Time-gated Luminescence Imaging And Biosensing In Cells And Tissues

BY

TING CHEN
B.Sc. Shanxi University, Taiyuan, China, 2008
M.Sc. Shanxi University, Taiyuan, China, 2011

THESIS

Submitted as a partial fulfillment of the requirements
for the degree of Doctor of Philosophy in Chemistry
in the Graduate College of the
University of Illinois at Chicago, 2018

Chicago, Illinois

Defense Committee:

Lawrence W. Miller, Chair and Advisor
Wonhwa Cho
Jung-Hyun Min
Xiaojing Yang
Mark McCauley, Medicine

This thesis is dedicated to

my dear husband Dezheng Li,

without whom it would never have been accomplished.

ACKNOWLEDGEMENTS

With so many people in my heart I feel deeply grateful for, I would like to thank my research advisor Professor Lawrence Miller first. His brilliant ideas about the project and his passion about the research guide me all the way to finish the thesis work. He always offers help when I am stuck in the problems, and usually just several sentences from him resolve my confusion and guide me to the next step. I cherish all our discussions about work and life. I am especially grateful for his generous support and encouragement during my maternity leaves. I couldn't imagine completing my PhD with two kids in another group or institute. Also, I would like to thank my dissertation committee members: Dr. Wonhwa Cho, Dr. Jung-Hyun Min, Dr. Xiaojing Yang and Dr. Mark McCauley for their support and assistance.

I am glad to work with so many friendly and cheerful people during my six years in the lab. Megha was my first and the best mentor. She patiently taught me all the skills I need to perform experiments, and always encouraged me to bravely express my ideas during group meeting. We still talk a lot even after she left the department. I am also grateful to Engin and Xiaoyan for their help in work and personal life. It is my great pleasure to work with Hamid, Yao, Ali, Claudia, Mona and Ha. They always offer suggestions and help if necessary.

I would like to thank Dr. George Papadantonakis and Silvia Solis for all their support and encouragement. They arranged short discussion classes for my convenience when I returned from maternity leaves. And special thanks to Rhonda Staudohar and Margaret Shortall for helping with the administrative work.

I would like to express my special thanks to my husband. He sacrificed a lot to come here and support me. He is the light in the dark, always stands behind me and cheers me up. With his love, I would never feel lonely or stressful. He also gave me the most valuable gifts in this world:

my two little boys Kevin and Owen. I just couldn't love them enough. This happy family is what matters most to me. Last, but not least, I owe big thanks to my family and my parents-in-law. They have offered a lot of help in the process of raising my two little boys. I don't think I can complete the doctoral work without their support.

TC

Contribution of Authors

Chapter 1 describes characteristics of lanthanide complexes, principle of time-gated method and background on relevant scientific concepts. The extracellular Tb-to-QD FRET biosensing experiment in Chapter 2 is part of a published paper (Afsari, H. A. ; Cardoso Dos Santos, M.; Lindén S.; Chen, T.; et,al. Time-gated FRET nanoassemblies for rapid and sensitive intra- and extracellular fluorescence imaging. Science Advances 2(6): e1600265, 2016) for which I was the fourth author. I performed all the experiments related to extracellular Tb-to-QD FRET imaging and generated Figures 5 and 6. Time-gated illuminescence imaging of immunolabeled human tissues is a published manuscript (Chen,T.; Hong, R.; Magda, D.; Bieniarz, C.; Morrison, L.; Miller, L. Anal. Chem. 89(23): 12713-12719, 2017.) for which I was the primary author and major drive of the research. I performed all the microscopy experiments and generated all the figures. My research mentor, Dr. Larry Miller contributed to the writing of the manuscript. Chapter 3 represents a series of my own unpublished experiments to develop lanthanide-based FRET biosensors with high dynamic range for time-gated microscopy and high throughput screening of protein-protein interactions in live cells. The final chapter of the thesis describes further application of the biosensors developed in Chapter 3, and a new method is proposed for mapping protein network or identifying potential hits of designated PPIs in living mammalian cells.

TABLE OF CONTENTS

LIST OF FIGURES

FIGURE PAGE

LIST OF ABBREVIATIONS

AEC	3-amino-9-ethylcarbazole
ALPHA	Amplified Luminescent Proximity Homogeneous assay
BAD	Bcl-2 Antagonist of cell Death
BAK	Bcl-2 Antagonist/Killer
Bcl-2	B-cell lymphoma 2
BRET	Bioluminescence Resonance Energy Transfer
CARD	Catalyzed Reporter Deposition
CFP	Cyan-Emitting Variant of Green Fluorescent Protein
DAB	3,3'-diaminobenzidine
DELFIA	Dissociation-Enhanced Lanthanide Fluorescent Immunoassay
DMEM	Dulbecco's Modified Eagle's Medium
DMSO	Dimethyl Sulfoxide
DOLs	Degrees Of Labeling
DPBS	Dulbecco's Phosphate Buffer Saline
DTPA	Diethylenetriaminepentaacetic Acid
EDHFR	*Escherichia Coli* Dihydrofolate Reductase
EGFP	Enhanced Green Fluorescent Protein
EGFR	Epidermal Growth Factor Receptor
ELISA	Enzyme-Linked Immunosorbant Assay
EMEM	Eagle's Minimum Essential Medium
FACS	Fluorescence-Activated Cell Sorting
FFPE	Formalin-Fixed Paraffin Embedded

FKBP12	FK506 Binding Protein 12
FP	Fluorescence Polarization
Fps	Fluorescent Proteins
FRB	Rapamycin Binding Domain of mTor
FRET	Förster Resonance Energy Transfer
GAM	Goat-Anti-Mouse
GAR	Goat-Anti-Rabbit
GFP	Green Fluorescent Protein
GPCR	G-Protein Coupled Receptors
H & E	Hematoxylin & Eosin
HDM2	Human Double Minute 2 Homolog
HEPES	4-(2-Hydroxyethyl)-1-Piperazineethanesulfonic Acid
HER	Human Epidermal Growth Factor Receptor
HPV	Human Papilloma Virus
HTS	High-Throughput Screening
ICCD	Intensified Charge Coupled Device
IF	Immunofluorescent
IFM	Immunofluorescence Microscopy
IHC	Immunohistochemistry
IL-2	Interleukin-2
IL-2Rα	α-chain of the IL-2 receptor
ITC	Isothermal Titration Calorimetry
IVTC	In Vitro Compartmentalization

Keap1	Kelch-Like ECH Associated Protein 1
LED	Light-Emitting Diode
Ln	Lanthanide
LTCs	Luminescent Tb^{3+} Complexes
MEM	Minimum Essential Media
mIHC	Multiplexed Immunohistochemistry
MSIHC	Mass Spectrometry Immunohistochemistry
NADPH	Nicotinamide Adenine Dinucleotide Phosphate
NEAA	Non Essential Amino Acids
NLR	Non-Linear Regression
NMR	Nuclear Magnetic Resonance
Nrf2	Nuclear Factor Erythroid Related Factor 2
PBS	Dulbecco's Phosphate Buffered Saline
PCAs	Protein-Fragment Complementation Assays
PPI	Protein-Protein Interaction
PPIMs	PPI Modulators
PPP1CA	Protein Phosphatase Catalytic Subunit Alpha Isozyme
PPP1R12C	Protein Phosphatase 1 Regulatory Subunit 12C
QC	Quality Control
ROI	Region Of Interest
S:B	Signal-to-Background
S:N	Signal-to-Noise
shRNA	Short Hairpin RNA

siRNA	Short-Interfering RNA
SPR	Surface Plasmon Resonance
SS	Steady State
SSMD	Strictly Standardized Mean Difference
TCF	T-Cell Factor
TGLM	Time-Gated Luminescence Microscopy
TMP	Trimethoprim
TNF	Tumor-Necrosis Factor
TNFR	Tumor-Necrosis Factor Receptor
TR-FRET	Time-Resolved Fluorescence Resonance Energy Transfer
TTHA	Triethylenetetraaminehexaacetic Acid
UV-Vis	Ultraviolet-Visible
Y2H	Yeast Two-Hybrid
YFP	Yellow-Emitting Variant of Green Fluorescent Protein

SUMMARY

The specific immunofluorescent (IF) staining of biomarkers, and the development of fluorescent biosensors, are common strategies to visualize and identify proteins, or protein-protein interactions (PPIs) in cells and tissues. Fluorescence-based high-throughput screening (HTS) assays that identify small molecules inhibitors of PPIs have proven to be useful tools in drug discovery. However, substantial improvements in the sensitivity and multiplexing capabilities of fluorescence-based protein imaging and screening technologies are needed to enable continued advancement in mechanistic biology and therapeutic development. Multiplexed IF is limited by the crosstalk between overlapping dye emission spectra and non-specific background, such as light scattering or sample autofluorescence. Similarly, non-specific background and the overlapping spectra of genetically encoded fluorescent proteins limit the multiplexing potential of dynamic, live-cell imaging of PPIs. HTS based on cell–free systems depends on the ability to obtain purified proteins. It occurs in artificial contexts that do not consider subcellular localization, post-translational modifications or competitive interaction with other cellular factors. Therefore, it does not discriminate against cytotoxic or membrane-impermeable compounds. Several cell-based HTS screening methods, such as protein-fragment complementation assays (PCAs) and bioluminescence resonance energy transfer (BRET) based assays are well established, but they suffer from low signal-to-background ratio, or high rates of false positives/negatives.

Time-gated luminescence imaging and detection using brightly emitting complexes of the lanthanide elements Tb(III) and Eu(III) offer several distinct advantages for immunofluorescence microscopy and for designing biosensors of protein function. Lanthanide complexes emit in multiple, well separated bands, and lanthanide emission lifetimes are on the

order of milleseconds. These features can be leveraged to develop highly sensitive, multiplexed protein imaging and screening assays based on Förster resonance energy transfer (FRET) between a Tb(III) or Eu(III) complex donor and a fluorescent protein acceptor. The donor emission can be easily filtered from sensitized acceptor emission, and is able to sensitize multiple differentially colored acceptors. While short-lived non-specific background, directly excited acceptor fluorescence, and autofluorescence are eliminated by time-gating, where pulsed light excites specimens and a short delay is implemented before the detector starts collecting light.

The main objectives of the studies in this dissertation were to expand the application of time-gated luminescence imaging in live cells and tissues, and to develop lanthanide-based biosensors for quantitative FRET imaging and HTS of PPIs in living cells with high sensitivity and signal-to-noise ratio. Chapter 1 describes characteristics of lanthanide complexes, principle of time-gated method and background on relevant scientific concepts. In Chapter 2, the feasibility of extracellular Tb-to-QD FRET biosensing was demonstrated by immunostaining different epitopes of epidermal growth factor receptor (EGFR) with QD- and Tb-antibody conjugates in A431 cells. By eliminating the non-specific background, time-gated luminescence microscopy (TGLM) enables the visualization of various markers and intermolecular, Tb(III)-to-dye FRET on FFPE tissue. Results also indicate the compatibility of TGLM with H&E staining in certain protocols. In Chapter 3, quantitative TGLM results from single chain lanthanide-based FRET biosensors were provided. Time-gated detection of PPIs and/or their inhibition were performed in multi-well plate with lysised cells or live mammalian cells. High quality data were obtained by the indication of Z' factor and strictly standardized mean difference (SSMD). The results strongly implicate the potential of lanthanide-based single-chain biosensors for hit

selection in HTS assays.

The final chapter of the thesis describes further application of the biosensors developed in Chapter 3. The interaction between protein phosphatase 1 regulatory subunit 12C (PPP1R12C) and its catalytic subunit alpha isozyme (PPP1CA), and their inhibition with a short peptide or other regulatory domain will be investigated to validate the ability of the biosensors to be utilized in HTS to discover effective small molecule inhibitors of PPIs. Finally, a new method, which combines split-DHFR and time-gated FRET, is proposed for mapping protein network or identifying potential hits of designated PPIs in living mammalian cells.

CHAPTER 1

INTRODUCTION

This thesis details the efforts for time-gated luminescence imaging on immunolabeled cells and human tissues, and development of lanthanide-based biosensors for quantitative FRET imaging and HTS of PPIs in living cells. The introductory part explicitly illustrates the photo-physical characteristics of lanthanide complexes, principle of time-gated method, the concept of FRET and the development of FRET biosensors. Additionally, it provides background information about multiplexed immunohistochemistry (mIHC). The importance of PPIs and HTS in drug discovery is also described with stage of current investigating technologies.

1.1 Lanthanide complexes as luminescent probes and time-gated detection

1.1.1 Chemical and photo-physical properties of lanthanide complexes

Complexes of the lanthanide elements Tb(III) and Eu(III) emit in multiple narrow-line bands and possess μs-ms long lifetime (**Figure 1A and B**). These two unique characteristics have been extensively leveraged for intracellular imaging and biosensing of protein-protein interactions.

Shielding of lanthanide 4f orbitals by larger radial expansion of their $5s^2 5p^6$ orbitals results in minimal perturbation by the ligand field, and therefore four narrow spectral bandwidths at 490 nm, 545 nm, 587 nm, and 620 nm, separately. Parity forbidden 4f-4f transitions of lanthanide elements lead to their long life time and low molar absorption coefficient ($< 1\ M^{-1}cm^{-1}$)[2]. Hence, an "antenna" moiety is required to overcome the low extinction coefficients of lanthanide ions to achieve efficient excitation[2]. The chelate in antenna is usually polyaminocarboxylate chelate, such as diethylenetriaminepentaacetic acid (DTPA), or triethylenetetraaminehexaacetic acid (TTHA). It binds to Tb(III) or Eu(III), and protects it from the solvent environment. The organic chromophore in antenna contains small singlet-triplet energy gap and a triplet energy at least 1500 cm^{-1} above the lanthanide emissive energy[3]. DTPA

or TTHA moieties are commonly attached to 7-amino-4-methyl-2(1H)-quinolinone (carbostyril 124; or cs124) fluorophore to serve as the antenna[4]. After chelating with Tb(III), these complexes exhibit high extinction coefficients and quantum yields at their long-wavelength absorption maxima of 342 nm[5]. Lumi4 is a macrocyclic probe, which incorporates four hydroxyisophthalamide sensitizers directly into the chelating portion of the molecule (**Figure 1C**). A variety of Lumi4-Tb(III) complexes have been developed for time-resolved FRET imaging and biosensing, owing to their high extinction coefficient (21,000 M^{-1} cm^{-1}) at 340 nm, excellent stability and quantum yield (>50%)[6].

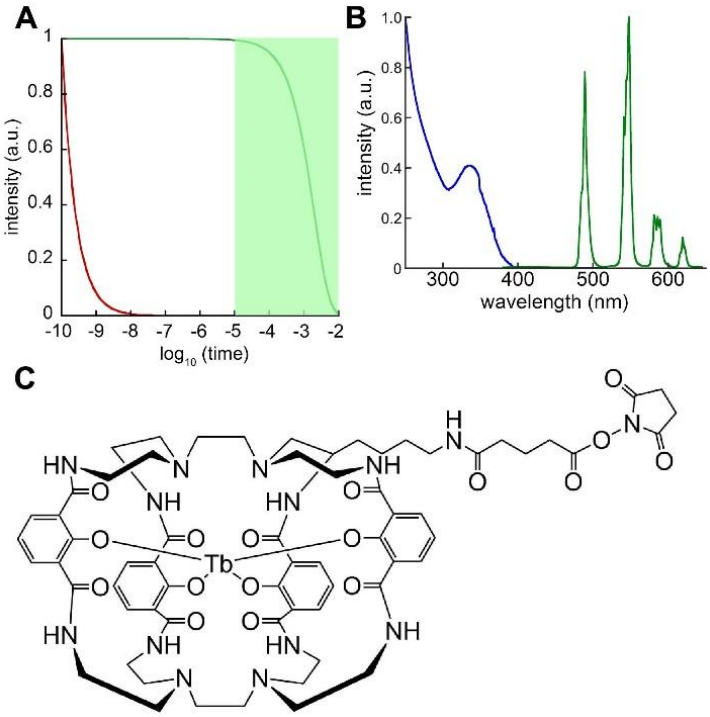

Figure 1. Characteristics of Tb(III) complex and Structure of Lumi4-Tb. (A) Time-gating detection of luminescence signals in the microsecond to millisecond range (green-shaded region) and elimination of nanosecond-scale fluorescence background. Depicted are single exponential decay curves with time constants of 2 ns (red line) and 2 ms (green line). The x axis is log10 time in seconds. (B) Normalized absorption (blue) and emission (green) spectra of Lumi4-Tb. (C) Amine-reactive analog of Lumi4-Tb. Reprinted with permission from Chen,T.; Hong, R.; Magda, D.; Bieniarz, C.; Morrison, L.; Miller, L. *Anal. Chem.*, 89(23): 12713-12719, 2017. Copyright 2017 American Chemical Society.

1.1.2 Application of lanthanide complexes in time-resolved FRET study

FRET-based biosensors are extensively utilized in solution-phase assays[7,8] , biomolecular imaging with time-gated luminescence microscope[9], and HTS applications[10]. Conventional FRET techniques using steady-state detection mode restrict the practical application of FRET biosensors, because the sensitivity of fluorescence detection is severely compromised by interference of non-specific background and autofluorescence, especially for those involving the UV-excited organic dyes or QDs[11]. Whereas, time-resolved FRET employing bright lanthanide complexes as donors provides remarkably high signal-to-noise ratio for luminescent biodetection[12,4].

The multiple, narrow emission bands of lanthanide complexes not only attenuate the donor emission bleedthrough into acceptor detection channel, but also afford multiplexing imaging or detection possibility, where two or more different colored acceptors are sensitized with single-wavelength, near-UV excitation. Long-lived (ms) lanthanide-sensitized acceptor emission can be distinctly measured after a 50-150 μs delay in the time-resolved detection method, when the ns-scale background, and directly excited acceptor luminescence rapidly decay and be extinguished (**Figure 2**). Hence, lanthanide-based time-resolved FRET is an effective strategy to completely eliminate the optical interference and cell/tissue autofluorescence in microscopy imaging[4], and bypass background fluorescence from assay buffer and reagents in HTS assay[13].

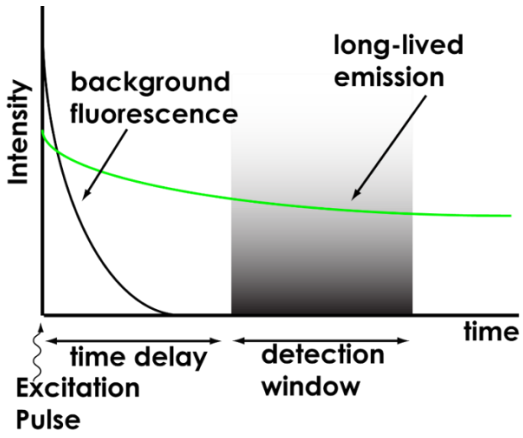

Figure 2. Principle of time gated detection method

1.2 FRET imaging and FRET-based biosensors

1.2.1 FRET and FRET imaging

Förster resonance energy transfer (FRET) is the non-radiational transfer of energy between an excited donor and a nearby acceptor. The FRET efficiency is defined as the probability of energy transfer per donor excitation event. It is inversely proportional to the sixth power of the distance between the donor and the acceptor, and therefore sensitive to small distance changes in a scale of <10 nm[14]. Usually, bimolecular FRET constructs are suitable for monitoring protein-protein interactions (PPIs), whereas unimolecular FRET constructs are used to detect protein conformational changes[14].

In a FRET pair, excitation of a donor results in the quenching of donor emission and the increase of acceptor emission. Intensity-based FRET imaging methods monitor the intensity of donor fluorescence with/without the photobleaching of acceptor, the sensitized fluorescence changes of acceptor, or the ratio between the donor and acceptor intensity[15]. While fluorescence decay-kinetics methods are established by determining the donor phtotobleaching rate, the

decrease of donor lifetime[16], or measuring fluorescence polarization[17].

Acceptor bleaching is a straightforward method to quantify FRET, especially between cyan-emitting variant of green fluorescent protein (CFP) and yellow-emitting variant (YFP)[18]. However, this method is destructive and therefore not compatible with timelapse imaging in living cells. The dual-emission ratio method, or two-color ratio imaging, is used to assess sensitized acceptor emission. It excites the sample at donor excitation wavelength, and repetitively measures the ratio of fluorescence intensity at corresponding donor emission peaks versus those of the acceptor[19]. Yet, the simple measurement of donor/acceptor intensity and their ratio can be affected by some interfering factors, such as uncertain stoichiometry of acceptor to donor, direct excitation of acceptor at donor excitation wavelength (cross talk), and leakage of donor emission to FRET channel (bleed-through). Thus the dual-emission method is not as quantitative as monitoring donor fluorescence. Various strategies, for example, the usage of different filter combinations with samples that only contain the donor or the acceptor, have been developed to correct above interfering factors, or to incorporate wide-field and confocal microscopes[20,21]. FRET can also be quantified by fluorescence lifetime imaging microscopy (FLIM), as lifetime is independent of fluorophore concentrations and insensitive to photobleaching. The time-domain fluorescence lifetime measurement in combination with two-photo excitation microscopy provides high sensitivity and spatial resolution, but requires long image acquisition time and complex data analysis[22]. Faster image acquisition can be achieved in frequency-domain lifetime measurement by equipment of a wide-field microscope with an image intensifier[23]. However, the requirement for donors with multiexponential decay excludes the use of many fluorescent proteins (FP).

1.2.2 Fluorescent proteins-based FRET biosensors

FRET-based biosensors are commonly involved in biomedical processes to monitor protein-protein interactions, study dynamics of enzyme activities, or metabolite concentrations[24,25]. With the combination of multiple FRET biosensors, the spatial and temporal resolution of several biological events can be investigated in the same cell[26]. But introduction of exogenous biosensors into one cell for multispectral imaging can increase phototoxicity and cause perturbation to the cell physiology.

Over the past decade, integrated FRET biosensors based on two differently colored fluorescent proteins have been developed for intermolecular and intramolecular FRET study (**Figure 3**). Unlike organic dyes, fluorescent proteins are designed to target subcellular compartments, introduced into various tissues or intact organisms, but rarely cause phototoxicity. Thus, fluorescent proteins are capable of responding to a much great variety of biological events. Dual-chain biosensors detect intermolecular FRET in real time upon interaction between two protein partners. So far, they have been utilized to study oligomerization state of different G-protein coupled receptors (GPCR)[27], transcription factor homo- or heterodimerization[28], and many other PPIs. But the variation in the expression level of two proteins hinders the accurate ratiometric imaging of dual-chain biosensors. On the other hand, single-chain biosensors contain two fluorescent proteins connected by a linker. Conformational change of the linker alters the distance or orientation between two partners, leading to a change in the FRET signal. This design has been applied successfully for ratiometic microscopy to detect NS3-4A protease activities in hepatitis C virus[29], Ca^{2+} dynamics[30], or Rho GTPase activities[31].

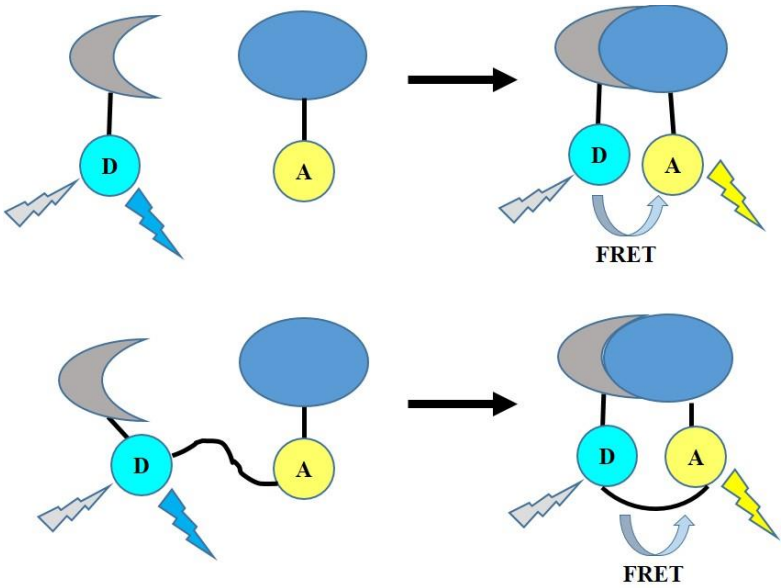

Figure 3. Design of FRET biosensors. Conformational change in single-chain biosensor and interaction between dual-chain biosensor results in change in sensitized acceptor emission due to FRET. D: donor fluorophore; A: acceptor fluorophore.

Advances in fluorescence microscopy and the continuing efforts to engineer new variants of GFP with altered colors and improved photophysical properties render the FP-based FRET biosensors as powerful tools to investigate complex biological processes in living cells. However, some limitations need to be taken into consideration when design and use the FP-based FRET biosensors. First, in spite of the various color variants reported, cross talk caused by the broad excitation and emission spectra profiles of FPs (**Figure 4A**) still hampers the development of compatible FRET pairs for simultaneous ratiometric imaging of multiple cellular events in a single cell[32]. Second, the large size of FPs results in the maximal FRET efficiencies as low as 40% in practical[33]. Third, the weak dimerization of FPs should be eliminated by including mutations in the experiments[34]. Overall, numerous efforts are undergoing to improve the quality of FPs-based FRET biosensors for multiplexed imaging in live cells to fully explore the colocalization and interaction of analytes. This involves the development of fluorescent

probes with novel spectral properties[35], increase of the response kinetics or detecting specificity[36].

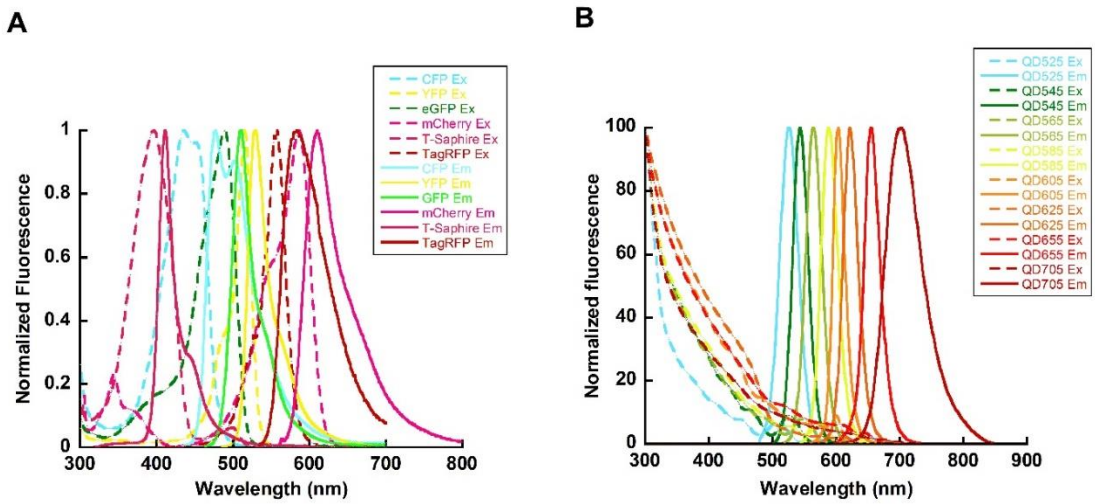

Figure 4. Excitation and emission spectra profiles of FPs (A), and QDs (B).

1.2.3. Quantum dots-based FRET biosensors

The remarkable properties of colloidal nanocrystalline semiconductors-quantum dots (QDs) have gained them great reputation as FRET biosensors in biological context. QDs have broad and strong absorption spectra, which span from the ultraviolet to the visible wavelengths depending on the particle size. Their narrow, size-tunable photoluminescence (**Figure 4B**), high phtotostability, strong resistance to photobleaching, and high sensitivity when conjugated with other biomolecular probes also contribute to their unique properties [37,38]. Hence, a series of QDs-based biosensors have been employed to detect small molecules, enzymatic processes, and protein cancer markers[39,40].

QDs often act as FRET donors in the QDs-based FRET biosensors. As their spectral overlap integral can be tuned and optimized to minimize direct acceptor excitation, crosstalk between QDs and dye is therefore reduced; the assemble of concentric multiple acceptors increases FRET efficiency, and facilitates multiplexed imaging in bioanalytical assays. In contrast, it is complicated to use QDs as FRET acceptors. The principle challenge arises from the fact that QDs are more efficiently excited than most potential donors because of their broad absorption and large extinction coefficients (**Figure 4B**). Additionally, the energy transfer using optical excitation and QDs is not viable due to the longer excited-state lifetimes of QDs ($\geq$ 10 ns) than those of fluorescent dye donors ($\leq$ 5 ns)[34]. So far, several solutions have been provided to overcome above limitations. Luminescent lanthanide (Ln) complexes with millisecond excited-state lifetime have been employed as donors, allowing the QDs excited-state to decay prior to energy transfer. This method offers several advantages, such as improved sensitivity of biosensor by the high brightness of QDs and signal amplification resulting from sequential FRET of several Ln complexes to the same QD, the versatility provided by attaching several biomolecules and fluorophores to the QD surface, and excellent capacity for multiplexing offered by the large spectral overlap of lanthanide-QD FRET pairs[41,42,43,44]. Alternatively, bioluminescent luciferase can be selected as donor to avoid optical excitation, while QDs can be preserved as ground state acceptors. A two-color protease assay and a four color in vivo imaging have been demonstrated with this strategy[45]. Moreover, chemiluminescent donors can be utilized for multiplexed configurations sensing[46].

1.3 Multiplexed immunohistochemistry

1.3.1 Immunohistochemistry on formalin-fixed paraffin embedded tissue

Formalin-fixation and paraffin-embedding (FFPE) is a typical method for preparation of

histological tissue in clinics worldwide to diagnose many diseases. The routine formalin-fixation process cross-links proteins via the formation of methylene bridges among amino groups of basic amino acids[47]. Then the samples undergo dehydration in alcohol series, and are finally embedded in paraffin. In this way, both proteins and their post modifications (e.g., phosphorylations, glycosylations) are preserved so that tissues are kept in an excellent condition for histopathological analysis soon or even years later[48]. These samples present an incredible opportunity yet huge challenges to researchers.

The antibody-based immunohistochemistry (IHC) is the standard method for protein detection in cells and tissue sections for clinical diagnosis. It provides valuable information about abundance and subcellular location of many biomarkers within a single biopsy, by using either brightfield (chromogenic) or fluorescent techniques. However, more powerful multiplexed IHC (mIHC) approaches are in strong demand to help investigate disease heterogeneity and disease-driven biology mechanisms, as well as conserve limited tissues.

1.3.2 Current techniques and their limitations

Chromogenic mIHC involves one single primary antibody at a time, and multivalent (e.g.biotinylated) secondary antibodies conjugated to enzymatic reporters (horseradish peroxidase or alkaline phosphatase), that generate colored pigments by reacting with substrates, such as 3,3'-diaminobenzidine(DAB), or 3-amino-9-ethylcarbazole (AEC). Despite its robustness and liableness for image acquisition and scoring, it is still challenging for colorimetric detection of more than three antigens using multiple enzyme-linked secondary antibodies[49]. Because the insoluble and dense deposits saturate easily, making it difficult for quantitative analysis due to nonlinear optical effects and low achievable dynamic ranges[50]. Moreover, virtually opaque regions will emerge in the tissue if multiple contrast agents are used in one

single tissue section.

On the other hand, immunofluorescence (IF) techniques based on fluorescent reporters provide higher signal-to-noise ratio than chromogenic methods, offer larger fields of view and are compatible with common light microscopes[51,52]. Multiple fluorophores, such as Alexa or Cy dyes, are available for IHC applications, but the multiplexing capability is limited by spectra overlap of fluorophores and the requirement for a complicated repertoire of species- and subtype-matched primary/secondary antibodies in indirect labeling protocol. Through careful selection of paired excitation/emission filter sets specific to the fluorophores, dichroic mirrors, and primary/secondary antibodies, a high level of multiplexing (> 4 labels at a time) is possible using conventional fluorescence microscope equipment[53]. Besides, great efforts have been put on extending the level of multiplexing by sequential cycles of staining, imaging and enzyme quenching. Here, methods to inactivate the enzyme include low-pH elution, high-temperature denaturation, and photoleaching[54,55]. Nevertheless, this labor intensive protocol still limits multiplexing due to tissue degradation after successive serial IHC assays[54.] Recently, mass spectrometry immunohistochemistry (MSIHC) have been extensively reported for achieving simultaneous, high-order (potentially up to 100 elemental mass tag-labeled antibodies at the same time) multiplexed imaging, while avoiding the extended labeling and washing process[56,57]. MSIHC use antibodies labeled with metal chelator tags, such as isotopically pure lanthanides, to overcome the spectral overlap of fluorophores. The narrow and potentially completely resolvable peaks corresponding to the metals are measured by mass differences. Yet, the field of view with this technique is presently restricted to a few hundred μm[58].

Another limitation of IF is that non-specific background, such as autofluorescence from FFPE tissues, lowers sensitivity and dynamic range[59]. As a solution, time-gated luminescence

microscopy (TGLM) can be adopted to eliminate non-specific background and increase the multiplexing potential of IF.

1.3.3 Signal amplification methods

Since 1980s, catalyzed reporter deposition (CARD) has been introduced as an important tool to confidently detect cellular markers of low abundance, therefore deepens the understanding of complexed protein and gene expression pathways that define cancer-related diseases. It is later adopted for usage in IHC on FFPE tissue[60], where specific signals arise from covalent binding of radical intermediate to proteins on tissue in close proximity to the site of generation. So far, two methods have been incorporated under the umbrella of CARD: tyramide signal amplification (TSA) and quinone methide signal amplification (QMSA).

TSA method utilizes the catalytic activity of horseradish peroxidase (HRP) in the presence of H_2O_2 to convert tyramine to a highly reactive tyramide, which reacts preferentially with electron-rich amino acid residues on proteins in close proximity to label a target protein or nucleic acid sequence in situ[61]. QMSA method takes advantage of the reaction between an alkaline phosphatase (AP) and latent quinone methides (QMs) for signal amplification in IHC assays[62]. The covalent bonding make these two methods quantitative and uniquely suited for serial staining. If used at the same protocol, these two methods are ideal for fluorescent multiplexing by skipping the antibody elution and enzyme deactivation steps[62].

1.3.4 Hematoxylin & Eosin (H & E) staining

A large number of archived clinical tissue specimens have been primarily stained with H&E for cancer diagnosis. Hematoxylin stains nucleic acids with a deep blue-purple color, while eosin stains proteins nonspecifically with a pink color. In a typical HE stained tissue, nuclei are stained blue and able to show varying cell-type- and cancer-type-specific patterns of

condensation of heterochromatin, while nucleoli stains with eosin show pink color. The cytoplasm and extracellular matrix have varying degrees of pink staining. If abundant polyribosomes are present, the cytoplasm will have a distinct blue cast[10]. Therefore, abundant structural information, with specific functional implications can be disclosed by H&E staining and used for prediagnosis.

Nevertheless, the hematoxylin staining is incompatible with immunofluorescence protocols due to the block of light by hematoxylin and eosin. By using TGLM, we demonstrate that H&E stained specimens could be further immunostained to show subcellular localization of particular biomarkers.

1.4 Protein-protein interactions as targets in drug discovery

1.4.1 The importance of PPIs as therapeutic targets

Within the biological processes of a cell, a giant and sophisticated network is formed by numerous molecular interactions. PPIs play pivotal roles among these interactions, as they are involved in many crucial pathways, such as signal transduction and immune responses[63]. Therefore, PPIs are closely linked to a wide variety of diseases, such as cancer, diabetes, and viral infections, thus represent a highly populated class of pharmaceutical targets in drug discovery[64,65]. For instance, infection with human papilloma virus (HPV) is the causative agent of some benign warts and cervical cancers, the interaction between viral transcription factor E2 and viral helicase E1 is required for the viral life cycle and thus is an attractive target for antiviral therapies[66]. Small molecules or peptides that can disrupt the interaction between cytokine tumor-necrosis factor (TNF) and its receptors TNFR1 and TNFR2, have been approved for treating arthritis[67]. Furthermore, interaction between substrate adaptor protein Kelch-like ECH associated protein 1 (Keap1) and the nuclear factor erythroid related factor 2 (Nrf2) gained

growing interest as a therapeutic target in the regulation of cytoprotective responses in cells upon exposure to stressors[51].

1.4.2 Challenges and current strategies for targeting PPIs

Despite the huge therapeutic potentials, enormous challenges still exist in targeting the interfaces between proteins by small molecules, which generally are cheaper, easier to synthesize and can be administered orally instead of by injection. The challenges include large and relatively flat PPIs sites, lack of deep pockets where a small molecule can dock, lack of natural ligands as starting points, and significant differences in the chemical space between PPI modulators (PPIMs) and conventional drug-like compounds [68,69]. Fortunately, "hot spot", or a sub-region with comparable dimension as the size of small organic molecules has been discovered. "Hot spot" contains a limited number of amino acid residues, but the particular spatial arrangement of functional groups mediates key interactions that contribute to binding affinity and selectivity. Therefore "hot spot" becomes a highly popular target to study small-molecule perturbations[70,71, 72]. So far, a number of successful studies have been showed to target PPIs for treatment of some human diseases. Those PPIs include: interleukin-2 (IL-2) and the α-chain of the IL-2 receptor (IL-2Rα)[73], β-catenin and T-cell factor (TCF)[74], B-cell lymphoma 2 (Bcl-2) and Bcl-2-antagonist/killer (BAK)/ Bcl-2 antagonist of cell death (BAD)[75,76].

Over the past decade, huge progress has been made toward new strategies for targeting "hot spots" of PPIs. Structural-based designs (e.g. computational molecular modeling) can help with the identification of key peptide fragments and amino acids residues[77]. But various screening methods is required if the structural information is limited or unavailable. Usually, PPIs are studied by either in vitro or in vivo assays. In vitro assays employ commonly used spectroscopic, electrophoretic, or affinity matrix–based techniques, such as nuclear magnetic

resonance (NMR) spectroscopy[78], isothermal titration calorimetry (ITC)[79], surface plasmon resonance (SPR)[80], and pull-down assays[6]. These techniques are widely adopted for PPIs discovery and confirmation, but require protein purification, appropriate post-translational modification and careful control of interacting conditions (e.g. buffer composition, pH and co-factor), as these assays are not performed in the cellular context of the PPIs and may lead to artifacts that do not reflect the native cell state. On the other hand, cell-based in vivo assays incorporate the physiological cellular environment for PPIs study, and are often designed based on yeast two-hybrid (Y2H) system, protein–fragment complementation, immunofluorescence, or FRET.

Ever since its first development, Y2H has been modified into many variants and commonly applied for PPIs detection. Generally, it is accomplished by attaching two distinct domains of eukaryotic transcription factors onto two proteins of interest. The following activation of a related reporter gene indicates the interaction. Y2H is sensitive to detect weak PPIs, but it is also known that Y2H generates false positives due to the fact that the assays take place artificially in a specific cellular location (nucleus or plasma membrane)[81]. Protein–fragment complementation assays (PCAs) and their variants are based on reconstitution of a fluorescent reporter or functional enzymatic protein from the interaction of two proteins or protein fragments. They have been adopted to sensitively visualize synapses between specific sets of neurons and map membrane PPIs[34, 60]. Recently, reversible PCAs were developed to screen for compounds disrupting PPIs[82,83]. In addition, fluorescent two-hybrid (F2H) assays with assistance of microscope have been exploited to detect more than 50 PPIs located in different subcellular compartments, such as the nucleus, cytoplasm, and mitochondria[14, 84,85]. The reversibility feature of the F2H approach allows the visualization of PPI dynamics in real time within the

physiologically relevant environment. Alternative approaches utilizing FRET or bioluminescence resonance energy transfer (BRET) are also reported[51,86,87,88].

In pharmacology field, a variety of screening approaches (e.g. high-throughput screening) combined with above assays, are being developed to identify small molecules that target "hot-spots" of PPI interface, especially on the condition of the limited or unavailable structurally information.

1.5 High-throughput screening assay

In modern drug discovery, pharmaceutical industries invest heavily in HTS systems to design and screen for drugs that target PPIs in pathways. As HTS is able to assess large numbers of compounds, proteins or genes within the biological events by automation and large dataset processing. The term of "High throughput" is now defined as testing of up to 100,000 compounds per day by fully automated robotic systems[26]. 96-well microtiter plates are usually used in preliminary assays for rapid evaluation of compound bioactivity, and 384 or 1,536 microliter plates are commonly found in parallel assays where the potential "hits" in chemical libraries tremendously increase.

When combined with other cell-free or cell-based PPIs detection methods, HTS assays can help identify stimulators, inhibitors, or other biologically active small molecules from the vast small molecule libraries, protein libraries, genome wide siRNA/shRNA libraries or cDNA libraries. Target-based HTS assays identify molecules that selectively bind to and modulate the activity of a biological target; and phenotype-based HTS assays screen for molecules that selectively induce a desired phenotype in the cell or organism of interest.

1.5.1 HTS assay design

To perform effective HTS assays, both the primary and subsequent secondary designs

should be considered carefully[89]. The basic format of primary HTS is defined with the nature of response (increase, decrease, change in nature or location) to be measured, measurement parameter output, false positives in conditional assays, and duration of the response. Secondary screens, also referred to as follow-up assays, validate compounds targeting the intended biological interaction and eliminate false positives-generating compounds by testing in an independent assay that uses alternative biological readout of target activity or a different methodology.

Regardless of the approach taken, several parameters must be optimized in the HTS protocols[89]: 1) sufficient sensitivity to identify compounds with low potency or efficacy; 2) stability of the biological response between wells and plates (reproducibility), which depends on assay reagents and hardware; 3) accuracy of the controls (positive and negative) as compared with the known targets; 4) economic feasibility as measured as cost per well.

1.5.2 Quality control and hit selection

An explosion in the rate of data generating in HTS assays necessitates appropriate experimental designs and analytic methods for both quality control (QC) and hit selection[90]. A variety of quality-assessment measurements, such as signal window, dynamic range, signal-to-noise ratio, signal-to-background ratio, and Z' factor, have been proposed to evaluate data quality[91]. Signal window measures the statistically significant difference between the maximum and minimum signal; dynamic range measures the ratio of mean signals between the positive and negative controls; signal-to-background ratio is defined as ratio between mean signal and mean background, which doesn't contain any data variation information; signal-to-noise ratio is defined as:

$$S{:}N = \frac{\text{mean signal} - \text{mean background}}{\text{standard deviation of background}} \qquad \text{Eqn. (I)}$$

It is only an indication of the degree of confidence that a signal can be distinguished from background noise. All of these parameters do not consider variations from signal and background. Therefore, Z' factor was proposed and then widely used in HTS as an indicator of data quality. It is calculated from the standard deviations and means of the maximum and minimum observed signal levels under controlled conditions (i.e., without library compounds present) according to equation I.

$$Z' = 1 - \frac{3(\sigma_p + \sigma_n)}{|\mu_p - \mu_n|} \qquad \text{Eqn. (II)}$$

Z'-factor can vary between -1 and 1, with values >0.5 considered to be a very good assay, values > 0 considered acceptable, and < 0 an unacceptable assay [92]. However, a high Z' factor can be generated by very strong positive control, but may not realistically represent more moderate screening positives. A less conservative indicator of quality, SSMD, can be calculated to accurately capture the clear differences between the high and low populations and used for hit identification[93]. For example, short-interfering RNA (siRNA) or short hairpin RNA (shRNA) libraries are screened in large-scale to identify new factors involved in the molecular pathways of diseases[94]. However, siRNA screens were less robust than small-molecule screens and contain more moderate screening positives[93]. Roughly speaking, SSMD is the ratio of mean to the standard deviation of the difference between two groups (e.g., plate wells containing positive and negative controls). For positive and negative controls in a plate with sample means μ_p and μ_n, and sample variances σ_p^2 and σ_n^2, SSMD may be calculated as,

$$\beta = \frac{\mu_p - \mu_n}{\sqrt{\sigma_p^2 + \sigma_n^2}} \qquad \text{Eqn. (III)}$$

The value of SSMD will be positive or negative depending on the assay type (activation or inhibition), and the SSMD-based quality control criteria for evaluating assay performance using

a very strong positive control is as follows: extremely strong, $\beta \geq 5$; very strong, $5 > \beta \geq 3$; strong, $3 > \beta \geq 2$; fairly strong, $2 > \beta \geq 1.645$; moderate, $1.645 > \beta \geq 1.28$; fairly moderate, $1.28 > \beta \geq 1$; fairly weak, $1 > \beta \geq 0.75$; weak, $0.75 > \beta \geq 0.5$; very weak, $0.5 > \beta \geq 0.25$; and extremely weak, $\beta \leq 0.25$[95].

Overall, two or more metrics can be calculated simultaneously to effectively validate the HTS assay protocol, or to determine the assay performance.

1.5.3 HTS assay formats

HTS assays can be performed in the cell-free biochemical context or cell-based native environment, providing benefits and limitations from different aspects. Biochemical HTS incorporate enzyme-linked immunosorbant assay (ELISA)-type assay formats, mix-and-read assay formats and bead-based assays. And cell-based HTS assays are categorized as reporter complementation, resonance energy transfer and protein redistribution method[89].

ELISA-type assays are based on the antibody and enzyme-based detection. They are very sensitive, as the readouts are amplified by an enzyme. They are also flexible designs in the ways of protein attachment to the plate surface (passive adsorption or biotinylation/avidin capture), second protein detection methods (direct or indirect labeling), or enzyme detection methods (colorimetric, fluorogenic, or luminogenic reactions)[96]. Its non-enzymatic format is called dissociation-enhanced lanthanide fluorescent immunoassay (DELFIA), where the lanthanide ion is bound to the affinity reagent through a chemical linkage, emits fluorescence upon adding of a proprietary detergent mixture and the signal is detected through time-resolved fluorescence. However, ELISA-type assays involve multiple incubation and washing steps, which disrupt the weak PPIs ($K_d > 1$ μM), and make the assays time-consuming for automated screening. In addition, extra assays with different formats or methods are required to demonstrate

the specificity of potential inhibitors.

Fluorescence-based detection methods, such as fluorescence polarization (FP)[97], FRET[98], time-resolved FRET[10], and fluorescence-activated cell sorting (FACS)[99], are extensively used as mix-and-read HTS formats. FP assays monitor the change in polarization upon the binding of a fluorescently labeled small molecule or peptide to a protein. No washing, incubation or separation steps are required during the assay. But FP is sensitive to optical interference and fluorescence from the test compounds. FRET and TR-FRET methods are flexible with a large number of available dyes and fluorescent proteins. They are usually performed in ratiometric assays to reduce the effects of autofluorescence and spectral interference from media and test compounds. FACS is also common in application of surface display, in vitro compartmentalization (IVTC), GFP-reporter assays and product entrapment to study enzyme activities.

Amplified luminescent proximity homogeneous assay (ALPHA), one of the bead-based formats, monitors fluorescent signal as energy transfer from donor beads (containing a photosensitizer-phthalocyanine to convert ambient oxygen to singlet oxygen upon illumination at 680 nm) to acceptor beads (rubrene or europium chelate as the final fluorophore) upon binding of two molecules captured on the beads. The high sensitivity and large distance range (200 nm) increase their application in HTS settings.

In summary, the cell-free biochemical assays provide data set easily to validate and interpret, and lack of interference from components in a complex cell environment yields robust results (e.g. high dynamic range, or Z' factor). However, accomplishments of the assays require significant quantities of pure proteins, optimization of potential hits for cell permeability and acceptable toxicity profile.

Cell-based reporter assays are adopted to overcome the limitations of biomedical assay. Intracellular PPIs can be studied in a physiological context, where co-activators, co-repressors, post-translational modifications or some other cellular factors are provided. Proteins that are difficult or costly to be purified (e.g. membrane proteins) can also be incorporated. Moreover, multiple PPIs in the pathways are possible to be detected and screened via multiplexing methods, while cytotoxic or membrane-impermeable compounds are discriminated. Protein-fragment complementation assays (PCA) involve two proteins of interest fused to complementary fragments of a reporter protein (β-lactamase, GFP, YFP or luciferase). The reporter protein activity is recovered only if PPI occurs[82,34]. The low sensitivity of the method has been improved by engineering two split horseradish peroxidase fragments through screening of 17 cut sites in HRP and directed evolution, fusing them to two extracellular proteins to enable sensitive visualization of synapses between specific sets of neurons[34]. FRET and TR-FRET assays are very popular due to their high sensitivity and multiplexing potential[100,10]. In bioluminescence resonance energy transfer (BRET) based assays, a bioluminescent enzyme acting as a donor to provide photos to an acceptor fluorophore in close proximity and generate a signal, which can be measured quickly and reversibly for detection of dynamic PPIs[101]. BRET is also extremely valuable for real-time monitoring of PPIs for functional and regulatory research[61]. Finally, successful high content screening assays for monitoring protein relocalization has been developed by combining FRET with microscopy imaging within cells[102,103].

Despite the multiple advantages provided by cell-based screening assays, their broad application in HTS to discover potential "hits" are still hindered by some problems, such as protein sequestration at non-physiological sites, low signal-to-background ratio, or high rates of false positives/negatives. Ideally, HTS assays with different formats should be performed

simultaneously to exclude all possible artifacts or interferences, and identify small molecules as potential drugs.

CHAPTER 2

TIME GATED LUMINESCENCE IMAGING OF IMMUNOLABELED CELLS AND HUMAN TISSUES

The extracellular Tb-to-QD FRET biosensing experiment is part of the paper originally published as "Afsari, H. A. ; Cardoso Dos Santos, M.; Lindén S.; Chen, T.; et,al. Time-gated FRET nanoassemblies for rapid and sensitive intra- and extracellular fluorescence imaging. *Science Advances* 2(6): e1600265, 2016". Reprinted with permission from AAAS.

Time-gated luminescence imaging of human tissues results are published as "Chen,T.; Hong, R.; Magda, D.; Bieniarz, C.; Morrison, L.; Miller, L. Anal. Chem. 89(23): 12713-12719, 2017". Copyright 2017 American Chemical Society".

2.1 Introduction

To date, the specific and sensitive immunostaining of biomarkers in cells or tissues with antibodies remains the common choice for fluorescence imaging. Immunofluorescence microscopy (IFM) enables quantitative analysis of protein expression levels, heterogeneity and spatial relationships among multiple markers with dimensions ranging from the sub-cellular to tissue level[104,105,106], as it offers high spatial resolution (sub-micron) and a large field of view[52].

A variety of FRET-based biosensors have been developed for immunofluorescence imaging of PPIs, second messenger dynamics and enzyme activities in live cell context[25]. The toolbox of FP-based FRET biosensors continues to fill as enormous research are undergoing to expand the spectra file of fluorescent proteins and improve the microscopic technology[107]. However, the broad excitation and emission spectra profiles of FPs hamper the development of compatible FRET pairs for simultaneous ratiometric imaging of multiple cellular events in a single cell[105]. And the requirement for acquisition and processing of two or three images per frame leads to lower signal-to-noise ratio and temporal resolution[108,109].

On the other hand, the multiplexing potential of IFM suffers from the limited number of secondary antibodies that can be applied to a single sample. Sequential cycles of staining,

imaging and enzyme quenching can overcome these limitations to a certain extent, but problems such as tissue degradation and experimental complexity still exist[49]. Another limitation of IFM is that non-specific background, such as light scattering or autofluorescence from FFPE tissues, lowers sensitivity and dynamic range. Being considered as the next generation approach in IHC, mass spectrometry can potentially detect up to 100 elemental mass tag-labeled antibodies, yet the field of view is presently limited to a few hundred μm[58,57]. Therefore, strong demand arises for a straightforward approach to visualize several markers on a single sample with maximized sensitivity, simple instrumentation and sample preparation.

The FRET pair combination of luminescent Tb^{3+} complexes (LTCs) as donors and QDs as acceptors, along with time-gated luminescence microscopy (TGLM) offer several unique advantages over FP-based IF imaging systems. LTCs emit at multiple narrow bands, which reduce the bleedthrough of Tb signal to sensitized acceptor channel and facilitate multiplexing. The ms-long excited-state lifetime of LTCs allows decay of the ns-scale light scattering, directly excited acceptor fluorescence, and autofluorescence background before the detector start collecting light in time-gating method. These features have been successfully leveraged in the solution phase assays to quantify human epidermal receptor (HER) expression and dimerization in patients' tumor samples[8], or realize ultrasensitive multiplexed biosensing[7]. They are also engaged in biomolecular imaging to detect protein-protein interactions on cell membranes[110], visually inspect lanthanide-stained microorganisms[111], or reveal the impact of GPCR oligomerization on internalization processes[112].

The color tunability and spectrally broad molar absorptivity of QDs further improve the LTCs-based FRET in several aspects: the Tb-QD FRET pairs enlarge the FRET distance range from <10 nm to ~ 20 nm because they already provided up to 11 nm Förster distances (the donor-

acceptor distance of 50% FRET efficiency)[113]; high sensitivity is achieved by the high brightness of QDs and sequential FRET from several Tb^{3+} complexes to the same QD; the ability to attach several biomolecules and fluorophores to the QD surface provides versatility. Therefore, Tb-to-QD FRET has been applied extensively for spectroscopic biosensing and cellular imaging[114,115,41]. Yet so far, Tb-QD FRET immunolabeling has only been used for heterogeneous and homogeneous solutions[116,42], its application for intra- and extracellular imaging is still missing.

Herein, we demonstrate the feasibility of extracellular Tb-to-QD FRET biosensing by immunostaining different epitopes of epidermal growth factor receptor (EGFR) with QD- and Tb-antibody conjugates in A431 cells. Two different therapeutic antibodies (cetuximab and matuzumab), or nanobodies (EgA1 and EgB4) that recognize different epitopes on the EGFR R17-18 were conjugated to Tb and QDs, respectively. A robust intramolecular Tb-to-QD FRET signal was observed on the surface of cultured A431 cells.

In addition, as TGLM provides higher contrast than conventional, steady state (SS) IF due to the elimination of non-specific background, we were able to visualize various markers including Ki-67, e-cadherin (E-cad), Bcl-6, Bcl-2, MSH-6 and CD-20 immulabled by Lumi4-Tb-conjugated, secondary antibodies. Two-component imaging of Tb(III) and fluorescent dye signals on the same specimens are also demonstrated. Tyramide signal amplification (TSA) method enables us to visualize intermolecular, Tb(III)-to-dye FRET by co-depositing both Lumi4-Tb alone or with various organic dyes to the same target protein. Finally, we show that TGLM with Lumi4-Tb is compatible with H&E staining in certain protocols, a potentially useful trait for further evaluation of archived FFPE tissues.

2.2 Materials and Methods

2.2.1 Materials

A431 cells (CRL-1555) and HeLa cells (CCL-2) were purchased from American Type Culture Collection. Dulbecco's modified eagle medium (DMEM, 10-014 CV), Eagle's minimum essential medium (EMEM, 10-010 CV), Phosphate buffer saline (PBS, 21-014 CV), Dulbecco's phosphate buffer saline (DPBS, 21-030 and 21-031), 0.25% trypsin/0.53 mM EDTA and 0.25% trypsin/2.21 mM EDTA were purchased from Corning Cellgro®. MEM non-essential amino acids (11140), DMEM (no phenol red, 21063) and HEPES (15630-080) were purchased from Gibco®. Antibodies (Cetuximab-QD650 and Matuzumab-Lumi4(Tb)) and nanobodies (EgA1-Lumi4(Tb) and EgB4-QD650) were provided by Prof. Niko Hildebrandt. Lumi4-NH2 was provided by Lumiphore, Inc. 8-well chambered coverglass (12-565-470) was purchased from Nunc™.

2.2.2 Cell culture

A431 cells were maintained in EMEM (+) (Eagle's minimum essential medium supplemented with 10% FBS, 1X MEM non-essential amino acids) at 37 °C and 5% CO2. The cells were passaged with 0.25% trypsin/0.53 mM EDTA. HeLa cells were maintained in DMEM (+) (DMEM supplemented with 10% FBS, 1X MEM non-essential amino acids and 15 mM HEPES) at 37 °C and 5% CO_2. The cells were passaged with 0.25% trypsin/2.21 mM EDTA.

2.2.3 Cell surface labeling with antibodies/nanobodies

Cells were trypsinized and seeded at 23,000 cells/well in an 8-well chambered coverglass and incubated at 37 °C and 5% CO_2 overnight. The following day, the cells were washed three times with DPBS (+Ca/+Mg), 100 μL of various combination of QD/Tb attached

antibodies or nanobodies (in DMEM without FBS) were added to different wells, and the cells were incubated for 30 min at 37 °C and 5% CO_2 incubator. The cells were washed again with DPBS (+Ca/+Mg) and 150 µL of 1mM patent blue V solution in DMEM (without phenol red) was added to the well to quench extracellular luminescence from non-specifically adsorbed probe.

2.2.4 Immunolabeled FFPE tissues

All the tissue treatment and staining procedures were performed by Ventana.

2.2.5 Time-gated and steady-state microscopies

Images of Tb(III) labeled markers and Tb-mediated FRET were acquired using a wide-field, time-gated luminescence microscope that uses a UV light-emitting diode(LED) for pulsed excitation and an ICCD camera for gated detection. The design, operation, and characterization of the microscope system have been described extensively[117,118]. For each TG image acquisition, the signal from multiple excitation/emission events was accumulated on the ICCD sensor and read out at the end of the camera frame. The camera control software enabled summation of multiple frames to yield a single composite TIFF image with a bit depth equal to 1024 multiplied by the number of frames. All images were summations of four frames (bit depth, 4096), and a feature of the camera control software was enabled that removes large variations in signal resulting from ion feedback noise of the intensifier. The UV LED source and the ICCD timing parameters were the same for all of the time-resolved images and data presented here: excitation pulse width, 1500 µs, pulse period, 3000 µs, delay time, 10 µs, intensifier on-time, 1480 µs. Sensitivity was modulated by either varying the frame length (and thus, the number of integrations) or the intensifier gain voltage. All TG images were acquired at an intensifier gain of

833 V. The emission filters and all detector timing and gain parameters for each tissue imaging figure in the text are provided in **Table 1**.

Steady state fluorescence images of markers labeled with various dyes or QDs were captured by a conventional CCD camera (Axiocam MrM, Carl Zeiss, Inc.) mounted on the front port of the microscope. A white light LED (UHP-T-LED-White, Stanford Photonics, Inc.) was available for continuous wave fluorescence excitation. Filter cubes containing the appropriate excitation and emission filters and dichroic allowed for wavelength selection.

2.2.6 Image processing

Raw, 12-bit images were imported into NIH ImageJ (v1.42q or v1.51j8) for all processing operations including cropping, contrast adjustment, and quantitative analysis[119]. TG FRET images were corrected for spectral bleedthrough of the Tb donor signal into the FRET channel. Bleedthrough correction for Tb-to-QD FRET images was accomplished by measuring signals from many cells (>100) containing Lumi4-NH2(Tb) probe in both the Tb emission channel (494 ± 10 nm) and the FRET emission channels (655 ± 20 nm). Bleedthrough correction for immunolabeled tissues was accomplished by measuring signals from many ROIs (>20) of cells containing Lumi4-Tb probe in both the Tb emission channel (494 ± 10 nm) and the FRET emission channels (605 ± 7 nm, 520 ± 10 nm, and 710 ± 20 nm). The FRET channel signal was plotted as a function of the Tb channel signal, a line was fit to the data, and the slope of that line was taken to be the correction constant. The correction constant for the 655 ± 20 nm and 605 ± 7 emission channels was 0.142, 0.122, respectively. Bleedthrough of Tb signal into the 520± 10 nm and 710 ±10 nm were negligible. The Tb channel image was multiplied by the appropriate bleedthrough correction constant, and the resulting image was subtracted from the FRET channel image to yield the true FRET image. Heatmap representations of image S/N were prepared by

measuring the mean pixel gray value from multiple ROIs within a given image that lacked cells. Then, the original image was divided by the mean background value, and a color lookup table was applied to generate the S/N map.

Brightfield images of hematoxylin staining were generated with the same monochrome camera used for recording luminescence images by switching to the microscope transmission mode with tungsten lamp illumination. Images were recorded with a red (Edmund Optics, 46545), green (Edmund Optics, 46546), and blue (Edmund Optics, 46547) transmitting filters placed in the light path and flat-field correction in each bright field channel were performed as follows. For each channel, 20 dark frames and 20 bright field images were stacked, converted to 32 bits, and median-filtered (radius 1), and each stack was averaged. The flat-field average was divided by the mean intensity of its central nine pixels to generate a normalized flat-field image. For each sample image, a median filter (radius 1) was applied and the master dark frame was subtracted. The resulting image was then divided by the normalized, master flat-field image, and the mean value of the detector offset was added back to the image. The processed images were then merged to form the brightfield color composite image. For combining with a luminescence image, each pixel of the red-filtered transmission image was divided by the maximum pixel value, the logarithm taken, and multiplied by -1 to approximate absorbance, and the absorbance image was then merged with the luminescence image.

2.3 Results and Discussion

2.3.1 Extracellular Tb-to-QD FRET using immunostaining

To demonstrate the feasibility of extracellular Tb-to-QD FRET biosensing by immunostaining with different kinds of antibodies, we used cetuximab and matuzumab antibodies and EgA1 and EgB4 single-domain V_HH (variable domain of heavy chain) antibodies

(nanobodies) that recognize different epitopes of EGFR[120,121]. eBioscience eFluor 650NC QDs emitting at 650 nm (QD650) were surface-functionalized with cetuximab and EgB4, and ultraviolet-visible (UV-Vis) absorption spectroscopy revealed that the average degrees of labeling (DOLs) were approximately 6.8 cetuximab per QD650 and 18.1 EgB4 per QD650. Matuzumab and EgA1 were reacted with N –hydroxysuccinimide (NHS) – functionalized Lumi4-Tb, and the DOLs were ca. 4.1 Tb per matuzumab and 2.2 Tb per EgA1. We then incubated live A431 cells in culture medium that contained QD650-cetuximab (9.5 nM) and matuzumab-Tb (100 nM) for 30 min, washed the cells, and mounted them immediately on the microscope slide for imaging. TG imaging revealed robust, long-lived PL signals in both the Tb (494 nm) and the QD (650 nm) detection channels (**Fig. 5A**). Similar results were seen when A431 cells were co-incubated with the nanobody conjugates QD650-EgB4 and EgA1-Tb (**Fig. 5B**). By contrast, hardly any appreciable long-lived TG signal was detectable in the QD channel when cells were incubated with QD conjugates or Tb conjugates alone (**Fig. 5, C and D**).

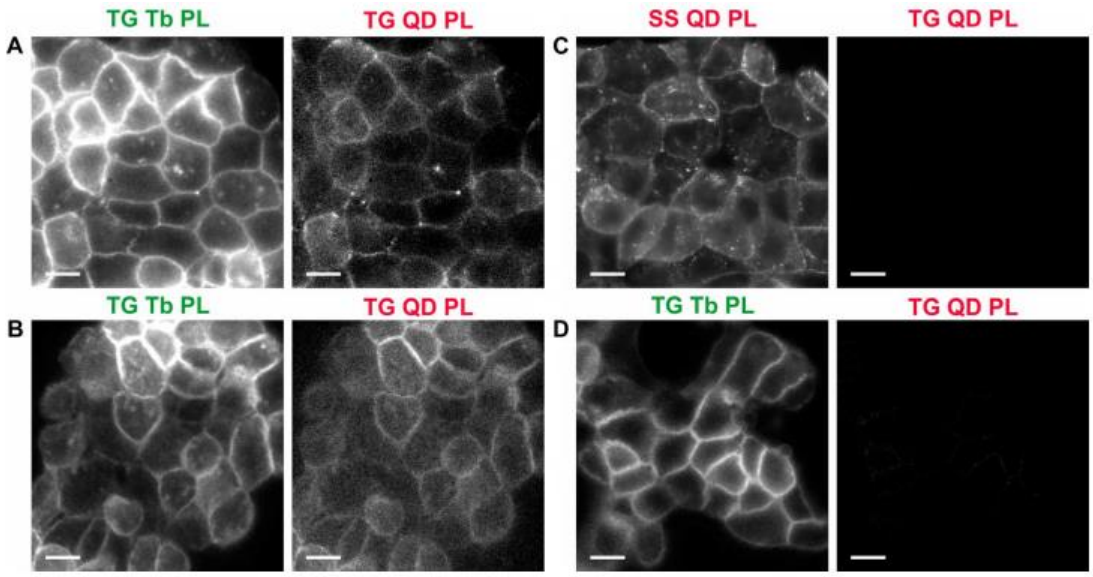

Figure 5. Extracellular Tb-to-QD FRET using immunostaining of EGFR. (A and B) Tb-to-QD FRET detected on A431 cells with QD- and Tb-conjugated antibodies (A) and nanobodies (B). For both immunostaining approaches, the time-gated Tb (TG Tb PL) and QD (TG QD PL) channels reveal bright PL signals originating mainly from the cell membranes. (C and D) In contrast, staining with only QD-antibodies (C) or only Tb-antibodies (D) does not result in TG PL in the QD channel (TG QD PL, right), and only the pure QD SS PL (C, SS QD PL, left) or the pure TG Tb PL (D, left) become visible. Excitation and emission wavelengths for the different detection channels were as follows: λ_{ex} = 365 nm and λ_{em} = 494±10 nm for TG Tb PL, λ_{ex}= 365 nm and λ_{em} = 655 ± 20 nm for TG QD PL, and λ_{ex} = 545 ± 15 nm and λ_{em}= 610 ± 35 nm for SS QD PL. For TG images, the number of integrations was 220 and 110 for the TG Tb PL and TG QD PL channels, respectively. Tb-to-QD FRET channel images (TG QD PL) were corrected for spectral crosstalk, and each TG QD PL channel image in this figure ispresented at identical contrast. Scale bars, 20 µm. From (Afsari, H. A. ; Cardoso Dos Santos, M.; Lindén S.; Chen, T.; et,al. Time-gated FRET nanoassemblies for rapid and sensitive intra- and extracellular fluorescence imaging. *Science Advances* 2(6): e1600265, 2016). Reprinted with permission from AAAS.

Moreover, Tb-mediated FRET was undetectable on A431 cells colabeled with matuzumab-Tb and HER2-specific antibodies conjugated to a QD (**Fig. 6**), although TG Tb PL and steady-state (SS) QD PL could both be detected. Thus, by eliminating short-lived, nonspecific signals, intermolecular FRET between both two different immunoglobulin G antibodies and two different single-domain antibodies could be clearly visualized, which

demonstrated the applicability of the Tb-QD FRET pair for imaging protein-protein interactions on cell membranes. Moreover, this FRET system can also be used for a homogeneous (no separation or washing steps) imaging of proteins that express on cellular membranes, similar to FRET in vitro assays[42,122]. This application would be particularly interesting for live cell imaging or multiplexing.

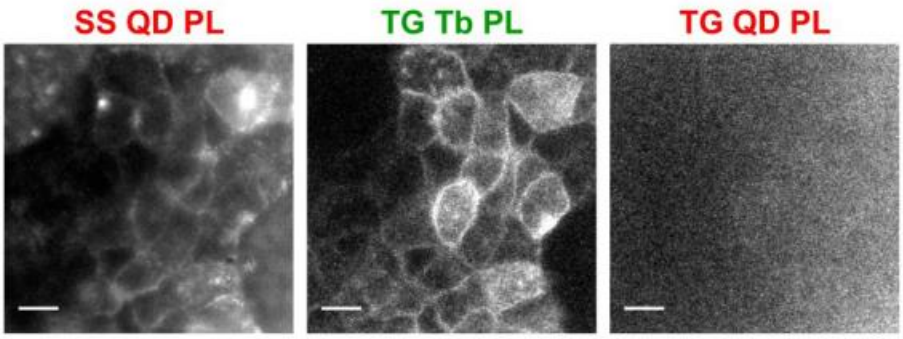

Figure 6. Extracellular Tb-to-QD FRET is undetectable when Tb- and QD-conjugated antibodies are localized to different targets. A431 cells were incubated in culture medium that contained Tb-conjugated Matuzumab (100 nM; DOL, 4.0 Tb/antibody) and QD-conjugated Pertuzumab (15 nM; DOL, 8 antibody/QD). Matuzumab and Pertuzumab recognize EGFR and HER2, respectively. While steady-state QD PL (left) and time-gated Tb PL (middle) are plainly visible, time-gated QD PL could not be detected, indicating a lack of FRET in this system. Excitation and emission wavelengths for the different detection channels were: λ_{ex} =365 nm and λ_{em} = 494 ± 10 nm for time-gated Tb (TG Tb PL), λ_{ex} = 365 nm and λ_{em}= 655 ± 20 nm for time-gated QD (TG QD PL), and λ_{ex} = 545±15 nm and λ_{em} = 610 ± 35 nm for steady-state QD (SS QD PL). For time-gated images, the number of integrations was 660 for both the TG Tb PL and TG QD PL channels. Scale Bars: 20 µm. From (Afsari, H. A. ; Cardoso Dos Santos, M.; Lindén S.; Chen, T.; et,al. Time-gated FRET nanoassemblies for rapid and sensitive intra- and extracellular fluorescence imaging. *Science Advances* 2(6): e1600265, 2016). Reprinted with permission from AAAS.

2.3.2 TGLM on unamplified tissue specimens.

We first sought to qualitatively compare TGLM and SS fluorescence images of indirectly labeled human tonsil tissue. FFPE specimens were stained with primary antibodies

targeting various markers including Ki-67, E-cadherin (E-cad), CD 20, Bcl-6. MSH-6, and Bcl-2. Following primary antibody labeling, the tissue specimens were labeled with the appropriate species-selective secondary antibodies that were conjugated to either Lumi4-Tb or Alexa Fluor 488 (AF488) and then imaged. Both SS and TGLM images exhibited the expected phenotype for each marker (**Fig. 7**).

In order to highlight the orthogonality of time-gated and SS signals, tonsil tissue slides were co-stained with two primary antibodies; one, a rabbit antibody, was selective for Ki-67 or E-cad and the other, a mouse antibody, was selective for Bcl-6, MSH-6 or CD20. The slides were then stained with goat-anti-rabbit (GAR) and goat-anti-mouse (GAM) secondary antibodies conjugated to either Lumi4-Tb or AF488 (GAR-Tb plus GAM-AF488 or GAM-Tb plus GAR-AF488). Visualization of both time-gated Tb(III) photoluminescence (TG Tb PL) and SS AF488 PL made it possible to separately detect Lumi4-Tb-labeled and AF488-labeled markers in the same field of view (Fig. 8 A-C), thus adding a second signal dimension for multi-component IF.

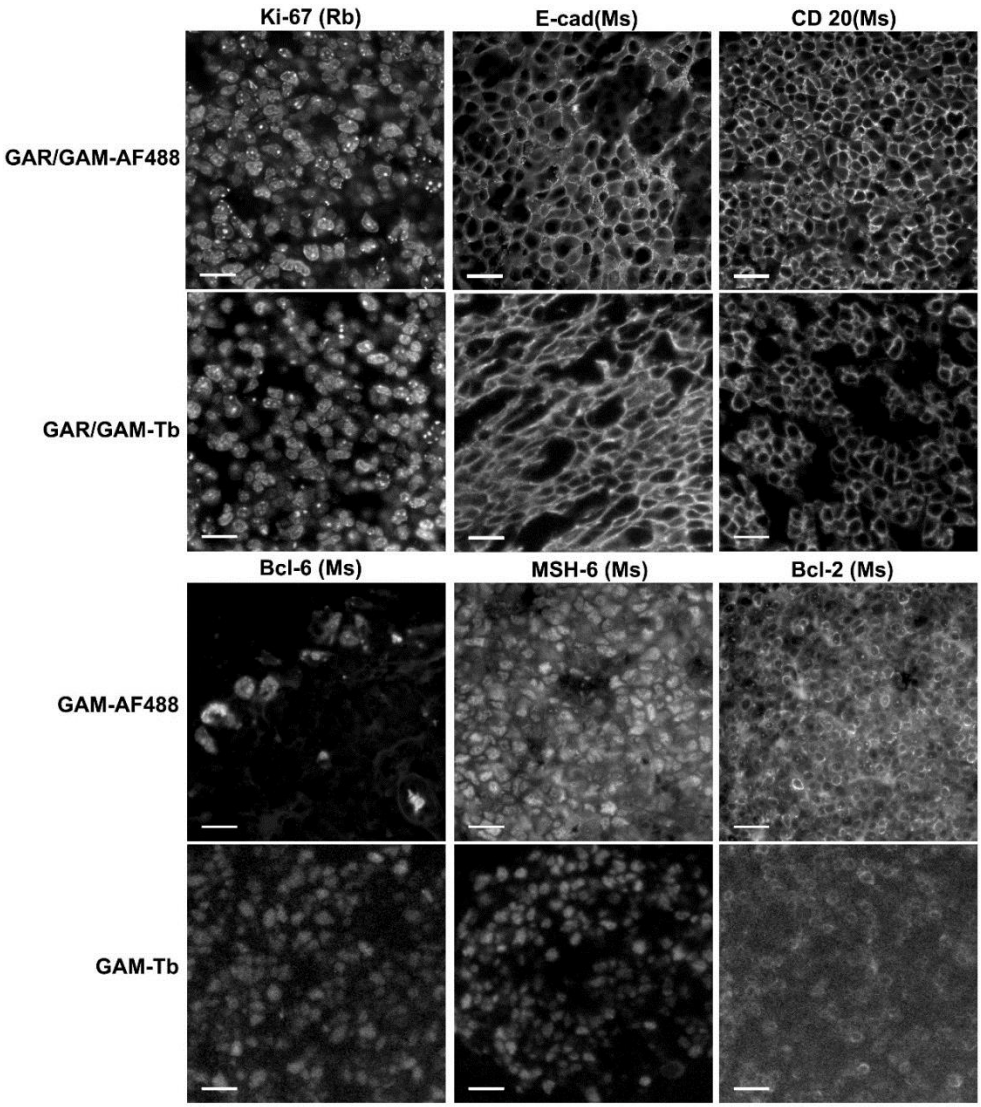

Figure 7. Steady state and time-gated microscopy of immunolabeled tonsil tissue.

FFPE slides were labeled with primary antibodies raised against Ki67, E-cad or CD-20 (A) or Bcl-6, MSH-6 or Bcl-2 (B), then stained with goat, anti-rabbit (GAR) or goat, anti-mouse (GAM) secondary antibodies conjugated to Lumi4-Tb or AF488 as indicated. Micrographs depict steady state AF488 fluorescence (λ_{ex}, 480 ± 20 nm and λ_{em}, 520 ± 10 nm) or time-gated Tb(III) luminescence (λ_{ex}, 365 nm and λ_{em}, 494 ± 10 nm). Scale Bars: 20 µm.

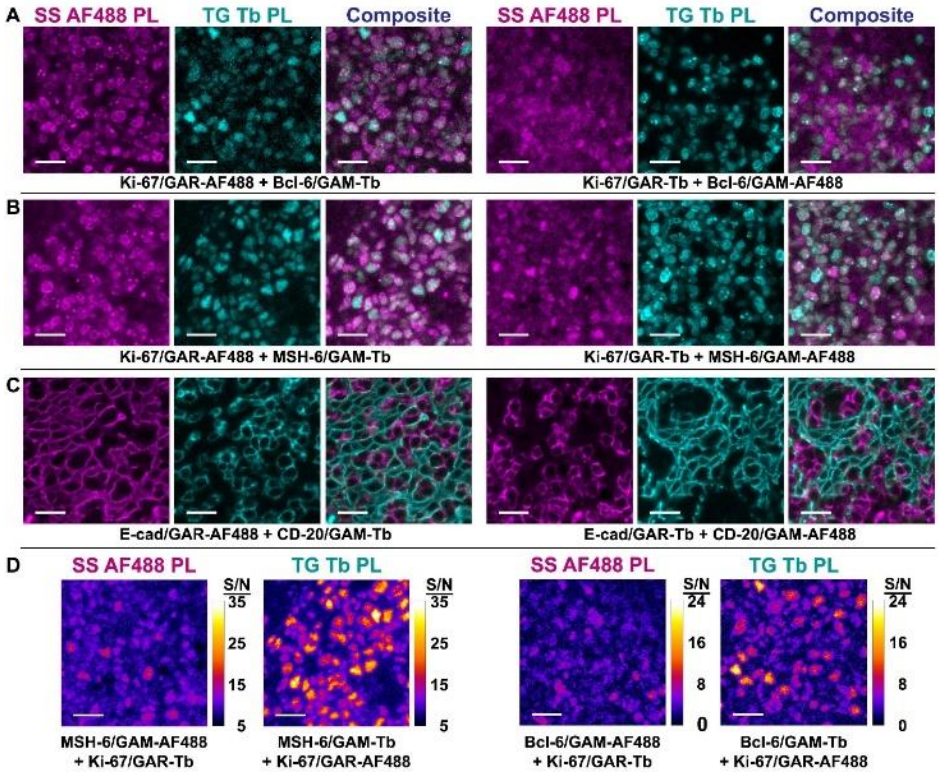

Figure 8. Time-gated detection eliminates non-specific fluorescence background, enhances signal-to-noise and separates unamplified Tb(III) luminescence from steady state fluorescence.

FFPE tonsil tissue slides were co-labeled with primary rabbit antibodies raised against Ki67 or E-cad and mouse antibodies raised against Bcl-6, MSH-6 or CD-20, then stained with goat, anti-rabbit (GAR) or goat, anti-mouse (GAM) secondary antibodies conjugated to Lumi4-Tb or AF488 as indicated. (A-C) Micrographs depict time-gated Tb(III) photoluminescence (TG Tb PL, cyan; delay, 10 μs; λ_{ex}, 365 nm; λ_{em}, 494 ± 10 nm), steady-state AF488 photoluminescence (SS AF PL, magenta; λ_{ex}, 480 ± 20 nm; λ_{em}, 520 ± 10 nm) or composite images of slides labeled with indicated antibody combinations. Complete time-gated imaging parameters are given in Table S1. Scale Bars: 20 μm. (D) Intensity modulated displays indicate signal-to-noise ratios (S/N) calculated from TG Tb PL and SS AF488 PL images of slides labeled with indicated antibody combinations. S/N maps were generated by subtracting the mean pixel gray values measured within image regions lacking specific signals, then dividing the background-subtracted images by the standard deviation of background gray values ($S/N = (S - \bar{B})/\sigma_B$). Reprinted with permission from Chen,T.; Hong, R.; Magda, D.; Bieniarz, C.; Morrison, L.; Miller, L. *Anal. Chem*. 89(23): 12713-12719, 2017. Copyright 2017 American Chemical Society.

The benefits of autofluorescence elimination can be seen by comparing TGLM images of Bcl-6 and MSH-6 to SS images of the same proteins (**Fig. 8 A-B**). Bcl-6 and MSH-6 are expressed at lower levels than Ki-67, as can be seen in diaminobenzidine (DAB) IHC images (**Fig. 9**). Whereas the SS AF488 PL signal of these relatively low-abundance markers is difficult to distinguish from background, TG Tb PL is more clearly visible in individual cells. The higher quality of TGLM images is emphasized in heat map representations of signal-to-noise ratio (S/N), calculated by dividing pixel gray value by the standard deviation of gray values measured in background regions of the respective images (**Fig. 8D**).

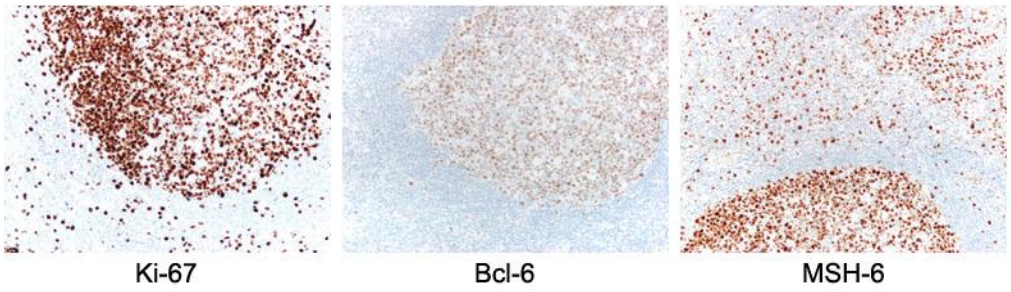

Figure 9. Ki-67 expressed at higher level than Bcl-6 or MSH-6. Brightfield images of FFPE tonsil tissue following diaminobenzidiene IHC.

2.3.3 TGLM with signal amplification

While unamplified Tb(III) signals are clearly visible above background (**Figs. 7 and 8**), signal strength, and therefore signal-to-noise ratio, is fundamentally limited by target abundance. Summation or averaging of many frames can be used to increase signal-to-noise ratio, but a strong signal is still needed for imaging rare targets. Therefore, we examined tyramide signal amplification (TSA) as a means of increasing overall Tb(III) signal strength.

TSA is an enzyme-catalyzed reporter deposition method that utilizes peroxidase-antibody conjugates and derivatized tyramine substrates, fluorophores coupled to tyramine in the present study, to covalently label targets with many copies of the tyramine derivatives [123] . TSA is particularly useful for multiplexing because individual primary/secondary antibody combinations can be applied and removed and peroxidase inactivated sequentially. We evaluated the feasibility of TSA for TGLM by labeling FFPE tonsil tissue specimens with primary antibodies against Ki-67, Bcl-6 or MSH-6. The specimens were subsequently labeled with complementary secondary antibodies conjugated to horseradish peroxidase (HRP) which catalyzed deposition of Lumi4-tyramide substrate. TSA labeling dramatically increased Tb(III) signal intensity levels and therefore S/N compared to un-amplified specimens. For example, 5-fold shorter exposure times were needed to acquire TGLM images of TSA-labeled Bcl-6 compared to unamplified Bcl-6 specimens, and S/N was substantially higher (**Fig. 10, Table 1**).

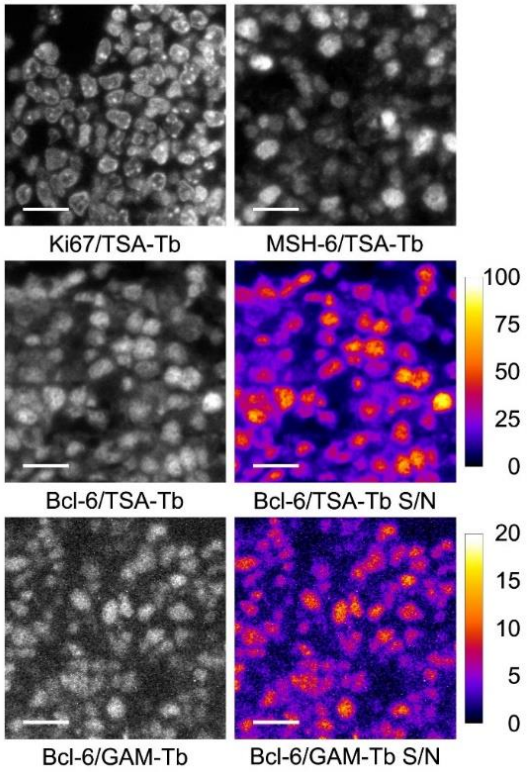

Figure 10. Tyramide signal amplification increases Tb(III) signal and S/N relative to indirect labeling with secondary antibodies.

Ki-67, MSH-6 or Bcl-6 on FFPE tonsil tissue was labeled with complementary secondary antibody conjugated to horseradish peroxidase (HRP) followed by catalyzed Lumi4-tyramide deposition (TSA-Tb) or else labeled with secondary antibody conjugated to Lumi4-Tb (GAM-Tb) as indicated. Acquisition times of 400 ms and 2 s were needed to obtain images of Bcl-6/TSA-Tb and Bcl-6/GAM-Tb, respectively (see Table S1 for imaging parameters). S/N of Bcl-6/TSA-Tb image was considerably greater than that of Bcl-6/GAM-Tb, as depicted in intensity modulated displays (right middle, right bottom). Scale Bars: 20 µm. Reprinted with permission from Chen,T.; Hong, R.; Magda, D.; Bieniarz, C.; Morrison, L.; Miller, L. *Anal. Chem.* 89(23): 12713-12719, 2017. Copyright 2017 American Chemical Society.

Image	λ_{em} (nm)	Excitation events	Frame length (ms)	Acquisition time (ms)[a]	Intensifier gain (V)
Fig. 8a, left	484-504	660	2000	8000	833
Fig. 8a, right	484-504	220	667	2700	833
Fig. 8b, left	484-504	440	1333	5332	833
Fig. 8b, right	484-504	220	667	2700	833
Fig. 8c, left	484-504	220	667	2700	833
Fig. 8c, right	484-504	440	1333	5332	833
Fig. 10, Ki-67	484-504	22	66.67	267	833
Fig. 10, MSH-6	484-504	33	99.99	400	833
Fig. 10, Bcl-6	484-504	33	99.99	400	833
Fig. 11a, middle	484-504	2	6	24	833
Fig. 11a, right	510-530	2	6	24	833
Fig. 11b, middle	484-504	4	12	48	833
Fig. 11b, right	700-720	4	12	48	833
Fig. 15a, Ki-67	484-504	22	66.67	267	833
Fig. 15a, E-cad	484-504	44	133	533	833
Fig. 15b, left	484-504	110	333	1333	833
Fig. 15b, right	484-504	110	333	1333	833
Fig. 7, Ki-67	484-504	110	333	1333	833
Fig. 7, E-cad	484-504	440	1333	5332	833
Fig. 7, CD 20	484-504	110	333	1333	833
Fig. 7, Bcl-6	484-504	660	2000	8000	833
Fig. 7, MSH-6	484-504	440	1333	5332	833
Fig. 7, Bcl-2	484-504	660	2000	8000	833
Fig. 12, 2nd	484-504	1	3	12	833
Fig. 12, 3rd	598-612	1	3	12	833

[a]Each image comprises four summed frames.

Table 1. Detection parameters for time-gated images of tissue sections

2.3.4 Time-gated FRET microscopy

FRET from a Tb(III) donor to an organic dye acceptor results in long-lifetime (~ms), sensitized dye emission that can be sensitively detected with time-gating methods. Moreover, the four major emission bands of Tb can sensitize differently colored fluorescent dyes, and this feature could be leveraged for multiplexing with single-wavelength excitation, as has been demonstrated in solution-phase immunoassays.[124]

We investigated the possibility of detecting intermolecular Tb(III)-to-dye FRET by using TSA to co-deposit Lumi4-Tb and one of three dyes (Fluorescein (FITC), sCy3, and Cy5) onto the same marker (Ki-67). Co-labeled tonsil tissue specimens were imaged in SS mode to detect dye fluorescence and in time-gated mode to detect long-lived Tb(III) donor luminescence and Tb(III)-sensitized dye emission. Unambiguous, long-lived photoluminescence signals at the acceptor dye emission wavelengths were observed for all Lumi4-Tb/dye pairs (Lumi4-Tb/FITC and Lumi4-Tb/Cy5, **Fig. 11**, and Lumi4-Tb/sCy3, **Fig. 12**).

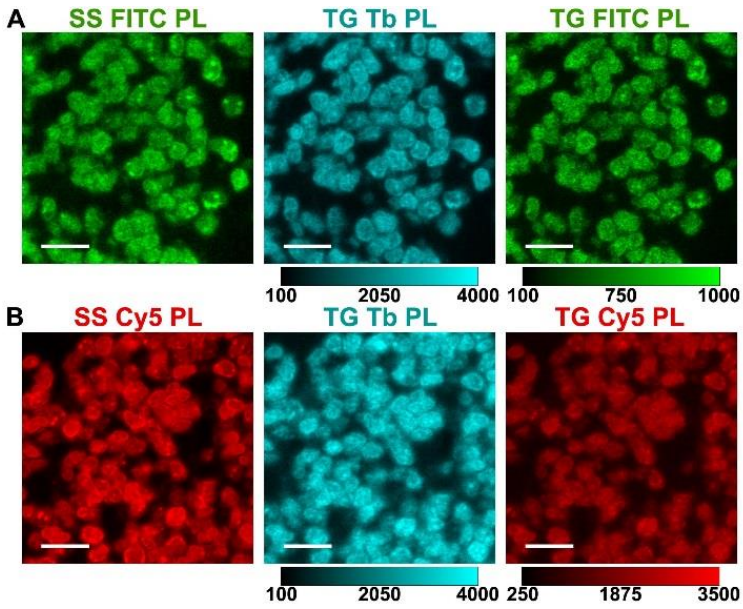

Figure 11. Tyramide Signal amplification (TSA) permitted visualization of intermolecular Tb(III)-to-dye FRET.

Ki-67 on human tonsil tissue was detected by co-depositing Lumi4Tb-tyramide as donor and Fluorescein-tyramide (A) or Cy5-tyramide (B) as acceptors. Micrographs depict steady-state (SS) dye, time-gated Tb(III), or time-gated Tb(III)-to-dye (FRET) photoluminescence as indicated: TG Tb PL, delay 10 µs, λ_{ex} 365 nm; λ_{em} 494±10 nm; SS FITC PL, λ_{ex} 480 ± 20 nm, λ_{em} 520 ± 10 nm; TG FITC PL, delay 10 µs, λ_{ex} 365 nm, λ_{em} 520±10 nm; SS Cy5 PL, λ_{ex} 655 ± 20 nm, λ_{em} 710 ± 20 nm; TG Cy5 PL, delay 10 µs, λ_{ex} 365 nm, λ_{em} 710 ± 20 nm. Scale Bars: 20 µm. Calibration bars depict ranges of grayscale values shown in corresponding 12-bit images. Reprinted with permission from Chen,T.; Hong, R.; Magda, D.; Bieniarz, C.; Morrison, L.; Miller, L. *Anal. Chem.* 89(23): 12713-12719, 2017. Copyright 2017 American Chemical Society.

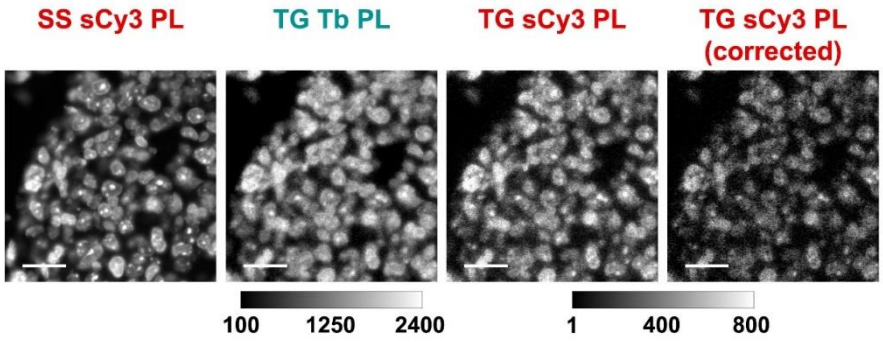

Figure 12. Tyramide Signal amplification (TSA) permitted visualization of intermolecular Tb(III)-to-dye FRET.

Ki-67 on human tonsil tissue was detected by co-depositing Lumi4Tb-tyramide as donor and sCy3-tyramide as acceptor. Micrographs depict steady-state (SS) dye, time-gated Tb(III), or time-gated Tb(III)-to-dye (FRET) photoluminescence as indicated: TG Tb PL, delay 10 µs, λ_{ex} 365 nm; λ_{em} 494±10 nm; SS sCy3 PL, λ_{ex} 545 ± 20 nm, λ_{em} 605 ± 7 nm; TG sCy3 PL, delay 10 µs, λ_{ex} 365 nm, λ_{em} 605 ± 7 nm. Scale Bars: 20 µm. Calibration bars depict ranges of grayscale values shown in corresponding 12-bit images.

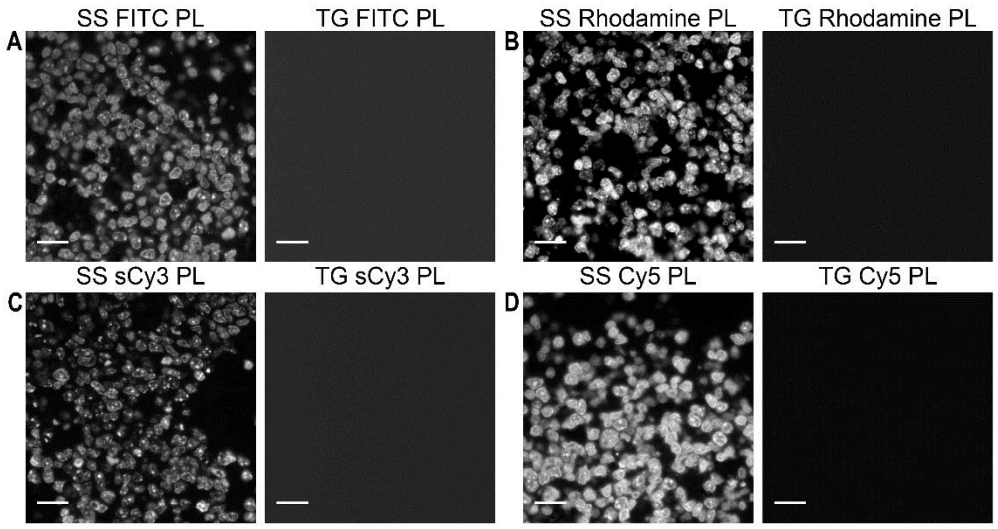

Figure 13. Time-gating eliminates organic dye emission signals.

Ki-67 on human tonsil tissue was labeled with various organic dyes as indicated using tyramide signal amplification. A delay of 10 µs was inserted between pulsed 365 nm excitation and detection for all time-gated (TG) images. Steady-state (SS) images were acquired using the following combinations of excitation and emission wavelengths (A) FITC, λ_{ex}, 480 ± 20 nm; λ_{em}, 520 ± 10 nm; (B) Rhodamine, λ_{ex}, 545 ± 15 nm; λ_{em}, 605 ± 7 nm; (C) sCy3, λ_{ex}, 545 ± 15 nm; λ_{em}, 605 ± 7 nm; (D) Cy5, λ_{ex}, 655 ± 20 nm; λ_{em}, 710 ± 20 nm. Scale Bars: 20 µm.

No long-lifetime signals were observed in specimens labeled only with dye (**Fig. 13**). We imaged control samples labeled only with Lumi4-Tb, and observed that bleedthrough of Tb(III) luminescence into the FITC or Cy5 channels was negligible (<3 %, **Fig. 14**), while bleedthrough of Tb(III) luminescence into the sCy3 emission channel (605 ± 7 nm) was equivalent to about 12% of the intensity seen in the Tb(III) channel (494 ± 10 nm, **Fig. 14**). After subtracting the bleedthrough component, we still observed high levels of intensity in the Tb(III)-to-sCy3 channel indicative of FRET (**Fig. 12**). Tb(III)-to-dye FRET could potentially enhance multiplexing by enabling the use of the same dye to label two different markers on the same specimen. For example, one marker could be stained with FITC for SS imaging and

another marker that is not co-localized with the first could be co-labeled with Tb(III) and FITC for visualization by TGLM.

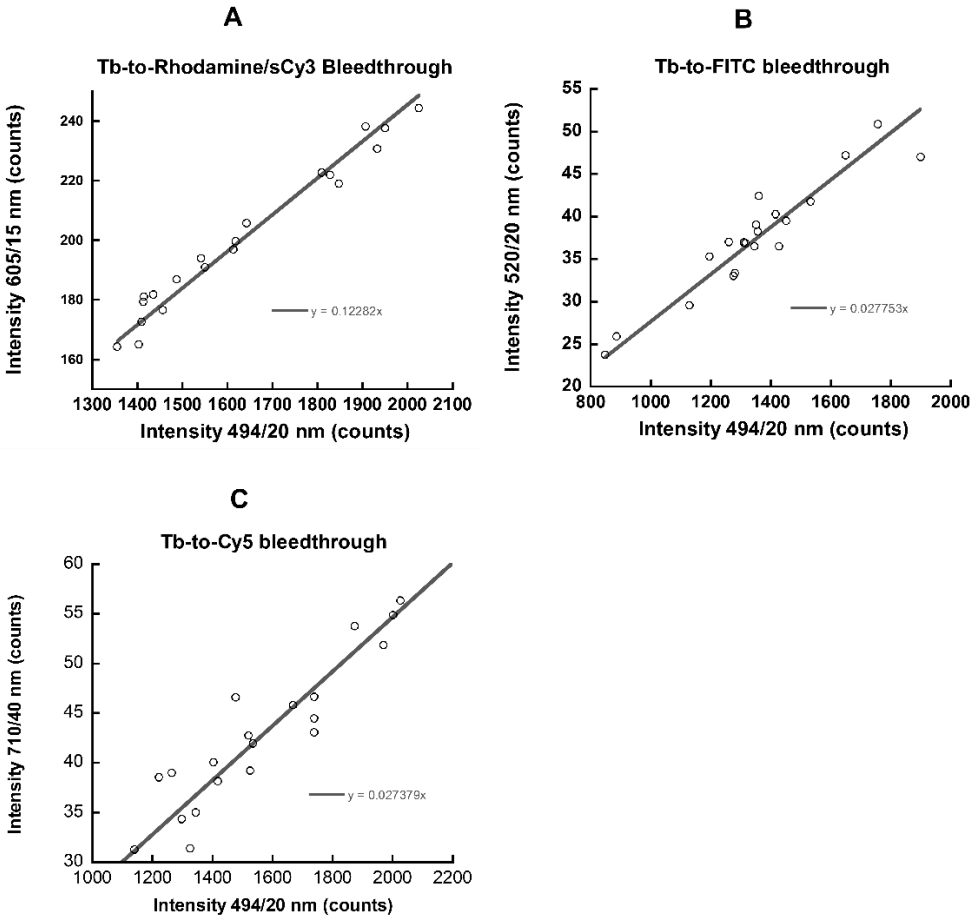

Figure 14. Bleed-through of Tb(III) signal into the sCy3, FITC, and Cy5 channels.

Plots of time-gated signal intensities in dye channel (y-axis, indicated emission wavelengths) vs. in Tb(III) channel (x-axis) prepared from TGLM images of Lumi4-Tb-labeled Ki-67 on FFPE tonsil tissue sections. Lines are linear fits to data with y-intercepts forced to 0. The slope of the sCy3 plot (A) is the bleed-through correction factor applied to the Tb(III)-to-dye FRET image in Figure S4. Slopes of FITC (B) and Cy5 (C) plots were less than 0.03, and bleed-through into these channels was considered to be negligible.

2.3.5 Compatibility with Hematoxylin and Eosin (HE) staining

Hematoxylin and eosin (H&E) staining is commonly used to distinguish cell components and morphological changes within tissues and is an essential component of contemporary cancer diagnosis. In addition, hematoxylin alone is also commonly used as a nuclear counterstain in IHC. However, due to overwhelmingly strong fluorescent emission for eosin or quenching of specific fluorescence by hematoxylin, these stains are usually incompatible with conventional IF. Here, we sought to determine whether H&E staining might be compatible with TGLM of Lumi4-Tb-labeled tissues. We first examined the impact of hematoxylin counterstain alone on both SS fluorescence microscopy and TGLM. Counterstained tissue specimens yielded robust, time-gated Tb(III) signals specific to E-cad or Ki-67. Corresponding brightfield images showed good nuclear hematoxylin staining which could be transformed to a darkfield representation and combined with the time gated Tb images to form color composite images (**Fig. 15A**). However, while membrane-localized E-cad was visible in SS PL images of FITC-labeled specimens, the nuclear marker Ki-67 could not be detected. In addition, no marker-specific fluorescence could be observed on rhodamine-labeled specimens that were counterstained with hematoxylin (not shown).

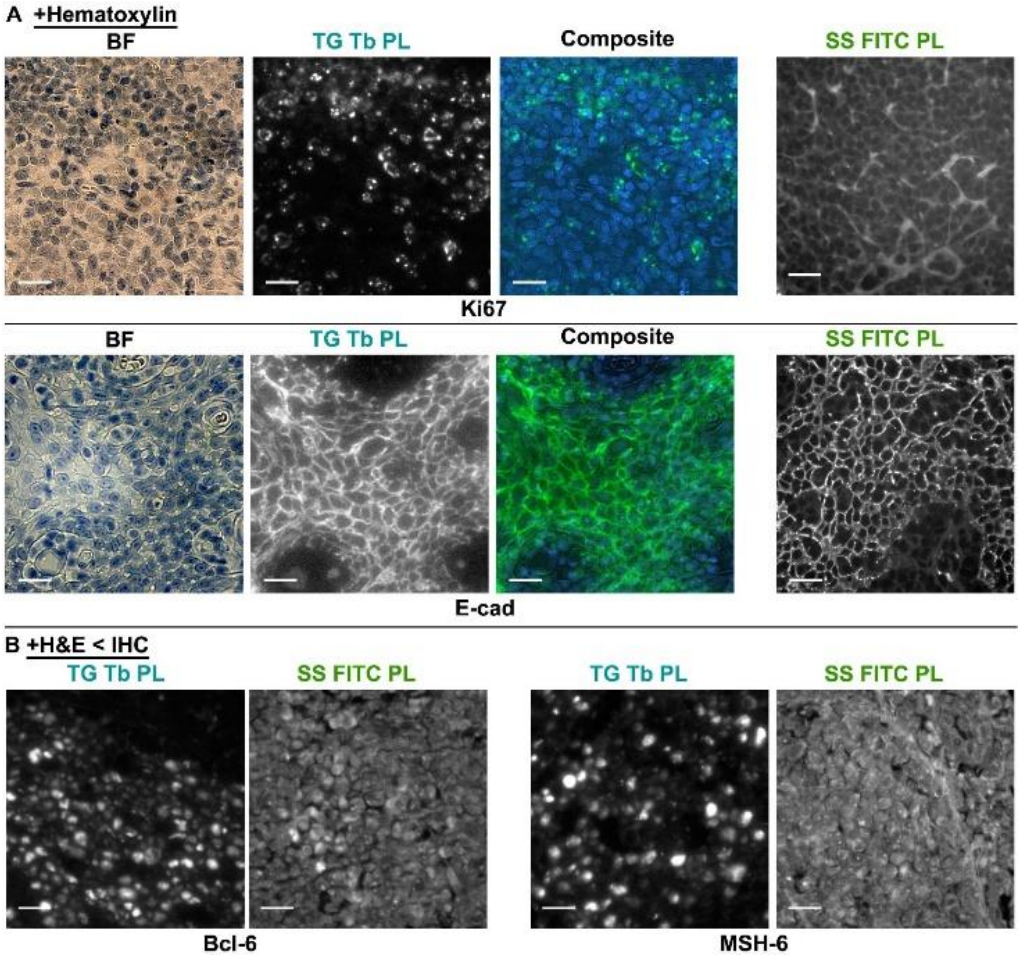

Figure 15. Lumi4-Tb labeling and TGLM are compatible with select hematoxylin and eosin staining protocols.

(A) FFPE tonsil tissue were stained with hematoxylin, labeled with primary antibodies against Ki-67 or E-cad and stained with Lumi4-Tb or FITC using tyramide signal amplification. Brightfield images were log-transformed into a pseudo-darkfield presentation and combined with TG Tb PL images. B. Tonsil tissue was stained with H&E prior to antigen retrieval, primary antibody labeling (Bcl-6 or MSH-6) and TSA-mediated deposition of Lumi4-Tb or FITC. Robust, specific Tb(III) signals were observed in time-gated images while SS FITC signals could not be detected above background. Micrographs: time-gated Tb(III) photoluminescence (TG Tb PL; delay, 10 μs; λ_{ex}, 365 nm; λ_{em}, 494 ± 10 nm), steady-state FITC photoluminescence (SS FITC PL,; λ_{ex}, 480 ± 20 nm; λ_{em}, 520 ± 10 nm) Scale Bars: 20 μm. Reprinted with permission from Chen,T.; Hong, R.; Magda, D.; Bieniarz, C.; Morrison, L.; Miller, L. *Anal. Chem.* 89(23): 12713-12719, 2017. Copyright 2017 American Chemical Society.

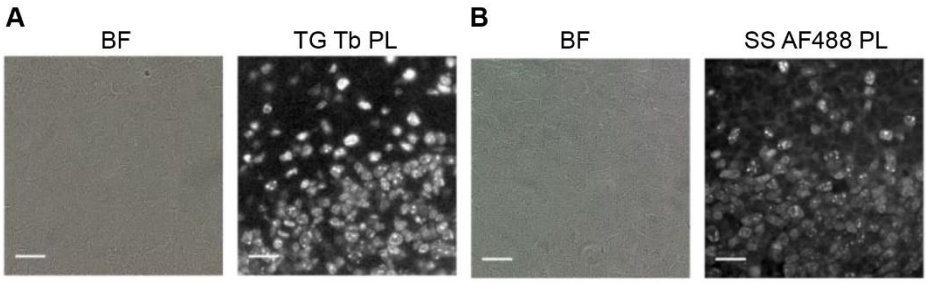

Figure 16. IHC including antigen retrieval removes H&E staining contrast but permits TSA-mediated labeling of Ki-67 and visualization in time-gated or steady-state mode.

Ki-67 on tonsil tissue labeled with either Lumi4-Tb (A) or AF488 (B) via TSA was imaged in time-gated or steady-state mode. Micrographs: BF, bright field; TG Tb PL, delay 10 µs, λ_{ex} 365 nm; λ_{em} 494±10 nm; SS AF488 PL, λ_{ex} 480 ± 20 nm, λ_{em} 520 ± 10 nm. Scale Bars: 20 µm.

Since a large number of archived clinical tissue specimens have been stained with H&E (the primary stain for cancer diagnosis), we examined whether these specimens could be further stained for particular biomarkers and visualized using either SS fluorescence or time-gated luminescence detection. To this end, we performed H&E staining prior to a standard IHC staining procedure that included antigen retrieval, primary antibody binding (Ki67, Bcl-6 or MSH-6) and subsequent TSA labeling with either Lumi4-Tb, FITC or AF488. Following this protocol, we observed strong, time-gated Tb(III) luminescence signals with all markers (**Fig. 15B**). Specific SS AF488 fluorescence could be observed on Ki-67-labeled specimens (**Fig. 16**), but the less abundant markers Bcl-6 and MSH-6 could not be detected above the autofluorescence background level following labeling with FITC (**Fig. 15B**). The IHC staining procedure appears to remove detectable H&E stain as evidenced by contrast-free brightfield images (**Fig. 16**). However, the residual eosin still generated enough background fluorescence to interfere with specific SS signal. These results suggest TGLM using Tb(III) labels can provide a

reliable method to perform IF on archived or other tissue specimens that are first subjected to H&E staining.

2.4 Conclusions

For extracellular IF imaging, we have demonstrated that Tb-to-QD FRET can be used for extracellular recognition of the membrane receptor EGFR by Tb- and QD-antibody conjugates that recognize different epitopes of EGFR. The application of commercial therapeutic antibodies (cetuximab and matuzumab) and single-domain V_HH antibodies (nanobodies) for successful EGFR FRET detection on live A431 cells showed the wide applicability of the Tb-to-QD FRET pair for immunostaining-based fluorescence imaging. The large versatility of single and multistep intra- and extracellular FRET, combined with the previously shown possibility of high-order multiplexing with Tb-to-QD–based FRET systems, will make Tb-to-QD FRET a very powerful tool for widely applicable intra- and extracellular fluorescence imaging and sensing.

For IFM on FFPE tissues, we directly compared TGLM with SS fluorescence microscopy by imaging FFPE tissue sections that had been labeled with either organic dyes or a luminescent Tb(III) complex, Lumi4-Tb. We found that TGLM delivered higher S/N, particularly when visualizing less abundant markers like MSH-6 or Bcl-6. Sensitivity was further enhanced by enzymatic amplified deposition of a Lumi4-tyramide derivative. Moreover, we found that Lumi4-Tb-labeled markers could be imaged in the presence of hematoxylin or on specimens that had been previously stained with H&E prior to IHC. In addition, we demonstrated the multiplexing potential of lanthanide-based TGLM by co-imaging Lumi4-Tb and organic dyes and by detecting intermolecular Tb(III)-to-dye FRET signals. All of these features could be utilized to access valuable information on multi-protein expression patterns and potentially on protein-protein interactions via intermolecular FRET. Moreover, our methods are

easy to adopt because they use conventional immunolabeling protocols and standard microscopes with commercially available modifications.

CHAPTER 3

HIGH DYNAMIC RANGE LANTHANIDE-BASED FRET BIOSENSORS FOR TIME-GATED LUMINESCENCE IMAGING AND HIGH THROUGHPUT SCREENING OF PPIS

3.1 Introduction

Most biological processes are mediated by proteins interacting transiently with one another in pairs or in multi-component complexes, and protein–protein interactions (PPIs) have come to represent an increasingly important class of therapeutic targets.[64, 91, 125] However, identification of drugs or leads that can inhibit PPIs is challenging due to the large area and flatness of the interfaces, a relative lack of small-molecule scaffolds from which to develop libraries, and the difficulty of characterizing interaction stoichiometry and sites of binding.[91, 126] Nevertheless, successful drugs have been developed that demonstrate the feasibility of targeting PPIs. These include agents targeting HPV E2/E1,[66, 127] BCL-X_L/BAD,[128] and HDM2/p53[129] interactions at doses as low as 1nM. High throughput screening (HTS) has been an important tool in identifying these agents, but the screening efforts have relied largely on cell-free systems that require protein purification. Apart from the impossibility of obtaining many proteins in pure form, *in vitro* assays necessarily occur in artificial contexts that do not account for factors such as subcellular localization of PPIs, competitive interaction with other cellular components and post-translational modifications[103]. Moreover, cell-free HTS systems do not discriminate against cytotoxic or membrane-impermeable compounds.[89, 130, 131] Thus, there is a need for high-throughput methods to discover PPI inhibitors that are performed directly within living mammalian cells.[132]

A limited number of methods for studying PPIs directly within living cells have been developed that can be adapted to at least a medium-throughput rate of analysis. These include methods based on sub-cellular redistribution of fluorescently labeled proteins (suitable for high-content imagers),[103, 133] reporter fragment complementation assays (e.g., split GFP, luciferase),[134] reporter gene hybrid-like systems,[60, 135] and methods based on Förster resonance energy transfer

(FRET) or bioluminescence resonance energy transfer (BRET).[13, 136] However, all of these available cell-based PPI assays suffer from one or more limitations, including low signal-to-background ratio (SBR), high rates of false positives/negatives, and protein sequestration at non-physiologic sites.

In this chapter, I present the development and characterization of Tb(III)-based FRET biosensors with high dynamic range to study PPIs and their inhibition in living cells by time-gated luminescence (TGL) microscopy or medium-to-high throughput TGL analysis in 96-well and 384-well plates. Our single-chain biosensor design leveraged the unique photophysical properties Tb(III) complexes that include a narrow-width, multi-line emission spectrum and excited state lifetimes greater than 1 ms. We characterized sensor performance using two model systems: 1) the well-studied, rapamycin-induced interaction between FK binding protein 12 (FKBP12) and the rapamycin binding domain of m-Tor (FRB);[137] and 2) the therapeutically relevant interaction between p53 and HDM2. The biosensors incorporated a rigid alpha-helical linker sequence comprised of multiple repeats of four glutamic acid or arginine residues alternated with four lysine residues (ER/K) flanked by EGFP and *Escherichia coli* dihydrofolate reductase (eDHFR). The affinity binding elements were positioned at the N- and C-termini of the sensors (Figure 1). The eDHFR domain binds with high specificity and affinity (K_D, ~1 nM) to heterodimers of trimethoprim linked to a luminescent Tb(III) complex,[138] permitting selective labeling of the sensor construct. TGL detection of Tb(III) luminescence or Tb(III)-to-GFP FRET allowed for sensitive imaging and detection of biosensor activity. Remarkable sensor dynamic ranges of over 500% and over 2500% were observed for rapamycin-induced activation of FKBP12/FRB interaction in live cell microscopic images and in 96-well plates, respectively. Statistically robust, high throughput detection of FKBP12/FRB interaction or inhibition and

p53/HDM2 inhibition was observed in 384-well plates. The high performance seen here with model systems and a modular sensor design show that Tb(III)-based, single-chain FRET biosensors can be applied to analyze a wide variety of PPIs in virtually any cell type.

3.2 Materials and Methods

3.2.1 Materials

Dulbecco's modified eagle medium with 1g/L glucose (DMEM,10-014CV), Dulbecco's modified eagle medium with 4.5g/L glucose (DMEM,10-013CV), Dulbecco's phosphate buffer saline (DPBS, 21-030 and 21-031), 0.25% trypsin/2.21 mM EDTA and 0.05% trypsin/2.21 mM EDTA (Corning, 25-053-Cl) were purchased from Corning cellgro ® . MEM non-essential amino acid (11140), DMEM (without phenol red, 21063), HEPES (15630-080) and Lipofectamine 2000 (11668-027) were purchased from Invitrogen^{TM}. FBS (S11150) was purchased from Atlanta Biologicals. Hygromycin (sc-29067) and Nutlin-3 (sc45061) were purchased from Santa Cruz Biotechnology. BSA (700-107P) was purchase from Gemini Bio-products. Rapamycin (553211-500UG) was purchased from Millipore. Ascomycin (11309) was purchase from Cayman Chemical. NADPH (N0411) and doxycycline (D9891) were purchased from Sigma. DMSO (D128-500) was purchased from Fisher Chemical. Patent V blue sodium salt (21605) was purchased from Fluka. Clotech In-fusion cloning kit (638909) was purchased from Takara. All enzymes and buffers used in cloning were purchased from New England biolabs. TMP-cs124-TTHA-Tb^{3+} was synthesized by Ali Mohamadi. TMP-Lumi4Tb^{3+} and Lumi4-cysTEGTMP-CR9 were provided by Lumiphore, Inc.

3.2.2 Plasmids

All following constructs were sequenced at UIC Research Resources Center (RRC).

pCMV-FKBP12-EGFP and pTREtight-FRB-eDHFR. The gene encoding (CMV Promoter)-EGFP-FKBP-(bGH Poly(A) Signal Sequence) was subcloned from plasmid pEGFP-FKBP12 to pPBH-TREtight-FRB-eDHFR to generate pPBH-TREtight-FRB-eDHFR/GFP-FKBP12. A 1850 bp fragment encoding (CMV Promoter)-EGFP-FKBP12-(bGH Poly (A) Signal Sequence) was amplified by PCR from pEGFP-FKBP12 using the primers 5' – GCC CGT CCC ACC AGG TGA GTT CCG CGT TAC ATA ACT TAC G – 3' (SexAI, coding strand) and 5' – CGC CTG TTG ACC TGG TCG CGT TAA GAT ACA TTG ATG AG – 3' (SexAI, non-coding strand). This fragment was inserted at the SexAI site in pPBH-TREtight-FRB-eDHFR with In-Fusion® Cloning Kit to give to pPBH-TREtight-FRB-eDHFR/GFP-FKBP12.

pPBH-TREtight-FRB-eDHFR-$(ER/K)_{10nm}$-EGFP-FKBP12. The FRB-eDHFR-$(ER/K)_{10nm}$-EGFP-FKBP12 was prepared by GenScript by synthesizing the open reading frame FRB-eDHFR-$(ER/K)_{10nm}$ -EGFP-FKBP12 with $(ER/K)_{10nm}$ linker with the sequence of 5' – GAA GAG GAA GAG AAA AAA AAA CAG CAG GAA GAG GAA GCA GAA AGG CTG AGG CGT ATT CAA GAA GAA ATG GAA AAG GAA AGA AAA AGA CGT GAA GAA GAC GAA AAA CGT CGA AGA AAG GAA GAG GAG GAA AGG CGG ATG AAA CTT GAG ATG GAA GCA AAG AGA AAA CAA GAA GAA GAA GAG AGA AAG AAA AGG GAA GAT GAT GAA AAA CGC AAG AAG AAG. The synthesized fragment was inserted into pPBH-TREtight vector between KpnI site and NheI site to give pPBH-TREtight-FRB-eDHFR-$(ER/K)_{10nm}$ -EGFP-FKBP12.

pPBH-TREtight-FRB-eDHFR-$(ER/K)_{30nm}$-EGFP-FKBP12. The 630 bp $(ER/K)_{30nm}$ linker fragment was prepared and cloned into pUC57 vector by GenScript . The genes encoding FRB-eDHFR, $(ER/K)_{30nm}$, EGFP-FKBP12 were subcloned from plasmids pPBH-TREtight-FRB-eDHFR-$(ER/K)_{30nm}$-EGFP-FKBP12 and $(ER/K)_{30nm}$ in pUC57 to pPBH-TREtight to generate

pPBH-TREtight-FRB-eDHFR-$(ER/K)_{30nm}$ -EGFP-FKBP12. A 753 bp fragment encoding FRB-eDHFR was prepared by PCR from pPBH-TREtight-FRB-eDHFR-$(ER/K)_{10nm}$ -EGFP-FKBP12 using the primers 5'-ACT CTG CAG TCG ACG GTA CCA TGA TCC TCT GGC ATG AGA TGT GGC -3' (coding strand) and 5'-TCG GAT CCT CCG CTT CCC CGC CG -3' (non-coding strand). A 630 bp fragment encoding $(ER/K)_{30nm}$ was prepared by PCR from $(ER/K)_{30nm}$ in pUC57 using the primers 5'-AAG CGG AGG ATC CGA AGA GGA GGA GAA AAA GAA GGA -3' (coding strand) and 5'-CCA GAG CCA CCG GTT CTC TGT TTT CGC TCT GC -3' (non-coding strand). A 1041 bp fragment encoding EGFP-FKBP12 was prepared by PCR from pPBH-TREtight-FRB-eDHFR-$(ER/K)_{10nm}$-EGFP-FKBP12 using the primers 5'-AAC CGG TGG CTC TGG CAT GGT GAG CA -3' (coding strand) and 5'-ATG CGG CCG CGC TAG-3' (non-coding strand). These 3 fragments were inserted between the KpnI site and the NheI site in pPBH-TREtight by Clontech In-Fusion® Cloning Kit to get pPBH-TREtight-FRB-eDHFR-$(ER/K)_{30nm}$-EGFP-FKBP12.

pPBH-TREtight-FRB-eDHFR-$(ER/K)_{20nm}$-EGFP-FKBP12. The $(ER/K)_{20nm}$ linker is the first 396 bp of $(ER/K)_{30nm}$ linker. The genes encoding FRB-eDHFR, $(ER/K)_{20nm}$, EGFP-FKBP12 were subcloned from plasmids pPBH-TREtight-FRB-eDHFR-$(ER/K)_{10nm}$-EGFP-FKBP12 and $(ER/K)_{30nm}$ in pUC57 to pPBH-TREtight to generate pPBH-TREtight-FRB-eDHFR-$(ER/K)_{20nm}$-EGFP-FKBP12. A 753 bp fragment encoding FRB-eDHFR was prepared by PCR from pPBH-TREtight-FRB-eDHFR-$(ER/K)_{10nm}$ -EGFP-FKBP12 using the primers 5'-ACT CTG CAG TCG ACG GTA CCA TGA TCC TCT GGC ATG AGA TGT GGC -3' (coding strand) and 5'-TCG GAT CCT CCG CTT CCC CGC CG -3' (non-coding strand). A 396 bp fragment encoding $(ER/K)_{20nm}$ was prepared by PCR from $(ER/K)_{30nm}$ in pUC57 using the primers 5'-AAG CGG AGG ATC CGA AGA GGA GGA GAA AAA GAA GGA -3' (coding strand) and 5'-CCA

GAG CCA CCG GTC TCT TCC TTG GCC TTT TTC TCC TGC -3’ (non-coding strand). A 1041 bp fragment encoding EGFP-FKBP12 was prepared by PCR from pPBH-TREtight-FRB-eDHFR-$(ER/K)_{10nm}$ -EGFP-FKBP12 using the primers 5’-GAA GAG ACC GGT GGC TCT GGC ATG GTG AGC A -3’ (coding strand) and 5’-ATG CGG CCG CGC TAG-3’ (non-coding strand). These 3 fragments were inserted between the KpnI site and the NheI site in pPBH-TREtight by Clontech In-Fusion® Cloning Kit to get pPBH-TREtight-FRB-eDHFR-$(ER/K)_{20nm}$ -EGFP-FKBP12.

pPBH-TREtight-p53 (1-92 a.a.)-eDHFR-$(ER/K)_n$-EGFP-HDM2 (1-128 a.a.). The genes encoding p53(1-92 a.a.), eDHFR-(ER/K)n-EGFP(n=10 nm, 20nm or 30 nm), and HDM2 (1-128 a.a.) were subcloned from plasmids p53-GFP, pPBH-TREtight-FRB-eDHFR-(ER/K)n-EGFP-FKBP12 (n=10 nm, 20nm or 30 nm) and pCMV-HDM2(C464A) to pPBH-TREtight to generate pPBH-TREtight-p53 (1-92 a.a.)-eDHFR-(ER/K)n-EGFP-HDM2(1-128 a.a.). A 276 bp fragment encoding p53 (1-92 a.a.) was prepared by PCR from p53-GFP using the primers 5’-ACT CTG CAG TCG ACG GTA CCA TGG AGG AGC CGC AGT CA -3’ (coding strand) and 5’-CCA GAT CCG GGC CAG GAG GGG G -3’ (non-coding strand). A 1446 bp, 1620 bp, or 1845 bp fragments encoding eDHFR-(ER/K)n-EGFP (n=10 nm, 20nm or 30 nm) respectively were prepared by PCR from pPBH-TREtight-FRB-eDHFR-(ER/K)n-EGFP-FKBP12 (n=10 nm, 20nm or 30 nm) using the primers 5’-CTG GCC CGG ATC TGG AGG ATC TGG AAT CAG TC -3’ (coding strand) and 5’-TTG CAC ATT CGA GAT CTG AGT CCG GAC TTG TA -3’ (non-coding strand). A 384 bp fragment encoding HDM2(1-128 a.a.) was prepared by PCR from pCMV-HDM2(C464A) using the primers 5’-ATC TCG AAT GTG CAA TAC CAA CAT GTC TGT ACC -3’ (coding strand) and 5’-ATG CGG CCG CGC TAG CCT ATT CAA GGT GAC ACC TGT TCT CAC TC -3’ (non-coding strand). These 3 fragments were inserted between the

KpnI site and the NheI site in pPBH-TREtight by Clontech In-Fusion® Cloning Kit to get pPBH-TREtight-p53 (1-92 a.a.)-eDHFR-(ER/K)n-EGFP-HDM2(1-128 a.a.) (n=10 nm, 20nm or 30 nm)

3.2.3 Stable expression of biosensor plasmids

All FRB/FKBP12 biosensor plasmids were transfected to NIH 3T3 cells, while all p53/HDM2 biosensors were transfected to Hela cells.

Cells were grown to 70-80% confluency in a sterile 10 cm dish. The cells were transfected with 12 μg of biosensor plasmids and their recombination helper plasmid pSPB-Transposase with a Lipofectamine:plasmid ratio of 2.5μg:1μg per plasmid. Plasmid and Lipofectamine solutions were first prepared in separate microcentrifuge tubes in OptiMEM I with a total volume of 1.5 mL. After 5 minutes of incubation at room temperature, the solutions were mixed and kept at room temperature for an additional 20 minutes. The media in 10 cm dish was aspirated and the Lipofectamine + plasmids solution was added into it. The cells were incubated with the solution for 4 hours in tissue culture incubator at 37 ^{o}C with 5% CO_2 and then the solution was replaced with 10 mL of fresh DMEM(+) (DMEM supplied with 15 mM HEPES, 10% FBS and 100 mg/mL Hygromycin). The transfections were confirmed with microscopy and/or flow cytometry by using the GFP emissions.

3.2.4 Probe delivery for TGLM

Cells were trypsinized and seeded at 20,000 cells/well in an 8-well chambered coverglass (Nunc™, 12-565-470) with fresh DMEM (+) containing 100 ng/mL Doxycycline to induce the expression of proteins and incubated at 37 °C and 5% CO_2 overnight. For FRB/FKBP12 stable transfected cell lines, on the following day the cells were washed twice with DPBS (+Ca/+Mg), 100 μL of TMP-Lumi4-R9 (12 μM in DMEM without phenol red) was

added, and the cells were incubated for 15 min at room temperature. Cells were washed again with DPBS (+Ca/+Mg) and 150 μL of Rapamycin (1 μM in DMEM without phenol red) was added to the sample well(control well had 1μM DMSO in DMEM without phenol red), and the cells were incubated for 15 min at 37 °C and 5% CO_2 incubator. Before microscope imaging, 20μL of 10 mM patent blue V solution (final concentration: 1 mM) were added to quench extracellular luminescence from non-specifically adsorbed probe. To obtain the time-lapse images of FRB/FKBP12 interaction induced by rapamycin, 50 μM rapamycin was added (final concentration: 2 μM) to sample well containing patent blue V solution after incubation with probe solution, steady-state GFP fluorescence, time-gated luminescence of Tb and Tb-to-GFP FRET were then acquired by TGLM.

For p53/HDM2 biosensor stable transfected cell lines, on the following day after seeding, the cells were incubated with Nutlin-3 or DMSO (10 μM in DMEM without FBS) for 90 min at 37 °C and 5% CO2 incubator. Then, cells were washed twice with DPBS (+Ca/+Mg), 100 μL of TMP-Lumi4-R9 (12 μM in DMEM without phenol red) was added, and the cells were incubated for 20 min at room temperature. Cells were washed again with DPBS (+Ca/+Mg) and 150 μL of patent blue V solution (1 μM in DMEM without phenol red, containing 10 μM Nutlin-3) was added to the sample well (control well had 10 μM DMSO) for microscope imaging. To obtain the time-lapse images of p53/HDM2 interaction inhibited by Nutlin-3, 516 μM Nutlin-3 was added (final concentration: 20 μM) to sample well containing patent blue V solution after incubation with probe solution. Steady-state GFP fluorescence, time-gated luminescence of Tb and Tb-to-GFP FRET were then acquired by TGLM.

3.2.5 Time-gated Luminescence Microscopy and image processing

TGLM and steady state microscopy were performed as described in Chapter 2.

Raw, 12-bit images were imported into NIH ImageJ (v1.42q) for all processing operations including cropping, contrast adjustment, and quantitative analysis[119]. For each channel, 20 dark frames and 20 bright field images were stacked, converted to 32 bits, and median-filtered (radius 1), and each stack was averaged. The flat-field average was divided by the mean intensity of its central nine pixels to generate a normalized flat-field image. For each sample image, a median filter (radius 1) was applied and the master dark frame was subtracted. The resulting image was then divided by the normalized, master flat-field image, and the mean value of the detector offset was added back to the image. For ratiometric images and measurements, a binary mask was created by first averaging a series of GFP images and then applying a threshold to highlight only regions exhibiting signal. The mask was applied to background-subtracted time-gated FRET images, and the FRET images were then divided by the GFP or Tb image. Intensity-modulated ratiometric displays were generated using the Fire lookup table in ImageJ and a color lookup table was applied.

3.2.6 Multi-well plate assays

3.2.6.1 Rapamycin stimulation assay with permeabilized mammalian cells

pPBH-TRE$_{tight}$-FRB-eDHFR-(ER/K)$_n$ -EGFP-FKBP12 (n=10nm, 20nm or 30 nm) stable transfected cells were seeded at a density of 1.6×10^5 cells/mL in a multi-well plate and incubated (37 ^oC, 5% CO_2) for 24 h in culture medium (250 µL for 96-well plate, 50 µL for 384-well plate) containing 100 ng/mL doxycycline. The following day, for the titration assay, growth media in the wells were discarded carefully and 50 µL lysis buffer (50 nM TMP-Lumi4Tb^{3+}, 5 µM NADPH, 0.1% BSA, 0.1% Triton X-100 and rapamycin with the range of 5 µM – 0.47 nM in DPBS solution) was added into the wells; for the stimulation assay, growth media in the wells

were discarded carefully and lysis buffer (50 μL for 96-well plate, 30 μL for 384-well plate containing 25 nM TMP-cs124-TTHA-Tb^{3+}, 5 μM NADPH, 0.1% BSA, 0.1% Triton X-100 and 1 μM rapamycin in DPBS solution) was added into the wells. Then the plate was kept at room temperature in dark for 15 minutes and the first measurement was taken afterwards. Negative control wells contained no cells, but only the same lysis buffer as sample wells.

3.2.6.2 <u>Ascomycin inhibition assay with permeabilized mammalian cells</u>

pPBH-TRE_{tight}-FRB-eDHFR-$(ER/K)_n$-EGFP-FKBP12 (n=10nm, 20nm or 30 nm) stable transfected cells were seeded at a density of 1.6×10^5 cells/mL in a multi-well plate and incubated (37 ^oC, 5% CO_2) for 24 h in culture medium (250 μL for 96-well plate, 50 μL for 384-well plate) containing 100 ng/mL doxycycline. The following day, for the titration assay, growth media in the wells were discarded carefully and 50 uL of lysis buffer (50 nM TMP-cs124-TTHA-Tb^{3+}, 5 μM NADPH, 0.1% BSA, 0.1% Triton X-100, 0.333 μM rapamycin and ascomycin with 2-fold serial dilution in the range of 40 μM – 0.02 μM in DPBS solution) was added into the wells; for the inhibition assay, growth media in the wells were discarded carefully and lysis buffer (50 μL for 96-well plate, 30 μL for 384-well plate containing 50 nM TMP-cs124-TTHA-Tb^{3+} ,5 μM NADPH, 0.1% BSA, 0.1% Triton X-100, 0.333 μM rapamycin and 20 μM ascomycin in DPBS solution) was added into the wells. Then the plate was kept at room temperature in dark for 20 minutes and the first measurement was taken afterwards, measurements were recorded every 10 minutes up to 2.5 hours. Negative control wells contained cells without protein expression, but the same lysis buffer as sample wells.

3.2.6.3 Nutlin-3 inhibition assay with permeabilized mammalian cells

pPBH-TRE$_{tight}$-p53(1-92a.a.)-eDHFR-(ER/K)$_n$-EGFP-HDM2(1-128a.a.)(n=10 nm, 20 nm or 30 nm) stable transfected cells were seeded at a density of 1.6×10^5 cells/mL in a multi-well plate and incubated (37 ^oC, 5% CO_2) for 24 h in culture medium (250 µL for 96-well plate, 50 µL for 384-well plate) containing 100 ng/mL doxycycline. The following day, for the titration assay, growth media in the wells were discarded carefully and lysis buffer (50 nM TMP-cs124-TTHA-Tb^{3+}, 5 µM NADPH, 0.1% BSA, 0.1% Triton X-100, and Nutlin-3 with 2-fold serial dilution in the range of 200 µM – 0.098 µM in DPBS solution) was added into the wells; for the inhibition assay, growth media in the wells were discarded carefully and lysis buffer (50 µL for 96-well plate, 30 µL for 384-well plate containing 50 nM TMP-cs124-TTHA-Tb^{3+}, 5 µM NADPH, 0.1% BSA, 0.1% Triton X-100, 10 µM Nutlin-3 in DPBS solution) was added into the wells. Then the plate was kept at room temperature in dark for 20 minutes and the first measurement was taken afterwards. Negative control wells contained cells without protein expression, but the same lysis buffer as sample wells.

3.2.6.4 Nutlin-3 inhibition assay with live mammalian cells

pPBH-TRE$_{tight}$-p53(1-92a.a.)-eDHFR-(ER/K)$_n$-EGFP-HDM2(1-128a.a.)(n=20 nm or 30 nm) stable transfected cells were seeded at a density of 1.6×10^5 cells/mL in a 96-well plate and incubated (37 ^oC, 5% CO_2) for 24 h in 250 µL culture medium containing 100 ng/mL doxycycline. The following day, growth media were discarded carefully and the wells were washed twice with DPBS solution.The cells were incubated with 10 µM TMP-Lumi4Tb-Arg9 in DMEM (without phenol red) at room temperature for 30 min; after washing with DPBS twice, DMEM (phenol red free) containing either 10 µM DMSO or 10 µM Nutlin-3 was added into the

wells. Then the plate was kept at room temperature in dark for 40 minutes and the first measurement was taken afterwards. Negative control wells contained cells without protein expression, but the same solution as sample wells.

3.3 Results and Discussion

3.3.1 Time-gated luminescence microscopy of single-chain biosensors in live cells

The term "dynamic range" as it applies to FRET biosensor generally refers to the maximum observed difference in the FRET signal between the "On" state and "Off" state of the sensor. However, there are subtle distinctions in the way this quantity is measured and reported in the literature. For example, Komatsu, *et al.* define dynamic range as the theoretical range of FRET/donor signal ratio between the on state biosensor and that in the off state.[139] This quantity could be measured either microscopically or spectroscopically by averaging the measured ratios from two cell populations expressing biosensor constructs with appropriate mutations that keep the sensors in the On and Off states. The same authors make a distinction between FRET dynamic range and the "gain" of a biosensor, where gain is the relative increase or decrease in the FRET ratio following stimulation of a sensor-expressing cell population. The gain would be dependent on the biosensor itself, the fraction of the sensor in the On-state under basal conditions, and the amount of stimulant (or inhibitor) added to the cells. In another example, Lam *et al.* define dynamic range as the range of FRET efficiency between the donor and acceptor fluorophores of the sensor.[140] In this study, we define dynamic range as the maximum observed difference in either the mean, donor-denominated or acceptor-denominated FRET ratios.

While dual-chain biosensors typically exhibit a high dynamic range, quantitative analysis of intermolecular FRET between is complicated by substantial differences in the local

concentrations of donor-labeled and acceptor labeled proteins. Single-chain biosensors overcome this problem by maintaining a 1:1 donor:acceptor ratio. However, single-chain sensors may fold into an off-state conformation where the donor and acceptor labels are in close proximity, leading to high baseline FRET and low dynamic range. Dynamic range is also reduced when the donor and acceptor adopt an on-state conformation where the orientation of their relative dipole moments disfavors FRET. For these reasons, many single-chain biosensors yield FRET ratio changes lower than 50%.[139, 140] Efforts to improve single-chain FRET biosensor dynamic range have been undertaken with some success including circular permutation of fluorescent proteins to optimize fluorophore orientation, variation of inherent fluorescent protein dimerization and engineering of the linker sequence that separates affinity elements and fluorophores.[141,142]

We aimed to develop single-chain, Tb(III)-based biosensors but were concerned about high baseline FRET signals. Dipole orientation doesn't affect lanthanide-based FRET because Tb(III) or Eu(III) emit with multiple dipole moments at many different orientations.[143] However, FRET between lanthanides and organic fluorophores or fluorescent proteins can typically be observed over relatively long distances (10–20 nm) compared to conventional FRET.[144] Moreover, during the long excited state lifetime of a lanthanide chromophore, many conformations can be sampled, some of which might bring the donor and acceptor close to one another. In order to minimize baseline FRET signals, we incorporated into our sensor design a semi-rigid α-helix linker sequence, which consists of an alternating sequence of approximately four glutamic acid residues followed by approximately four arginine or lysine residues (an ER/K linker). As reported by Sivaramakrishnan and Spudich, the ER/K adopts an alpha-helical geometry in solution.[145] However, it was speculated that the ER/K helix can break

stochastically, permiting close approach of elements positioned on either end. Thus, insertion of the ER/K linker between affinity binding elements and FRET partners yields a biosensor with low baseline FRET because the donor and acceptor are held far apart in the Off-state, yet the ends can still bind one another. Because the affinity elements are tethered together, their effective concentration depends only on linker length and is independent of solution concentration. The overall fraction of an ER/K biosensor in the closed or On-state depends only on the K_D of the affinity elements and linker length. Consequently, protein-protein interactions may be observed and analyzed even when the overall sensor concentration is far below the K_D[146].

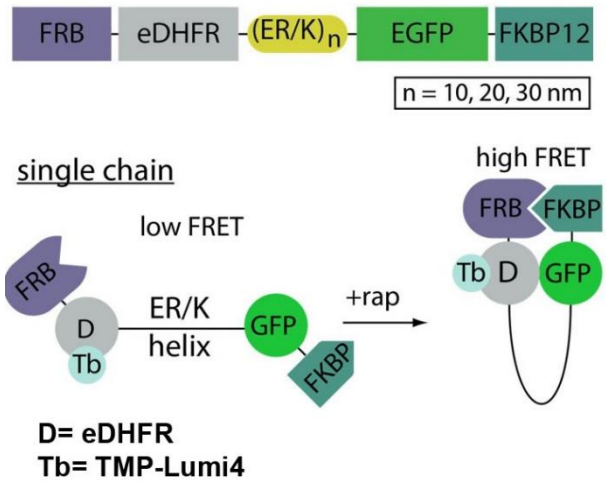

Figure 17. Design of a single-chain biosensor using model system of rapamycin-induced FRB/FKBP12 interaction.

NIH3T3 fibroblasts were stably transfected with plasmid DNA encoding a single fusion protein under control of a Tet-responsive promoter that contained the following elements (from *N- to C-* terminus): FRB, eDHFR, $(ER/K)_n$, GFP and FKBP12 (**Figure 17**). Three stably

transformed cell lines were created that expressed sensors with ER/K linker lengths of 10 nm, 20 nm or 30 nm. Following overnight induction of protein expression with doxycycline, cells were incubated in culture medium containing a cell-permeable, luminescent Tb(III) complex, TMP-Lumi4-R_9 (12 uM, 15 min, room temperature), washed with PBS, immersed in imaging medium and then imaged immediately. Steady-state images of GFP fluorescence and time-gated images of Tb(III) luminescence and Tb(III)-to-GFP sensitized emission reveal sensor distribution throughout the cytoplasm and Tb(III) probe distribution throughout the cytoplasm and nucleus (**Figure 18A**). In a time-series image sequence of cells expressing the sensor with 20 nm linker, the donor-denominated FRET (FRET/Tb) ratio increased to over 300% of its initial value about 15 min after rapamycin addition (**Figure 18B**). Very large increases in both FRET/Tb and the acceptor-denominated FRET ratio (FRET/GFP) were observed in rapamycin-stimulated cells expressing biosensors containing 10 nm, 20 nm, and 30 nm ER/K linkers (**Figure 18C**). The dynamic ranges of both FRET/Tb and FRET/GFP signals increased with linker length. In cells expressing FKBP12/FRB biosensors with 10, 20, and 30 nm ER/K linkers, the maximum observed changes in mean FRET/Tb were 87%, 288% and 525%, respectively. The maximum, microscopically observed increases in mean FRET/GFP were 61%, 378% and 470% for linker lengths of 10, 20 and 30 nm, respectively.

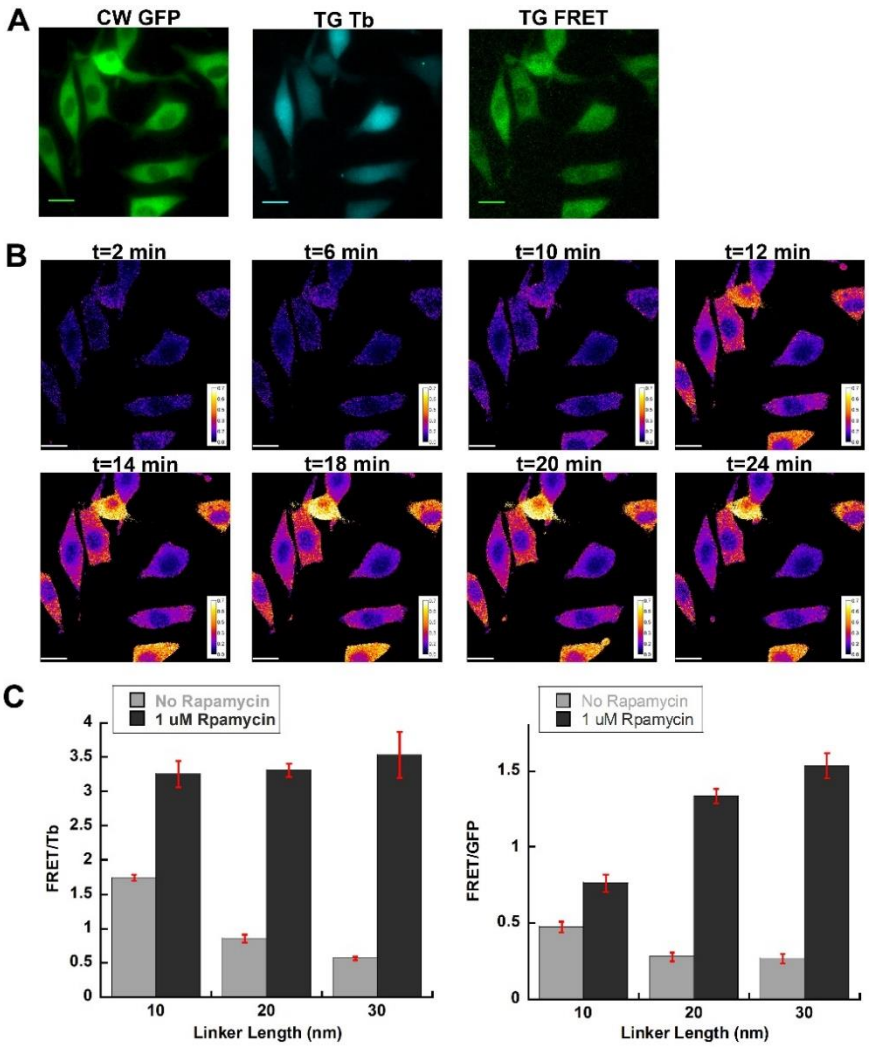

Figure 18. Time-gated luminescence microscopy with Tb(III) probes enables two-channel, ratiometric imaging with high dynamic range of single-chain FRET biosensors.

A. Representative images of NIH3T3 fibroblasts cells stably expressing FRB-eDHFR-$(ER/K)_{20}$-GFP-FKBP12 approximately 20 min after stimulation with 2 μM rapamycin.

Micrographs: CW GFP, steady-state GFP fluorescence (λ_{ex}, 480 ± 20 nm; λ_{em}, 535 nm ± 25 nm); TG-Tb, time-gated Tb(III) luminescence (λ_{ex}, 365 nm, λ_{em}, 620 nm ± 10 nm, gate delay 10 μs); TG FRET, time-gated Tb(III)-to-GFP sensitized emission (λ_{ex}, 365 nm; λ_{em}, 520 ± 10 nm, gate delay 10 μs). Scale bar, 20 μm. Tb and FRET channel images were rendered at identical contrast. **B**. Color maps of the same cells shown in **A** depict the ratio of the TG FRET image to the TG-Tb image at various time points following rapamycin stimulation. **C.** Biosensor dynamic ranges increase with the length of ER/K linker due to reduction in baseline, or Off-State FRET signals. Bar graphs depict the mean, pixel-wise FRET/Tb or FRET/GFP ratios measured in regions of interest drawn within cells both before and 25 min after addition of rapamycin. Values given are averaged from 10 or more cells for each condition. Error bars, sem.

3.3.2 Detection of PPIs and their inhibition in multi-well plates

We next sought to assess the potential of our Tb(III) biosensors for detection and quantification of PPIs and their inhibition in multi-well plate format following expression in live mammalian cells. With rare exceptions, conventional FRET-based detection of cellular PPIs at medium throughput (96-well plate) or high-throughput (384-well plate) is impossible because of the aforementioned limitations in FRET S/N and dynamic range and the relatively small amounts of protein in each sample well.[13] NIH 3T3 cells stably expressing single-chain, FKBP/FRB biosensors (containing 10 nm, 20 nm, or 30 nm ER/K linkers) were seeded into 96-well plates (40,0000 cells/well) and grown overnight in medium containing doxycycline to induce protein expression. A rapamycin titration assay was first performed to obtain the EC_{50} values and the optimal rapamycin concentration to induce the FRB/FKBP12 interaction. Lysis buffer containing TMP-Lumi4-Tb (50 nM) and serial dilutions of rapamycin (final conc., 5 μM to 0.47 nM) were added to the wells, and time-gated emission at 520 nm and 615 nm was measured after

incubation at room temperature for 15 min. The mean 520 nm signal from 20 control wells containing non-expressing cells and the same lysis buffer solution was subtracted from each sample well, then the background-corrected Tb(III)-to-GFP FRET signal (at 520 nm) was divided by the Tb(III) signal (615 nm) in order to minimize well-to-well variability resulting from the differences in probe amounts or sample absorbance[147].

A non-linear regression (NLR) fit to a plot of FRET/Tb ratio vs. rapamycin concentration yielded EC_{50} values of 22.3 ± 1.5 nM and 18.0 ± 1.5 nM for cells expressing biosensors with 20 nm or 30 nm ER/K linkers, respectively (**Figure 19A**). To determine maximum response, we stimulated expressing cells with 1 μM rapamycin in the lysis buffer containing another TMP-Tb(III) complex conjugate, TMP-TTHA-cs124(Tb) (final conc., 25 nM). Again, the mean FRET signal from control wells (20) containing non-expressing cells and lysis buffer with TMP-cs124-TTHA(Tb) but lacking rapamycin was subtracted from FRET signals measured for each sample well, and the background-corrected FRET signals were ratioed to the corresponding Tb(III) signals. An increase in dynamic range with ER/K linker length was observed in the 96-well plate data, similar to that seen in microscopy data. However, the magnitude of the measured dynamic range was substantially higher. Cells expressing FKBP12/FRB biosensors with 10 nm, 20 nm, or 30 nm ER/K linkers exhibited dynamic ranges of 165%, 1700%, and 2500%, respectively (**Figure 19A**).

In order to further assess the performance of our model system, we calculated two quality metrics that are often used to evaluate HTS assays: Z'-factor and strictly standardized mean difference (SSMD)[148]. For measurement of FKBP12/FRB biosensor activation following cell permeabilization in 96-well plates, Z' ranged from 0.72 to 0.89, and SSMD value of more than 14 was obtained for all sensors (**Table 2**). While these results clearly indicate a highly

robust assay, high-throughput assays require the capability to measure at least 100,000 compounds per day, and this requires analysis in 384-well plates. In 384-well plates, we obtained relatively poor *Z'* factors around zero for all sensors, although this may be partly attributed to error introduced by manual plate preparation. According to SSMD criteria, however, the rapamycin activation assay may be considered to range from strong to extremely strong, based on SSMD values ranging from 2.5 to 6.4 (**Table 2**).

In order to further evaluate the potential of Tb(III) biosensors for multi-well plate applications, we measured the effects of ascomycin as an inhibitor of the rapamycin-induced, FKBP12/FRB interaction[149]. Ascomycin was titrated against a constant concentration of rapamycin (0.333 μM) in permeabilized cells expressing the FKBP/FRB sensors with either 20 or 30 nm ER/K linker lengths. Non-linear fitting yielded IC_{50} values of 0.4 ± 0.1 μM for both sensors (Figure 3B). Full inhibition with 20 μM ascomycin yielded FRET/Tb signal decreases of 65%, 92%, 92% in cells expressing 10 nm, 20 nm, 30 nm ER/K linker biosensors, respectively (**Figure 19B**). Z' factors > 0.68 and SSMD values >12 were obtained for all inhibition assay conditions (**Table 2**).

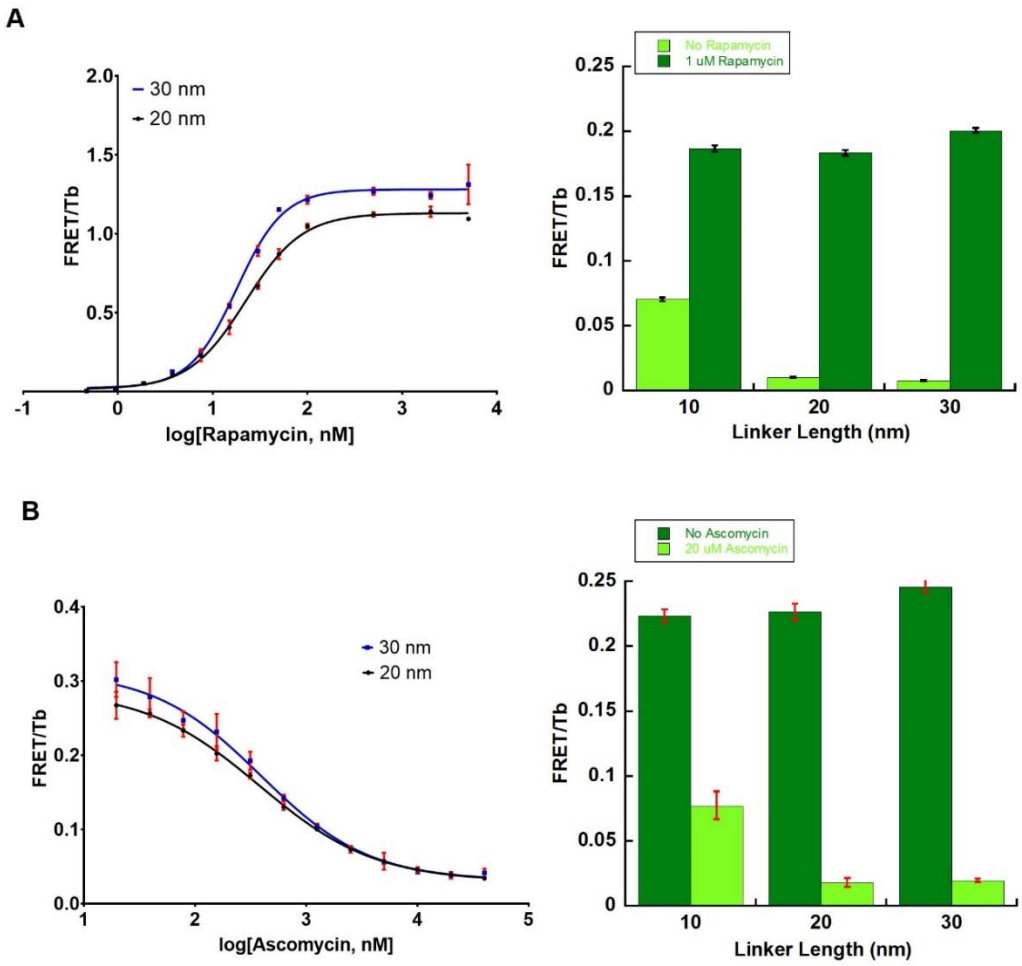

Figure 19. **Rapamycin stimulation titration and Ascomycin inhibition titration with permeablized cells in 96-well plate.**

A. **Left:** NIH 3T3 fibroblast cells were permeabilized and equilibrated with rapamycin concentrations ranging from 5 µM to 0.47 nM. The Non-linear regression fitted plot gave calculated EC_{50} values. **Right:** Substantial signal increase was observed in the positive control wells (1 µM rapamycin) relative to that seen in the negative controls (no rapamycin).Z' factor was obtained. **B. Left:** Ascomycin was titrated (from 40 µM to 0.02 µM) against a constant concentration of rapamycin (0.333 µM). NLR fit of the plot with concentration of ascomycin against FRET/Tb gave the IC_{50} values. **Right:** Great signal decrease was observed in positive control wells containing ascomycin, compared to negative control wells containing only rapamycin. Z' factor was obtained. For left graphs: each data point represents 3 replicates (3 wells); For right graphs: each bar from positive controls represents 16 replicates, while negative controls represents 8 replicates. Error bars indicate the SD.

3.3.3 Study on p53 - HDM2 interaction and its inhibition

The data obtained with the FKBP12/FRB model system clearly shows the strong potential of Tb(III)-based, single-chain FRET biosensors for both imaging and HTS analysis of PPIs. We further evaluated the potential of these sensors by measuring the inhibition of the interaction between p53 and HDM2. As a tumor suppressor, p53 plays a crucial role in human cancer. Its activity is controlled through a negative feedback mechanism by HDM2[150]. The small molecule inhibitor of p53/HDM2 interaction, Nutlin-3, was identified in a screening campaign and represents one of the early successes of discovery efforts to find drugs that target PPIs[151]. We replaced the FRB domain in our original biosensors with the N-terminal 92 amino acids of p53 and replaced the FKBP12 domain with the N-terminal 128 residues of HDM2. Again, we prepared sensor constructs with 10, 20 and 30 nm ER/K linkers, and we stably transformed HeLa cells with the constructs for evaluation with Nutlin-3 as a positive control.

We first examined the p53/HDM2 sensor performance microscopically. Stably transformed HeLa cells were incubated with medium containing either 10 μM DMSO (negative control), or 10 μM Nutlin-3 (positive control) at 37°C for 90 min. After incubation with cell permeable TMP-Lumi4-R_9, steady-state images of GFP fluorescence and time-gated images of Tb (III) luminescence and Tb(III)-to-GFP sensitized emission were acquired separately. A representative set of images obtained from cells expressing the p53/HDM2 sensor with a 20 nm ER/K linker clearly show a reduction in the FRET/Tb signal in cells with Nutlin-3 (**Figure 20A**). Quantitative image analysis once again showed that the maximum difference between On- and Off-states of the sensors increased with ER/K linker length; the mean decrease in FRET/Tb due to Nutlin-3 inhibition was measured to be 40%, 73%, and 84% in cells expressing sensors with 10, 20 and 30 nm linkers, respectively (**Figure 20B**). In addition, analysis of a time-lapse image

sequence shows that inhibition occurs rapidly, with near maximal sensor response occurring within minutes of Nutlin-3 addition to cell culture (**Figure 20C**).

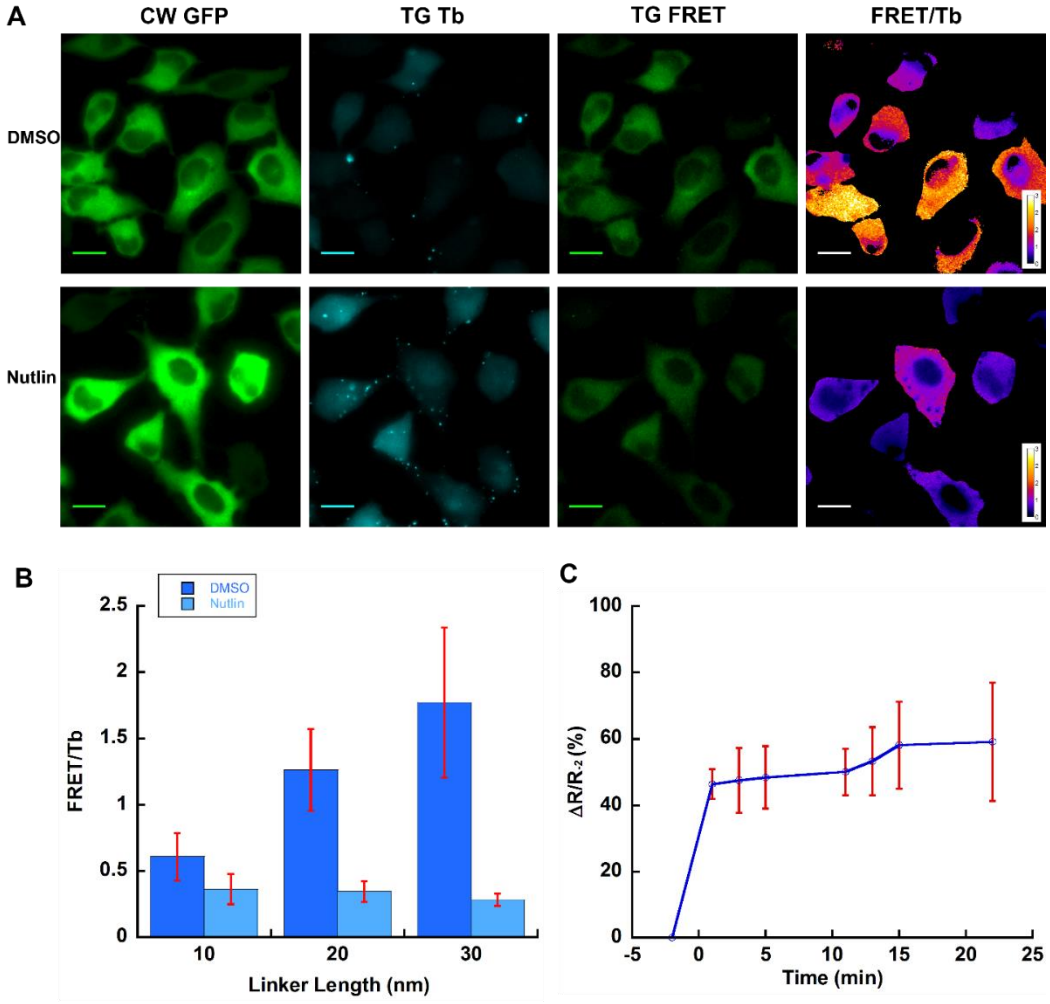

Figure 20. Decreased Tb-to-GFP FRET observed when Nutlin-3 inhibits p53/HDM2 interaction and high z' factor obtained in 96-well plate assay.
A. HeLa cells stably expressing p53(1-92 a.a.)-eDHFR-$(ER/K)_{20}$- GFP-HDM2(1-128 a.a.) incubated with media containing 10 µM Nutlin-3 for 90 min showed reduced Tb-to-GFP FRET, while control specimen lacking inhibitor showed high FRET signal. Micrograph: 1st column; continuous wave GFP fluorescence (λ_{ex}, 480 ± 20 nm; λ_{em}, 535 ± 25 nm); 2nd column: time-gated Tb luminescence (λ_{ex}, 365 nm; λ_{em}, 620 ± 10 nm); 3rd column: time-gated Tb-to-GFP FRET (λ_{ex}, 365 nm; λ_{em}, 520 ± 10 nm); 4th column: FRET/Tb ratio map images. Scale Bars: 20 µm. Tb and FRET channel images were rendered at identical contrast. **B**. Increasing FRET-to-Tb signals observed with the increase of linker length (10 nm to 20 nm to 30 nm), then the signals

decreased after incubation with Nutlin-3. Bar graphs depict the mean, pixel-wise FRET/Tb or FRET/GFP ratios measured in regions of interest drawn within cells. Values given are averaged from 10 or more cells for each condition. Error bars, SD. **C**. Absolute value of percent decrease in FRET/Tb at different time points after adding Nutlin-3 ($\Delta R/R_{-2}$). Values obtained from regions of interest drawn within cells, 7-cell sample. Error bars, SEM.

We also performed the inhibition assays with permeabilized cells in both 96-well and 384-well plates using similar conditions to those used with the FKBP/FRB biosensors. Following overnight induction of biosensor expression with doxycycline, lysis buffer containing TMP-TTHA-cs124(Tb) (final conc., 50 nm) was added to wells. Nutlin-3 (final conc., 10 μM) was also added with lysis buffer to positive control wells. Z' factor and SSMD values were calculated to determine data quality. In all assays, with cells expressing 10 nm linker biosensor, both Z' factor and SSMD values were very low due to the low response from positive controls, in other words, trivial FRET change after incubation with Nutlin-3. However, Z' factors ≥ 0.70, | SSMD | > 10 were obtained in 96-well plate assays with cell expressing 20 nm, 30 nm linker biosensor (Table 1). In 384-well plate assays, Z' factor values are negative, but |SSMD| > 2 indicate strong effect size and potential use for hit identification with moderate positive controls (**Table 2, Figure 21**).

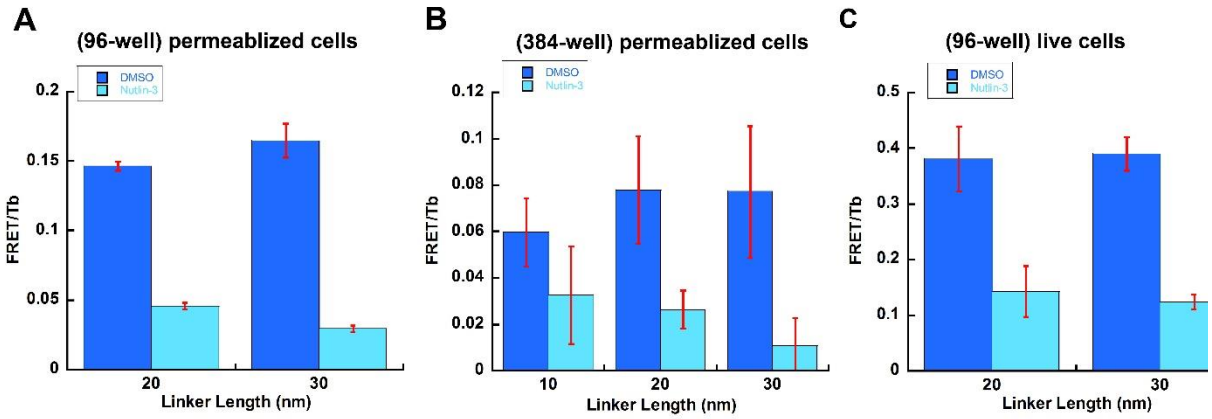

Figure 21. Nutlin-3 inhibition assays performed in multi-well plates with permeablized cells or live cells.

For A and B, cells stably expressing biosensors were permeabilized and equilibrated with 10μM Nutlin-3; For C, living cells were incubated with 10μM Nutlin-3 after incubation with12μM TMP-Lumi4Tb-R9 at RT. Error bars indicate the SD.

FRB/FKBP12 interaction					
	Z' factor	|SSMD|		Z' factor	|SSMD|
96-well plate			384-well plate		
Rapamycin stimulation			Rapamycin stimulation		
10 nm	0.72	14.67	10 nm	-0.03	3.55
20 nm	0.87	28.07	20 nm	-0.49	2.50
30 nm	0.89	35.29	30 nm	0.41	6.32
Ascomycin inhibition					
10 nm	0.69	12.52			
20 nm	0.86	29.15			
30 nm	0.92	46.79			
p53/HDM2 interaction					
	Z' factor	|SSMD|		Z' factor	|SSMD|
96-well plate			384-well plate		
Nutlin-3 inhibition			Nutlin-3 inhibition		
10 nm	-5.83	0.62	10 nm	-2.94	1.06
20 nm	0.82	23.40	20 nm	-0.83	2.09
30 nm	0.67	10.74	30 nm	-0.83	2.16
TMP-Lumi4-R9 incubation					
Nutlin-3 inhibition					
20 nm	-0.30	3.24			
30 nm	0.52	8.22			

Table 2. Z' factor and |SSMD| values for multi-well plate assays.

3.3.4 Time-gated detection of inhibition of p53 - HDM2 interaction in live cells

The ability to robustly detect PPIs or their inhibition in mammalian cell culture following cell permeabilization offers distinct benefits for drug discovery and HTS. First, no protein purification is required, and it may be possible to design expression constructs where one of the affinity partners is a transmembrane protein. Second, because the sensors are expressed directly in mammalian cells, PPIs that depend on phosphorylation or other post-translational modifications may be assessed. Finally, the assay is simple, requiring only addition of lysis buffer with detection reagent, no wash steps and immediate readout. These capabilities critically require TGL detection of lanthanide-based FRET as well as a single-chain biosensor design. For example, only ~8,000 cells are present in a single well of a 384-well plate with a solution volume of 50 μL. If we assume a cell volume of 3 pL and a moderate biosensor expression level such that effective cellular concentration is 5 μM, then only sub-picomolar amounts of protein are present in a well and the sensor concentration following cell lysis is in the low-nanomolar range. These concentrations are well below the detection limits of conventional FRET and far below the K_D of most relevant PPIs. Consequently, the affinity elements must be tethered to one another and the high sensitivity of TGL detection is needed.

While PPI detection following cell permeabilization offers substantial benefits, the ability to detect PPI changes within intact, live cells could offer more biologically relevant insights as it would allow for PPI analysis in the presence of other cellular factors. Moreover, HTS assays within live cells would further assess the ability of drugs to cross the plasma membrane and their inhibition or activation characteristics within the cellular milieu. We evaluated the performance of our sensors in live cells in 96-well plates using the same, cell permeable TMP-Lumi4-R_9 complex that we used for microscopic imaging. After overnight

induction in medium containing doxycycline, HeLa cells stably expressing single-chain p53/HDM2 affinity biosensors with 20 nm or 30 nm ER/K linker were washed and incubated in medium containing 10 μM TMP-Lumi4-R_9 at room temperature for 30 min. Following DPBS wash, PBS buffer solution containing either 10 μM DMSO (negative control), or 10 μM Nutlin-3 (positive control) was added to wells and left at room temperature for 40 min. Time-gated Tb and Tb-sensitized FRET signals were then recorded. We calculated the Z' factor and SSMD of the assay. Although low Z' factor is obtained, high |SSMD| for cells expressing 20 nm, or 30 nm linker biosensor is obtained with value 3.2 and 8.2, respectively. This very strong or extremely strong effect sizes advocate the application of the single-chain biosensor in HTS assay for live cell PPIs interaction or inhibition hit selection.

3.4 Conclusions

Tb(III)-based, single-chain FRET biosensors exhibit a remarkable dynamic signal range when used to microscopically image PPIs using TGL microscopy or when detecting interaction or inhibition in multi-well plates. Large FRET signal changes resulted from time-gated elimination of non-specific fluorescent signals and the incorporation of a rigid alpha-helical linker structure into the biosensor that held Tb(III) donors and GFP acceptors at a distance greater than the Förster distance when the sensor was in the Off-state. The single-chain design made it possible to robustly detect PPIs or their inhibition in 384-well plates following permeabilization of expressing cells. High throughput analysis capability will enhance drug discovery efforts by simplifying assay protocols and enabling access to a wider variety of PPIs than can currently be analyzed using assays with purified components. Direct visualization of PPI inhibition in living cells at medium-throughput mode will make it possible to design secondary, cell-based assays that can evaluate cell permeability of hit compounds. TGL

microscopy of PPIs also exhibits far higher dynamic range than conventional FRET imaging. While current acquisition speeds of TGL FRET are relatively slow (up to 8 s per time-gated FRET image), these rates could be improved with brighter Tb(III) probes. Taken together, the results presented here show that Tb(III)-based FRET biosensors offer a versatile platform technology for interrogating PPIs and their function in live cells.

CHAPTER 4

FUTURE PERSPECTIVE

The high sensitivity and dynamic range of the lanthanide-based FRET biosensors encourage the exploration of a wide variety of PPIs and their inhibitions. Herein, the interaction between protein phosphatase 1 regulatory subunit 12C (PPP1R12C) and its catalytic subunit alpha isozyme (PPP1CA), and their inhibition with a short peptide or another regulatory domain will be investigated for their potential of being utilized in HTS as therapeutic targets to discover effective small molecule inhibitors. In addition, a new method, which combines split-DHFR and time-gated FRET, is proposed for mapping protein network or identifying potential hits of designated PPIs in living mammalian cells.

4.1. Lanthanide-based FRET biosensor with PPP1R12C and PPP1CA

4.1.1. Introduction

Protein phosphatase-1 (PP1) is one of the major serine/threonine protein phosphatases ubiquitously distributed in eukaryotic cells. It regulates a wide variety of cellular functions, such as muscle relaxation, glycogen metabolism, and cell-cycle progression[131,146], through the interaction of its catalytic subunit (PP1C) with a large number of established regulatory subunits. Structure analysis indicates that the interaction involves primarily C-terminal domain of PP1[152], and the numerous PP1 regulatory subunits share one specific PP1 targeting sequence-the RVxF motif, which fits in a small hydrophobic groove on the surface of PP1C[146]. As one of the mammalian regulatory subunits of PP1C, PPP1R12C was found to specifically bind to PP1C with the N terminus, and this association is required for the regulation of the catalytic activities and the assembly of actin cytoskeleton[152]. The association of the PPP1R12C N terminus to PP1C leads to actin depolymerization, while the C terminus binding antagonizes this effect[152].

Thus, we designed the new lanthanide FRET biosensor by replacing FRB with N terminus (1-389 a.a.) of PPP1R12C, and FKBP12 with C terminus (161-387 a.a.) of PPP1CA.

Due to the difficulty of cloning, we requested Genscript to finish the cloning of two mammalian plasmid constructs: PPP1R12C(TEV)-eDHFR-ER/K_n-EGFP-PPP1CA (n= 10 nm, or 20 nm). I have stably transfected two plasmids into Hela cells and sorted out cells with low –to medium expression level by flow cytometry. For next step, we will test the interaction between PPP1R12C and PPP1CA in multi-well plate, and examine their inhibition with a short peptide or another competing regulatory domain.

4.1.2 Materials and methods

4.1.2.1 Materials

Hela cells were purchased from American Type Culture Collection (ATCC® CCL-2™). Dulbecco's modified eagle medium with 1g/L glucose (DMEM, 10-014CV), , Dulbecco's phosphate buffer saline (DPBS, 21-030), and 0.25% trypsin/2.21 mM EDTA were purchased from Corning cellgro ® . MEM non-essential amino acid (11140), DMEM (without phenol red, 21063), HEPES (15630-080) and Lipofectamine 2000 (11668-027) were purchased from InvitrogenTM. FBS (S11150) was purchased from Atlanta Biologicals. Hygromycin (sc-29067) was purchased from Santa Cruz Biotechnology. Doxycycline (D9891) was purchased from Sigma.

4.1.2.2 Stable expression of biosensor plasmids

Hela cells were grown to 70-80% confluency in a sterile 10 cm dish. The cells were transfected with 12 μg of biosensor plasmids and their recombination helper plasmid pSPB-Transposase with a Lipofectamine:plasmid ratio of 2.5μg:1μg per plasmid. Plasmid and Lipofectamine solutions were first prepared in separate microcentrifuge tubes in OptiMEM I with a total volume of 1.5 mL. After 5 minutes of incubation at room temperature, the solutions were mixed and kept at room temperature for an additional 20 minutes. The media in 10 cm dish

was aspirated and the Lipofectamine + plasmids solution was added into it. The cells were incubated with the solution for 4 hours in tissue culture incubator at 37 ^{o}C with 5% CO_2 and then the solution was replaced with 10 mL of fresh DMEM(+) (DMEM supplied with 15 mM HEPES, 10% FBS and 100 mg/mL Hygromycin). The transfections were confirmed with microscopy after induction with 100 ng/mL doxycycline. Cells with low-to medium level of GFP expression were sorted out with flow cytometry.

4.2 Development of a new assay for PPIs study and HTS screening in live mammalian cells

Protein fragment complementation and two-hybrid systems are two main technologies used in genetic in *vivo* study of PPIs in yeast, bacterial and other organisms. But their setup in mammalian cells to study PPIs as therapeutic targets for drug discovery are still undergoing with difficulties. Many mammalian proteins don't behave properly in yeast or bacterial cells, as they need different secondary modifications. A native cellular format is especially required to study the dynamic process of the protein interaction network, such as signaling pathways and flexibility of actin cytoskeleton. Moreover, HTS assay based on cell-free systems could not select cell-permeable and nontoxic small molecules or PPI modifiers.

In general, two-hybrid assays depend on the colocalization of two protein domains, which results in recruitment of prey to a specific cellular location (e.g., the reporter gene or plasma membrane) and finally an output signal (transcription activation, enzymatic activity or fluorescence). In most cases, reporter gene expression is used as a signal amplification readout to detect transient and weak associations. The efficiency of the system is further improved by the lack of cumbersome purification step. However, two-hybrid systems have a major limitation of false positives introduced by interactions between proteins that are normally present in separate cellular compartments, or autoactivation by the bait protein. On the other hand, PCAs are based

on the reconstitution of a functional reporter by PPI-induced refolding of two protein fragments. They do not require coexpression and specific localization of chimeric proteins, therefore can be used to analyze the native location of protein associations. They are also suitable for studies on the kinetics or spatiotemporal dynamics of PPIs. So far, several folding-dependent complementation methods have been successfully adapted to mammalian cell systems. Split-β-galactosidase assays based on ligand-dependent recruitment of β-arrestin[153] and endocytosis[154] have been exploited to study GPCR biology. Split-luciferase systems taking advantage of the reversible character of luciferase reassembly are more frequently used in mammalian cells to monitor fusion of cellular organelles[155], to detect intraviral PPIs[156], and actin polymerization[157]. Multicolor split-FP methods have been developed to simultaneously capture multiple PPIs in different subcellular locations[158], and their combination with FRET or BRET readouts allow study of complex formation[83]. Nevertheless, the application of split-FP in high throughput cDNA library screening is rather limited due to intrinsic topological constraints or strong fluctuations in signal intensity caused by variations of prey expression levels[159].

Herein, I propose a new method for HTS of cDNA library in living mammalian cells to map protein network or identify potential hits of designated PPIs. This method combines split-DHFR, FRET, and time-gated detection, thus is expected to offer high sensitivity and signal-to-noise ratio.

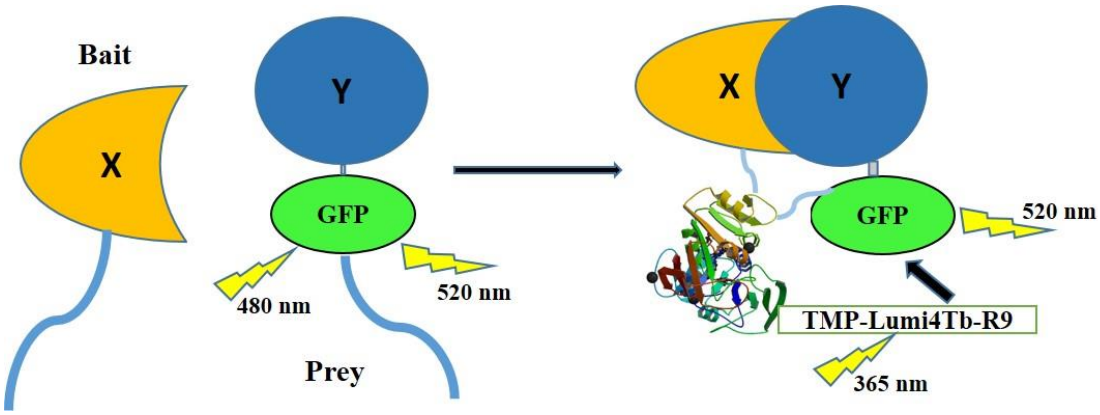

Figure 22. A new assay for PPIs study and HTS screening in live mammalian cells.
Two proteins of interest (X and Y) are each fused to a fixed eDHFR fragment. If there is no interaction between X and Y (left), the fragments remain unstructured and only GFP signal can be observed. Upon interaction between the bait and prey (right), the two fragments refold into a fully functional eDHFR protein. The specific binding between eDHFR and TMP enable the detection of Tb sensitized GFP signal. The image of the eDHFR is based on the Protein Data Bank (PDB) structure under accession number 1DRA[160].

Split-DHFR was originally explored in yeast cells, and then reported for murine DHFR in mammalian cells for growth selection in DHFR-deficient cells[159,161]. In the new design, E.coli. DHFR is utilized and separated into two fragments, the F[1,2] N-terminal and the F[3] C-terminal fragments. Protein X is fused to one of the fragments as bait, and is stably expressing in cells. For interaction study with model system (e.g. FRB/FKBP12), protein Y is fused to GFP and the other fragment of eDHFR as prey. For interaction screening, human cDNA library will be cloned with GFP and DHFR fragment genes, and the final translated protein will act as prey. Prey will be transiently transfected in cells and transfection can be validated by GFP signal. Then the cells will be incubated with TMP-Lumi4Tb-R9. In the absent of interaction, GFP and time-gated Tb signal can be observed. After determining the minimal time frame of physical contact between the two fragments to establish complete refolding, sensitized Tb-to-GFP FRET

will be detected and the cDNA sequence in the corresponding prey will be recovered by PCR using primers flanking the restriction sites of the vector. Furthermore, by attaching differently colored FPs to protein Y, this method offers multiplexing potential for investigating PPIs in signaling pathways or mapping PPIs network.

REFERENCES

1. Heffern, M. C.; Matosziuk, L. M.; Meade, T. J.: Lanthanide probes for bioresponsive imaging. *Chemical reviews 114* (8): 4496-4539,2014.

2. Selvin, P. R.: Principles and biophysical applications of lanthanide-based probes. *Annual review of biophysics and biomolecular structure 31*: 275-302,2002.

3. Armelao, L.; Quici, S.; Barigelletti, F.; Accorsi, G.; Bottaro, G.; Cavazzini, M.; Tondello, E.: Design of luminescent lanthanide complexes: From molecules to highly efficient photo-emitting materials. *Coordination Chemistry Reviews 254* (5-6): 487-505,2010.

4. Rajendran, M.; Yapici, E.; Miller, L. W.: Lanthanide-based imaging of protein-protein interactions in live cells. *Inorganic chemistry 53* (4): 1839-1853,2014.

5. Reddy, D. R.; Pedro Rosa, L. E.; Miller, L. W.: Luminescent trimethoprim-polyaminocarboxylate lanthanide complex conjugates for selective protein labeling and time-resolved bioassays. *Bioconjugate chemistry 22* (7): 1402-1409,2011.

6. Aggarwal, V.; Ha, T.: Single-molecule pull-down (SiMPull) for new-age biochemistry: methodology and biochemical applications of single-molecule pull-down (SiMPull) for probing biomolecular interactions in crude cell extracts. *BioEssays : news and reviews in molecular, cellular and developmental biology 36* (11): 1109-1119,2014.

7. Geissler, D.; Stufler, S.; Lohmannsroben, H. G.; Hildebrandt, N.: Six-color time-resolved Forster resonance energy transfer for ultrasensitive multiplexed biosensing. *Journal of the American Chemical Society 135* (3): 1102-1109,2013.

8. Ho-Pun-Cheung, A.; Bazin, H.; Gaborit, N.; Larbouret, C.; Garnero, P.; Assenat, E.; Castan, F.; Bascoul-Mollevi, C.; Ramos, J.; Ychou, M.; Pelegrin, A.; Mathis, G.; Lopez-Crapez, E.: Quantification of HER expression and dimerization in patients' tumor samples using time-resolved Forster resonance energy transfer. *PloS one 7* (7): e37065,2012.

9. Rajapakse, H. E.; Miller, L. W.: Time-resolved luminescence resonance energy transfer imaging of protein-protein interactions in living cells. *Methods in enzymology 505*: 329-345,2012.

10. Madiraju, C.; Welsh, K.; Cuddy, M. P.; Godoi, P. H.; Pass, I.; Ngo, T.; Vasile, S.; Sergienko, E. A.; Diaz, P.; Matsuzawa, S.; Reed, J. C.: TR-FRET-based high-throughput screening assay for identification of UBC13 inhibitors. *Journal of biomolecular screening 17* (2): 163-176,2012.

11. Tu, D.T.; Liu, L.Q.; Ju, Q.; Liu, Y.S.; Zhu, H.M.; Li, R.F.; Chen, X.Y.: Time-Resolved FRET Biosensor Based on Amine-Functionalized Lanthanide-Doped $NaYF_4$ Nanocrystals. *Angew. Chem. Int. Ed.* 50: 6306-6310, 2011.

12. Hildebrandt, N.; Wegner, K. D.; Algar, W. R.: Luminescent terbium complexes: Superior Förster resonance energy transfer donors for flexible and sensitive multiplexed biosensing.

Coordination Chemistry Reviews 273-274: 125-138,2014.

13. Song, Y.; Madahar, V.; Liao, J.: Development of FRET assay into quantitative and high-throughput screening technology platforms for protein-protein interactions. *Annals of biomedical engineering 39* (4): 1224-1234,2011.

14. Miyawaki, A.: Development of probes for cellular functions using fluorescent proteins and fluorescence resonance energy transfer. *Annual review of biochemistry 80*: 357-373,2011.

15. Wlodarczyk, J.; Woehler, A.; Kobe, F.; Ponimaskin, E.; Zeug, A.; Neher, E.: Analysis of FRET signals in the presence of free donors and acceptors. *Biophysical journal 94* (3): 986-1000,2008.

16. Yasuda, R.: Imaging spatiotemporal dynamics of neuronal signaling using fluorescence resonance energy transfer and fluorescence lifetime imaging microscopy. *Current opinion in neurobiology 16* (5): 551-561,2006.

17. Mattheyses, A. L.; Hoppe, A. D.; Axelrod, D.: Polarized fluorescence resonance energy transfer microscopy. *Biophysical journal 87* (4): 2787-2797,2004.

18. Thermo Scientific: Protein-Interactions-Handbook.

19. Fu, H.A.: PPIs methods and applications. *Methods in molecular biology* 261, 2004

20. Erickson, M. G.; Liang, H.; Mori, M. X.; Yue, D. T.: FRET Two-Hybrid Mapping Reveals Function and Location of L-Type Ca2+ Channel CaM Preassociation. *Neuron 39* (1): 97-107,2003.

21. Zal, T.; Gascoigne, N. R.: Photobleaching-corrected FRET efficiency imaging of live cells. *Biophysical journal 86* (6): 3923-3939,2004.

22. Sun, Y.; Day, R. N.; Periasamy, A.: Investigating protein-protein interactions in living cells using fluorescence lifetime imaging microscopy. *Nature protocols 6* (9): 1324-1340,2011.

23. Grecco, H. E.; Roda-Navarro, P.; Girod, A.; Hou, J.; Frahm, T.; Truxius, D. C.; Pepperkok, R.; Squire, A.; Bastiaens, P. I.: In situ analysis of tyrosine phosphorylation networks by FLIM on cell arrays. *Nature methods 7* (6): 467-472,2010.

24. Newman, R. H.; Fosbrink, M. D.; Zhang, J.: Genetically encodable fluorescent biosensors for tracking signaling dynamics in living cells. *Chemical reviews 111* (5): 3614-3666,2011.

25. VanEngelenburg, S. B.; Palmer, A. E.: Fluorescent biosensors of protein function. *Current opinion in chemical biology 12* (1): 60-65,2008.

26. Carlson, H. J.; Campbell, R. E.: Genetically encoded FRET-based biosensors for multiparameter fluorescence imaging. *Current opinion in biotechnology 20* (1): 19-

27,2009.

27. Rives, M. L.; Vol, C.; Fukazawa, Y.; Tinel, N.; Trinquet, E.; Ayoub, M. A.; Shigemoto, R.; Pin, J. P.; Prezeau, L.: Crosstalk between GABAB and mGlu1a receptors reveals new insight into GPCR signal integration. *The EMBO journal 28* (15): 2195-2208,2009.

28. Higueruelo, A. P.; Jubb, H.; Blundell, T. L.: Protein-protein interactions as druggable targets: recent technological advances. *Current opinion in pharmacology 13* (5): 791-796,2013.

29. Sabariegos, R.; Picazo, F.; Domingo, B.; Franco, S.; Martinez, M. A.; Llopis, J.: Fluorescence resonance energy transfer-based assay for characterization of hepatitis C virus NS3-4A protease activity in live cells. *Antimicrobial agents and chemotherapy 53* (2): 728-734,2009.

30. Palmer, A. E.; Tsien, R. Y.: Measuring calcium signaling using genetically targetable fluorescent indicators. *Nature protocols 1* (3): 1057-1065,2006.

31. Machacek, M.; Hodgson, L.; Welch, C.; Elliott, H.; Pertz, O.; Nalbant, P.; Abell, A.; Johnson, G. L.; Hahn, K. M.; Danuser, G.: Coordination of Rho GTPase activities during cell protrusion. *Nature 461* (7260): 99-103,2009.

32. Shaner, N. C.; Steinbach, P. A.; Tsien, R. Y.: A guide to choosing fluorescent proteins. *Nature methods 2* (12): 905-909,2005.

33. Patterson, G. H.; Piston, D. W.; Barisas, B. G.: Forster distances between green fluorescent protein pairs. *Analytical biochemistry 284* (2): 438-440,2000.

34. Martell, J. D.; Yamagata, M.; Deerinck, T. J.; Phan, S.; Kwa, C. G.; Ellisman, M. H.; Sanes, J. R.; Ting, A. Y.: A split horseradish peroxidase for the detection of intercellular protein-protein interactions and sensitive visualization of synapses. *Nature biotechnology 34* (7): 774-780,2016.

35. Shcherbakova, D. M.; Hink, M. A.; Joosen, L.; Gadella, T. W.; Verkhusha, V. V.: An orange fluorescent protein with a large Stokes shift for single-excitation multicolor FCCS and FRET imaging. *Journal of the American Chemical Society 134* (18): 7913-7923,2012.

36. Ibraheem, A.; Campbell, R. E.: Designs and applications of fluorescent protein-based biosensors. *Current opinion in chemical biology 14* (1): 30-36,2010.

37. Algar, W. R.; Susumu, K.; Delehanty, J. B.; Medintz, I. L.: Semiconductor quantum dots in bioanalysis: crossing the valley of death. *Analytical chemistry 83* (23): 8826-8837,2011.

38. Rosenthal, S. J.; Chang, J. C.; Kovtun, O.; McBride, J. R.; Tomlinson, I. D.: Biocompatible quantum dots for biological applications. *Chemistry & biology 18* (1): 10-24,2011.

39. Medintz, I. L.; Mattoussi, H.: Quantum dot-based resonance energy transfer and its growing application in biology. *Physical chemistry chemical physics : PCCP 11* (1): 17-45,2009.

40. Peng, C.-W.; Li, Y.: Application of Quantum Dots-Based Biotechnology in Cancer Diagnosis: Current Status and Future Perspectives. *Journal of Nanomaterials 2010*: 1-11,2010.

41. Algar, W. R.; Wegner, D.; Huston, A. L.; Blanco-Canosa, J. B.; Stewart, M. H.; Armstrong, A.; Dawson, P. E.; Hildebrandt, N.; Medintz, I. L.: Quantum dots as simultaneous acceptors and donors in time-gated Forster resonance energy transfer relays: characterization and biosensing. *Journal of the American Chemical Society 134* (3): 1876-1891,2012.

42. Siligardi, G.; Hussain, R.; Patching, S. G.; Phillips-Jones, M. K.: Ligand- and drug-binding studies of membrane proteins revealed through circular dichroism spectroscopy. *Biochimica et biophysica acta 1838* (1 Pt A): 34-42,2014.

43. Geissler, D.; Linden, S.; Liermann, K.; Wegner, K. D.; Charbonniere, L. J.; Hildebrandt, N.: Lanthanides and quantum dots as Forster resonance energy transfer agents for diagnostics and cellular imaging. *Inorganic chemistry 53* (4): 1824-1838,2014.

44. Boulant, S.; Kural, C.; Zeeh, J. C.; Ubelmann, F.; Kirchhausen, T.: Actin dynamics counteract membrane tension during clathrin-mediated endocytosis. *Nature cell biology 13* (9): 1124-1131,2011.

45. So, M. K.; Xu, C.; Loening, A. M.; Gambhir, S. S.; Rao, J.: Self-illuminating quantum dot conjugates for in vivo imaging. *Nature biotechnology 24* (3): 339-343,2006.

46. Freeman, R.; Liu, X.; Willner, I.: Chemiluminescent and chemiluminescence resonance energy transfer (CRET) detection of DNA, metal ions, and aptamer-substrate complexes using hemin/G-quadruplexes and CdSe/ZnS quantum dots. *Journal of the American Chemical Society 133* (30): 11597-11604,2011.

47. Nirmalan, N. J.; Harnden, P.; Selby, P. J.; Banks, R. E.: Mining the archival formalin-fixed paraffin-embedded tissue proteome: opportunities and challenges. *Molecular bioSystems 4* (7): 712-720,2008.

48. Lim, M. S.; Elenitoba-Johnson, K. S.: Proteomics in pathology research. *Laboratory investigation; a journal of technical methods and pathology 84* (10): 1227-1244,2004.

49. Stack, E. C.; Wang, C.; Roman, K. A.; Hoyt, C. C.: Multiplexed immunohistochemistry, imaging, and quantitation: a review, with an assessment of Tyramide signal amplification, multispectral imaging and multiplex analysis. *Methods 70* (1): 46-58,2014.

50. Rimm, D. L.:What brown cannot do for you.*Nature Biotechnology* 24(8): 914-916, 2006.

51. Schaap, M.; Hancock, R.; Wilderspin, A.; Wells, G.: Development of a steady-state FRET-

based assay to identify inhibitors of the Keap1-Nrf2 protein-protein interaction. *Protein science : a publication of the Protein Society* *22* (12): 1812-1819,2013.

52. Lubeck, E.; Cai, L.: Single-cell systems biology by super-resolution imaging and combinatorial labeling. *Nature methods* *9* (7): 743-748,2012.

53. Boichenko, I.; Deiss, S.; Bar, K.; Hartmann, M. D.; Hernandez Alvarez, B.: A FRET-Based Assay for the Identification and Characterization of Cereblon Ligands. *Journal of medicinal chemistry* *59* (2): 770-774,2016.

54. Glass, G.; Papin, J. A.; Mandell, J. W.: SIMPLE: a sequential immunoperoxidase labeling and erasing method. *The journal of histochemistry and cytochemistry : official journal of the Histochemistry Society* *57* (10): 899-905,2009.

55. Pirici, D.; Mogoanta, L.; Kumar-Singh, S.; Pirici, I.; Margaritescu, C.; Simionescu, C.; Stanescu, R.: Antibody elution method for multiple immunohistochemistry on primary antibodies raised in the same species and of the same subtype. *The journal of histochemistry and cytochemistry : official journal of the Histochemistry Society* *57* (6): 567-575,2009.

56. Giesen, C.; Wang, H. A.; Schapiro, D.; Zivanovic, N.; Jacobs, A.; Hattendorf, B.; Schuffler, P. J.; Grolimund, D.; Buhmann, J. M.; Brandt, S.; Varga, Z.; Wild, P. J.; Gunther, D.; Bodenmiller, B.: Highly multiplexed imaging of tumor tissues with subcellular resolution by mass cytometry. *Nature methods* *11* (4): 417-422,2014.

57. Angelo, M.; Bendall, S. C.; Finck, R.; Hale, M. B.; Hitzman, C.; Borowsky, A. D.; Levenson, R. M.; Lowe, J. B.; Liu, S. D.; Zhao, S.; Natkunam, Y.; Nolan, G. P.: Multiplexed ion beam imaging of human breast tumors. *Nature medicine* *20* (4): 436-442,2014.

58. Levenson, R. M.; Borowsky, A. D.; Angelo, M.: Immunohistochemistry and mass spectrometry for highly multiplexed cellular molecular imaging. *Laboratory investigation; a journal of technical methods and pathology* *95* (4): 397-405,2015.

59. Robertson, D.; Savage, K.; Reis-Filho, J. S.; Isacke, C. M.: Multiple immunofluorescence labelling of formalin-fixed paraffin-embedded (FFPE) tissue. *BMC cell biology* *9*: 13,2008.

60. Petschnigg, J.; Groisman, B.; Kotlyar, M.; Taipale, M.; Zheng, Y.; Kurat, C. F.; Sayad, A.; Sierra, J. R.; Mattiazzi Usaj, M.; Snider, J.; Nachman, A.; Krykbaeva, I.; Tsao, M. S.; Moffat, J.; Pawson, T.; Lindquist, S.; Jurisica, I.; Stagljar, I.: The mammalian-membrane two-hybrid assay (MaMTH) for probing membrane-protein interactions in human cells. *Nat Methods* *11* (5): 585-592,2014.

61. Li, Y. C.; Rodewald, L. W.; Hoppmann, C.; Wong, E. T.; Lebreton, S.; Safar, P.; Patek, M.; Wang, L.; Wertman, K. F.; Wahl, G. M.: A versatile platform to analyze low-affinity and transient protein-protein interactions in living cells in real time. *Cell reports* *9* (5): 1946-1958,2014.

62. Polaske, N. W.; Kelly, B. D.; Ashworth-Sharpe, J.; Bieniarz, C.: Quinone Methide Signal Amplification: Covalent Reporter Labeling of Cancer Epitopes using Alkaline Phosphatase Substrates. *Bioconjugate chemistry 27* (3): 660-666,2016.

63. Vidal, M.; Cusick, M. E.; Barabasi, A. L.: Interactome networks and human disease. *Cell 144* (6): 986-998,2011.

64. Wells, J. A.; McClendon, C. L.: Reaching for high-hanging fruit in drug discovery at protein-protein interfaces. *Nature 450* (7172): 1001-1009,2007.

65. Arkin, M. R.; Tang, Y.; Wells, J. A.: Small-molecule inhibitors of protein-protein interactions: progressing toward the reality. *Chemistry & biology 21* (9): 1102-1114,2014.

66. Goudreau, N.; Cameron, D. R.; Deziel, R.; Hache, B.; Jakalian, A.; Malenfant, E.; Naud, J.; Ogilvie, W. W.; O'Meara, J.; White, P. W.; Yoakim, C.: Optimization and determination of the absolute configuration of a series of potent inhibitors of human papillomavirus type-11 E1-E2 protein-protein interaction: a combined medicinal chemistry, NMR and computational chemistry approach. *Bioorganic & medicinal chemistry 15* (7): 2690-2700,2007.

67. Hino, N.; Okazaki, Y.; Kobayashi, T.; Hayashi, A.; Sakamoto, K.; Yokoyama, S.: Protein photo-cross-linking in mammalian cells by site-specific incorporation of a photoreactive amino acid. *Nature methods 2* (3): 201-206,2005.

68. Barker, A.; Kettle, J. G.; Nowak, T.; Pease, J. E.: Expanding medicinal chemistry space. *Drug discovery today 18* (5-6): 298-304,2013.

69. Sperandio, O.; Reynes, C. H.; Camproux, A. C.; Villoutreix, B. O.: Rationalizing the chemical space of protein-protein interaction inhibitors. *Drug discovery today 15* (5-6): 220-229,2010.

70. Moreira, I. S.; Fernandes, P. A.; Ramos, M. J.: Hot spots--a review of the protein-protein interface determinant amino-acid residues. *Proteins 68* (4): 803-812,2007.

71. Perot, S.; Sperandio, O.; Miteva, M. A.; Camproux, A. C.; Villoutreix, B. O.: Druggable pockets and binding site centric chemical space: a paradigm shift in drug discovery. *Drug discovery today 15* (15-16): 656-667,2010.

72. Fry, D. C.: Protein-protein interactions as targets for small molecule drug discovery. *Biopolymers 84* (6): 535-552,2006.

73. Raimundo, B.C.; Oslob, J.D.; Braisted, A.C.; Hyde, J.; McDowell, R.S.; Randal, M.; Waal, N.D.; Wilkinson, J.; Yu, C.H.; Arkin, M.R.: Integrating Fragment Assembly and Biophysical Methods in the Chemical Advancement of Small-Molecule Antagonists of IL-2: An Approach for Inhibiting Protein - Protein Interactions. *J. Med. Chem.* 47: 3111 - 3130, 2004.

74. Lepourcelet, M.; Chen, Y.N.; France, D.S.; Wang, H.S.; Crews, P.; Petersen, F.; Bruseo, C.; Wood, A.W.; Shivdasani, R.A.: Small-molecule antagonists of the oncogenic Tcf/ β-catenin protein complex. *Cancer Cell* 5: 91-102, 2004.

75. Sattler, M.; Liang, H.; Nettesheim, D.; Meadows, D.P.; Harlan, J.E.; Eberstadt,M.; Yoon, H.S.; Shuker, S.B.; Chang, B.S.; Minn, A.J.; Thompson, C.B.; Fesik, S.W.: Structure of Bcl-xL–Bak Peptide Complex: Recognition Between Regulators of Apoptosis. Science 275: 983-986, 1997.

76. Petros, A.M.; Nettesheim, D.G.; Wang, Y.; Olejniczak, E.T.; Meadows, R.P.; mack, J.; Awift, K.; matayoshi, E.D.; Zhang, H.C.: Thompson, C.B.; Fesik, S.W.: Rationale for Bcl-x_L/Bad peptide complex formation from structure, mutagenesis, and biophysical studies. *Protein Science* 9: 2528-2534, 2000.

77. Rubinstein, M.; Niv, M. Y.: Peptidic modulators of protein-protein interactions: progress and challenges in computational design. *Biopolymers 91* (7): 505-513,2009.

78. Lippens, G.; Landrieu, I.; Smet, C.; Huvent, I.; Gandhi, N. S.; Gigant, B.; Despres, C.; Qi, H.; Lopez, J.: NMR Meets Tau: Insights into Its Function and Pathology. *Biomolecules 6* (2),2016.

79. Situ, A. J.; Schmidt, T.; Mazumder, P.; Ulmer, T. S.: Characterization of membrane protein interactions by isothermal titration calorimetry. *Journal of molecular biology 426* (21): 3670-3680,2014.

80. Patching, S. G.: Surface plasmon resonance spectroscopy for characterisation of membrane protein-ligand interactions and its potential for drug discovery. *Biochimica et biophysica acta 1838* (1 Pt A): 43-55,2014.

81. Hamdi, A.; Colas, P.: Yeast two-hybrid methods and their applications in drug discovery. *Trends in pharmacological sciences 33* (2): 109-118,2012.

82. Tchekanda, E.; Sivanesan, D.; Michnick, S. W.: An infrared reporter to detect spatiotemporal dynamics of protein-protein interactions. *Nature methods 11* (6): 641-644,2014.

83. Rebois, R. V.; Robitaille, M.; Petrin, D.; Zylbergold, P.; Trieu, P.; Hebert, T. E.: Combining protein complementation assays with resonance energy transfer to detect multipartner protein complexes in living cells. *Methods 45* (3): 214-218,2008.

84. Fellinger, K.; Rothbauer, U.; Felle, M.; Langst, G.; Leonhardt, H.: Dimerization of DNA methyltransferase 1 is mediated by its regulatory domain. *Journal of cellular biochemistry 106* (4): 521-528,2009.

85. Meilinger, D.; Fellinger, K.; Bultmann, S.; Rothbauer, U.; Bonapace, I. M.; Klinkert, W. E.; Spada, F.; Leonhardt, H.: Np95 interacts with de novo DNA methyltransferases, Dnmt3a

and Dnmt3b, and mediates epigenetic silencing of the viral CMV promoter in embryonic stem cells. *EMBO reports 10* (11): 1259-1264,2009.

86. Sun, Y.; Rombola, C.; Jyothikumar, V.; Periasamy, A.: Forster resonance energy transfer microscopy and spectroscopy for localizing protein-protein interactions in living cells. *Cytometry. Part A : the journal of the International Society for Analytical Cytology 83* (9): 780-793,2013.

87. Padilla-Parra, S.; Tramier, M.: FRET microscopy in the living cell: different approaches, strengths and weaknesses. *BioEssays : news and reviews in molecular, cellular and developmental biology 34* (5): 369-376,2012.

88. Deriziotis, P.; Graham, S. A.; Estruch, S. B.; Fisher, S. E.: Investigating protein-protein interactions in live cells using bioluminescence resonance energy transfer. *Journal of visualized experiments : JoVE* (87),2014.

89. Inglese, J.; Johnson, R. L.; Simeonov, A.; Xia, M.; Zheng, W.; Austin, C. P.; Auld, D. S.: High-throughput screening assays for the identification of chemical probes. *Nature chemical biology 3* (8): 466-479,2007.

90. Piljic, A.; Schultz, C.: Simultaneous Recording of Multiple Cellular Events by FRET. Chemical Biology 3 (3):156-160, 2008.

91. Arkin, M. R.; Wells, J. A.: Small-molecule inhibitors of protein-protein interactions: progressing towards the dream. *Nature reviews. Drug discovery 3* (4): 301-317,2004.

92. Zhang J.H.; Chung, T.D.Y.: Oldenburg, K.R.: A simple statistical parameter for use in evaluation and validation of high throughput screening assays. Journal of Biomolecular Screening 4 (2): 67-73, 1999.

93. Birmingham, A.; Selfors, L. M.; Forster, T.; Wrobel, D.; Kennedy, C. J.; Shanks, E.; Santoyo-Lopez, J.; Dunican, D. J.; Long, A.; Kelleher, D.; Smith, Q.; Beijersbergen, R. L.; Ghazal, P.; Shamu, C. E.: Statistical methods for analysis of high-throughput RNA interference screens. *Nature methods 6* (8): 569-575,2009.

94. Kurreck, J.: RNA interference: Perspectives and caveats. *Journal of RNAi and Gene Silencing*, 1(2): 50-51, 2005.

95. Zhang, X. D.: Illustration of SSMD, z score, SSMD*, z* score, and t statistic for hit selection in RNAi high-throughput screens. *Journal of biomolecular screening 16* (7): 775-785,2011.

96. Arkin, M.R.; Glicksman, M.A.; Fu, H.A.; Havel, J.J.; Du, Y.H.: Inhibition of Protein-Protein Interactions Non-Cellular Assay. *Assay Guidance Manual* 2012.

97. Hall, M. D.; Yasgar, A.; Peryea, T.; Braisted, J. C.; Jadhav, A.; Simeonov, A.; Coussens, N.

P.: Fluorescence polarization assays in high-throughput screening and drug discovery: a review. *Methods and applications in fluorescence 4* (2): 022001,2016.

98. Sharma, K. K.; Przybilla, F.; Restle, T.; Godet, J.; Mely, Y.: FRET-based assay to screen inhibitors of HIV-1 reverse transcriptase and nucleocapsid protein. *Nucleic acids research 44* (8): e74,2016.

99. Yang, G.; Withers, S. G.: Ultrahigh-throughput FACS-based screening for directed enzyme evolution. *Chembiochem : a European journal of chemical biology 10* (17): 2704-2715,2009.

100. Rogers, M. S.; Cryan, L. M.; Habeshian, K. A.; Bazinet, L.; Caldwell, T. P.; Ackroyd, P. C.; Christensen, K. A.: A FRET-based high throughput screening assay to identify inhibitors of anthrax protective antigen binding to capillary morphogenesis gene 2 protein. *PloS one 7* (6): e39911,2012.

101. Sun, S.; Yang, X.; Wang, Y.; Shen, X.: In Vivo Analysis of Protein-Protein Interactions with Bioluminescence Resonance Energy Transfer (BRET): Progress and Prospects. *International journal of molecular sciences 17* (10),2016.

102. Lundholt,B.K.; Heydorn, A.; Bjørn, S.P.; Præstegaard, M.: A Simple Cell-Based HTS Assay System to Screen for Inhibitors of p53-Hdm2 Protein–Protein Interactions. ASSAY and Drug Development Technologies 4 (6): 679-688, 2006.

103. Herce, H. D.; Deng, W.; Helma, J.; Leonhardt, H.; Cardoso, M. C.: Visualization and targeted disruption of protein interactions in living cells. *Nature communications 4*: 2660,2013.

104. de Boer, P.; Hoogenboom, J. P.; Giepmans, B. N.: Correlated light and electron microscopy: ultrastructure lights up! *Nature methods 12* (6): 503-513,2015.

105. Kelleher, M. T.; Fruhwirth, G.; Patel, G.; Ofo, E.; Festy, F.; Barber, P. R.; Ameer-Beg, S. M.; Vojnovic, B.; Gillett, C.; Coolen, A.; Keri, G.; Ellis, P. A.; Ng, T.: The potential of optical proteomic technologies to individualize prognosis and guide rational treatment for cancer patients. *Targeted oncology 4* (3): 235-252,2009.

106. Martell, J. D.; Deerinck, T. J.; Sancak, Y.; Poulos, T. L.; Mootha, V. K.; Sosinsky, G. E.; Ellisman, M. H.; Ting, A. Y.: Engineered ascorbate peroxidase as a genetically encoded reporter for electron microscopy. *Nature biotechnology 30* (11): 1143-1148,2012.

107. Braslavsky, S.E.; Fron, E.; Rodriguez, H.B.; Roman, E.S.; Scholes, G.D.; Valeur, B.; Wirz, J.: Pitfalls and limitations in the practical use of F¨orster's theory of resonance energy transfer. *Photochemical & Photobiological Sciences* 7: 1444-1448, 2008.

108. Berney, C.; Danuser, G.: FRET or No FRET: A Quantitative Comparison. *Biophysical Journal* 84: 3992-4010, 2003.

109. Piston, D. W.; Kremers, G. J.: Fluorescent protein FRET: the good, the bad and the ugly. *Trends in biochemical sciences 32* (9): 407-414,2007.

110. Linden, S.; Singh, M. K.; Wegner, K. D.; Regairaz, M.; Dautry, F.; Treussart, F.; Hildebrandt, N.: Terbium-based time-gated Forster resonance energy transfer imaging for evaluating protein-protein interactions on cell membranes. *Dalton transactions 44* (11): 4994-5003,2015.

111. Jin, D.; Piper, J. A.: Time-gated luminescence microscopy allowing direct visual inspection of lanthanide-stained microorganisms in background-free condition. *Analytical chemistry 83* (6): 2294-2300,2011.

112. Faklaris, O.; Cottet, M.; Falco, A.; Villier, B.; Laget, M.; Zwier, J. M.; Trinquet, E.; Mouillac, B.; Pin, J. P.; Durroux, T.: Multicolor time-resolved Forster resonance energy transfer microscopy reveals the impact of GPCR oligomerization on internalization processes. *FASEB journal : official publication of the Federation of American Societies for Experimental Biology 29* (6): 2235-2246,2015.

113. Geissler, D.; Charbonniere, L. J.; Ziessel, R. F.; Butlin, N. G.; Lohmannsroben, H. G.; Hildebrandt, N.: Quantum dot biosensors for ultrasensitive multiplexed diagnostics. *Angewandte Chemie 49* (8): 1396-1401,2010.

114. Hildebrandt, N.; Charbonniere, L. J.; Lohmannsroben, H. G.: Time-resolved analysis of a highly sensitive Forster resonance energy transfer immunoassay using terbium complexes as donors and quantum dots as acceptors. *Journal of biomedicine & biotechnology 2007* (7): 79169,2007.

115. Algar, W. R.; Malanoski, A. P.; Susumu, K.; Stewart, M. H.; Hildebrandt, N.; Medintz, I. L.: Multiplexed tracking of protease activity using a single color of quantum dot vector and a time-gated Forster resonance energy transfer relay. *Analytical chemistry 84* (22): 10136-10146,2012.

116. Harma, H.; Soukka, T.; Shavel, A.; Gaponik, N.; Weller, H.: Luminescent energy transfer between cadmium telluride nanoparticle and lanthanide(III) chelate in competitive bioaffinity assays of biotin and estradiol. *Analytica chimica acta 604* (2): 177-183,2007.

117. Gahlaut, N.; Miller, L. W.: Time-resolved microscopy for imaging lanthanide luminescence in living cells. *Cytometry. Part A : the journal of the International Society for Analytical Cytology 77* (12): 1113-1125,2010.

118. Rajendran, M.; Miller, L. W.: Evaluating the performance of time-gated live-cell microscopy with lanthanide probes. *Biophysical journal 109* (2): 240-248,2015.

119. Schneider, C. A.; Rasband, W. S.; Eliceiri, K. W.: NIH Image to ImageJ: 25 years of image analysis. *Nature methods 9* (7): 671-675,2012.

120. Hofman, E. G.; Ruonala, M. O.; Bader, A. N.; van den Heuvel, D.; Voortman, J.; Roovers, R. C.; Verkleij, A. J.; Gerritsen, H. C.; van Bergen En Henegouwen, P. M.: EGF induces coalescence of different lipid rafts. *Journal of cell science 121* (Pt 15): 2519-2528,2008.

121. Martinelli, E.; De Palma, R.; Orditura, M.; De Vita, F.; Ciardiello, F.: Anti-epidermal growth factor receptor monoclonal antibodies in cancer therapy. *Clinical and experimental immunology 158* (1): 1-9,2009.

122. Wegner, K. D.; Linden, S.; Jin, Z.; Jennings, T. L.; el Khoulati, R.; van Bergen en Henegouwen, P. M.; Hildebrandt, N.: Nanobodies and nanocrystals: highly sensitive quantum dot-based homogeneous FRET immunoassay for serum-based EGFR detection. *Small 10* (4): 734-740,2014.

123. Bobrow, M. N.; Harris, T. D.; Shaughnessy, K. J.; Litt, G. J.: Catalyzed reporter deposition, a novel method of signal amplification. Application to immunoassays. *J Immunol Methods 125* (1-2): 279-285,1989.Bobrow, M. N.; Shaughnessy, K. J.; Litt, G. J.: Catalyzed reporter deposition, a novel method of signal amplification. II. Application to membrane immunoassays. *J Immunol Methods 137* (1): 103-112,1991.Polaske, N. W.; Kelly, B. D.; Ashworth-Sharpe, J.; Bieniarz, C.: Quinone Methide Signal Amplification: Covalent Reporter Labeling of Cancer Epitopes using Alkaline Phosphatase Substrates. *Bioconjugate Chemistry 27* (3): 660-666,2016.

124. Geissler, D.; Stufler, S.; Lohmannsroben, H. G.; Hildebrandt, N.: Six-color time-resolved Forster resonance energy transfer for ultrasensitive multiplexed biosensing. *J. Am. Chem. Soc. 135* (3): 1102-1109,2013.

125. Scott, D. E.; Bayly, A. R.; Abell, C.; Skidmore, J.: Small molecules, big targets: drug discovery faces the protein-protein interaction challenge. *Nat Rev Drug Discov 15* (8): 533-550,2016.

126. Cochran, A. G.: Antagonists of protein-protein interactions. *Chem Biol 7* (4): R85-94,2000.

127. Yoakim, C.; Ogilvie, W. W.; Goudreau, N.; Naud, J.; Hache, B.; O'Meara, J. A.; Cordingley, M. G.; Archambault, J.; White, P. W.: Discovery of the first series of inhibitors of human papillomavirus type 11: inhibition of the assembly of the E1-E2-Origin DNA complex. *Bioorg Med Chem Lett 13* (15): 2539-2541,2003.

128. Bruncko, M.; Oost, T. K.; Belli, B. A.; Ding, H.; Joseph, M. K.; Kunzer, A.; Martineau, D.; McClellan, W. J.; Mitten, M.; Ng, S. C.; Nimmer, P. M.; Oltersdorf, T.; Park, C. M.; Petros, A. M.; Shoemaker, A. R.; Song, X.; Wang, X.; Wendt, M. D.; Zhang, H.; Fesik, S. W.; Rosenberg, S. H.; Elmore, S. W.: Studies leading to potent, dual inhibitors of Bcl-2 and Bcl-xL. *J Med Chem 50* (4): 641-662,2007.

129. Grasberger, B. L.; Lu, T.; Schubert, C.; Parks, D. J.; Carver, T. E.; Koblish, H. K.; Cummings, M. D.; LaFrance, L. V.; Milkiewicz, K. L.; Calvo, R. R.; Maguire, D.; Lattanze, J.; Franks, C. F.; Zhao, S.; Ramachandren, K.; Bylebyl, G. R.; Zhang, M.; Manthey, C. L.;

Petrella, E. C.; Pantoliano, M. W.; Deckman, I. C.; Spurlino, J. C.; Maroney, A. C.; Tomczuk, B. E.; Molloy, C. J.; Bone, R. F.: Discovery and cocrystal structure of benzodiazepinedione HDM2 antagonists that activate p53 in cells. *J Med Chem 48* (4): 909-912,2005.Vassilev, L. T.; Vu, B. T.; Graves, B.; Carvajal, D.; Podlaski, F.; Filipovic, Z.; Kong, N.; Kammlott, U.; Lukacs, C.; Klein, C.; Fotouhi, N.; Liu, E. A.: In vivo activation of the p53 pathway by small-molecule antagonists of MDM2. *Science 303* (5659): 844-848,2004.

130. An, W. F.; Tolliday, N.: Cell-based assays for high-throughput screening. *Mol Biotechnol 45* (2): 180-186,2010.

131. Michelini, E.; Cevenini, L.; Mezzanotte, L.; Coppa, A.; Roda, A.: Cell-based assays: fuelling drug discovery. *Analytical and bioanalytical chemistry 398* (1): 227-238,2010.

132. Korn, K.; Krausz, E.: Cell-based high-content screening of small-molecule libraries. *Curr Opin Chem Biol 11* (5): 503-510,2007.

133. Lundholt, B. K.; Heydorn, A.; Bjorn, S. P.; Praestegaard, M.: A simple cell-based HTS assay system to screen for inhibitors of p53-Hdm2 protein-protein interactions. *Assay Drug Dev Technol 4* (6): 679-688,2006.

134. Michnick, S. W.; Ear, P. H.; Manderson, E. N.; Remy, I.; Stefan, E.: Universal strategies in research and drug discovery based on protein-fragment complementation assays. *Nature reviews. Drug discovery 6* (7): 569-582,2007.

135. Eyckerman, S.; Lemmens, I.; Catteeuw, D.; Verhee, A.; Vandekerckhove, J.; Lievens, S.; Tavernier, J.: Reverse MAPPIT: screening for protein-protein interaction modifiers in mammalian cells. *Nat Methods 2* (6): 427-433,2005.

136. Pfleger, K. D.; Eidne, K. A.: Illuminating insights into protein-protein interactions using bioluminescence resonance energy transfer (BRET). *Nature methods 3* (3): 165-174,2006.You, X.; Nguyen, A. W.; Jabaiah, A.; Sheff, M. A.; Thorn, K. S.; Daugherty, P. S.: Intracellular protein interaction mapping with FRET hybrids. *Proceedings of the National Academy of Sciences of the United States of America 103* (49): 18458-18463,2006.

137. Banaszynski, L. A.; Liu, C. W.; Wandless, T. J.: Characterization of the FKBP.rapamycin.FRB ternary complex. *J Am Chem Soc 127* (13): 4715-4721,2005.

138. Rajapakse, H. E.; Reddy, D. R.; Mohandessi, S.; Butlin, N. G.; Miller, L. W.: Luminescent terbium protein labels for time-resolved microscopy and screening. *Angewandte Chemie 48* (27): 4990-4992,2009.

139. Komatsu, N.; Aoki, K.; Yamada, M.; Yukinaga, H.; Fujita, Y.; Kamioka, Y.; Matsuda, M.: Development of an optimized backbone of FRET biosensors for kinases and GTPases. *Molecular biology of the cell 22* (23): 4647-4656,2011.

140. Lam, A. J.; St-Pierre, F.; Gong, Y.; Marshall, J. D.; Cranfill, P. J.; Baird, M. A.; McKeown, M. R.; Wiedenmann, J.; Davidson, M. W.; Schnitzer, M. J.; Tsien, R. Y.; Lin, M. Z.: Improving FRET dynamic range with bright green and red fluorescent proteins. *Nature methods 9* (10): 1005-1012,2012.

141. Nagai, T.; Yamada, S.; Tominaga, T.; Ichikawa, M.; Miyawaki, A.: Expanded dynamic range of fluorescent indicators for Ca(2+) by circularly permuted yellow fluorescent proteins. *Proceedings of the National Academy of Sciences of the United States of America 101* (29): 10554-10559,2004.

142. Allen, M. D.; Zhang, J.: Subcellular dynamics of protein kinase A activity visualized by FRET-based reporters. *Biochemical and biophysical research communications 348* (2): 716-721,2006.

143. Selvin, P. R.: Lanthanide-based resonance energy transfer. *IEEE Journal of Selected Topics in Quantum Electronics 2* (4): 1077-1087,1996.

144. Hildebrandt, N.; Wegner, K. D.; Algar, W. R.: Luminescent terbium complexes: Superior Förster resonance energy transfer donors for flexible and sensitive multiplexed biosensing. *Coordination Chemistry Reviews 273-274* (Supplement C): 125-138,2014.

145. Sivaramakrishnan, S.; Spudich, J. A.: Systematic control of protein interaction using a modular ER/K alpha-helix linker. *Proc Natl Acad Sci U S A 108* (51): 20467-20472,2011.

146. Swanson, C. J.; Sivaramakrishnan, S.: Harnessing the unique structural properties of isolated alpha-helices. *The Journal of biological chemistry 289* (37): 25460-25467,2014.

147. Mathis, Gerard: Probing Molecular Interactions with Homogeneous Techniques Based on Rare Earth Cryptates and Fluorescence Energy Transfer. *CLIN. CHEM.* 41(9):1391-1397, 1995.

148. Zhang, X. D.: A pair of new statistical parameters for quality control in RNA interference high-throughput screening assays. *Genomics 89* (4): 552-561,2007.

149. Kawai, M.; Lane, B.C.; Hsieh, G. C.; Mollison, K.W.; Carter, G.W.; Luly, J.R.: Structure-activity profiles of macrolactam immunosuppressant FK-506 analogues. FEBS LETTERS 316 (2): 107-113, 1993.

150. Boyd, S.D.; Tsai, K.Y.; Jacks, T.: An intact HDM2 RING-finger domain is required for nuclear exclusion of p53. Nature Cell Biology 2: 563-568, 2000.

151. Shangary, S.; Wang, S.: Small-molecule inhibitors of the MDM2-p53 protein-protein interaction to reactivate p53 function: a novel approach for cancer therapy. *Annual review of pharmacology and toxicology 49*: 223-241,2009.

152. Tan, I.; Ng, C. H.; Lim, L.; Leung, T.: Phosphorylation of a novel myosin binding subunit

of protein phosphatase 1 reveals a conserved mechanism in the regulation of actin cytoskeleton. *The Journal of biological chemistry 276* (24): 21209-21216,2001.

153. von Degenfeld, G.; Wehrman, T. S.; Hammer, M. M.; Blau, H. M.: A universal technology for monitoring G-protein-coupled receptor activation in vitro and noninvasively in live animals. *FASEB journal : official publication of the Federation of American Societies for Experimental Biology 21* (14): 3819-3826,2007.

154. Hammer, M. M.; Wehrman, T. S.; Blau, H. M.: A novel enzyme complementation-based assay for monitoring G-protein-coupled receptor internalization. *FASEB journal : official publication of the Federation of American Societies for Experimental Biology 21* (14): 3827-3834,2007.

155. Huang, H.; Choi, S. Y.; Frohman, M. A.: A quantitative assay for mitochondrial fusion using Renilla luciferase complementation. *Mitochondrion 10* (5): 559-566,2010.

156. Deng, Q.; Wang, D.; Xiang, X.; Gao, X.; Hardwidge, P. R.; Kaushik, R. S.; Wolff, T.; Chakravarty, S.; Li, F.: Application of a split luciferase complementation assay for the detection of viral protein-protein interactions. *Journal of virological methods 176* (1-2): 108-111,2011.

157. Ishimoto, T.; Ozawa, T.; Mori, H.: Real-time monitoring of actin polymerization in living cells using split luciferase. *Bioconjugate chemistry 22* (6): 1136-1144,2011.

158. Hu, C. D.; Kerppola, T. K.: Simultaneous visualization of multiple protein interactions in living cells using multicolor fluorescence complementation analysis. *Nature biotechnology 21* (5): 539-545,2003.

159. Remy, I.; Michnick, S. W., Mapping Biochemical Networks With Protein-Fragment Complementation Assays. In *Protein-Protein Interactions: Methods and Applications*, Fu, H., Ed. Humana Press: Totowa, NJ, 2004; pp 411-426.

160. Bystroff, C.: Oatley, S.J.: Kraut, J.: Crystal Structures of Escherichia coli Dihydrofolate Reductase: The NADP+ Holoenzyme and the Folate·NADP+ Ternary Complex. Substrate Binding and a Model for the Transition State. *Biochemistry* 29: 3263-3277, 1990.

161. Remy, I.; Michnick, S. W.: Visualization of biochemical networks in living cells. *Proceedings of the National Academy of Sciences of the United States of America 98* (14): 7678-7683,2001.

VITA

TING CHEN

EDUCATION:

B.Sc., Chemistry, Shanxi University, Taiyuan, China, 2008

M.Sc., Chemistry, Shanxi University, Taiyuan, China, 2011

Ph.D., Chemistry, University of Illinois at Chicago, Illinois, 2018

RESEARCH EXPERIENCE:

- Department of Chemistry, University of Illinois at Chicago — Chicago, IL,USA
  Research assistant; Advisor: Prof. Lawrence Miller. — 2012/06 - present
- Department of Chemistry, Shanxi University — Taiyuan, Shanxi, China
  Advisor: Prof. Shengwan Zhang. — 2008/09 – 2011/06
- Department of Chemistry, Shanxi University — Taiyuan, Shanxi, China
  Part time research trainee with Prof. Zhao Zhang — 2006/09 – 2007/06

TEACHING EXPERIENCE:

- Department of Chemistry, University of Illinois at Chicago — Chicago, IL,USA
  2011/08- 2017/05

  General chemistry (Chem 106 112 and 114),
  Inorganic chemistry (Chem 314),
  Organic chemistry (Chem 100)
  Biochemistry (Chem 452 and 455).

PUBLICATIONS:

- **Chen, T.**; Pham, H.; Yapici, E.; Miller, L.W.: High dynamic range lanthanide-based FRET biosensors for time-gated microscopy and high throughput screening of PPIs. In preparation.
- **Chen, T.**; Hong, R.; Magda, D.; Bieniarz, C.; Morrison, L.; Miller, L.: Time gated luminescence imaging of immunolabeled human tissues. Analytical Chemistry 89(23), 12713-12719, 2017.

- Afsari1, H.; Santos, M. C. D.; Lindén S.; **Chen, T.**; Qiu, X.; Henegouwen, P. M. P.; Jennings, T. L.; Susumu K.; Medintz, I. L.; Hildebrandt, N.; Miller, L. W.: Time-gated FRET nanoassemblies for rapid and sensitive intra- and extracellular fluorescence imaging. *ScienceAdvances* 2:e1600265, 2016.
- Ma, Y.H.; Qiao, H.; Wang, W.; **Chen, T.**; Du, X.W.; Zhai, X.L.; Zhang, S.W.: Variations in physicochemical properties of Chinese Fenjiu during storage and high-gravity technology of liquor aging. *International journal of food properties* 17(4), 923-936, 2014.

PRESENTATIONS:

- **Chen, T**.; Pham, H.; Miller, L.W.: Lanthanide-based FRET biosensors for time-gated imaging and detection of protein-protein interactions in live mammalian cells. Poster and Spotlight Oral presentation, *Experimental Biology* Chicago (IL), 2017
- **Chen, T**.; Pham, H.; Miller, L.W.: Lanthanide-based FRET biosensors for time-gated imaging and detection of protein-protein interactions in live mammalian cells. Poster presentation, *5th Annual International Chemical Biology Society Conference* Madison, (WI), 2016

APPENDIX

RightsLink®

Home | Create Account | Help

Title: Time gated luminescence imaging of immunolabeled human tissues.

Author: Ting Chen, Rui Hong, Darren Magda, et al

Publication: Analytical Chemistry

Publisher: American Chemical Society

Date: Nov 1, 2017

LOGIN

If you're a copyright.com user, you can login to RightsLink using your copyright.com credentials. Already **a RightsLink user** or want to learn more?

PERMISSION/LICENSE IS GRANTED FOR YOUR ORDER AT NO CHARGE

This type of permission/license, instead of the standard Terms & Conditions, is sent to you because no fee is being charged for your order. Please note the following:

- Permission is granted for your request in both print and electronic formats, and translations.
- If figures and/or tables were requested, they may be adapted or used in part.
- Please print this page for your records and send a copy of it to your publisher/graduate school.
- Appropriate credit for the requested material should be given as follows: "Reprinted (adapted) with permission from (COMPLETE REFERENCE CITATION). Copyright (YEAR) American Chemical Society." Insert appropriate information in place of the capitalized words.
- One-time permission is granted only for the use specified in your request. No additional uses are granted (such as derivative works or other editions). For any other uses, please submit a new request.

BACK | CLOSE WINDOW